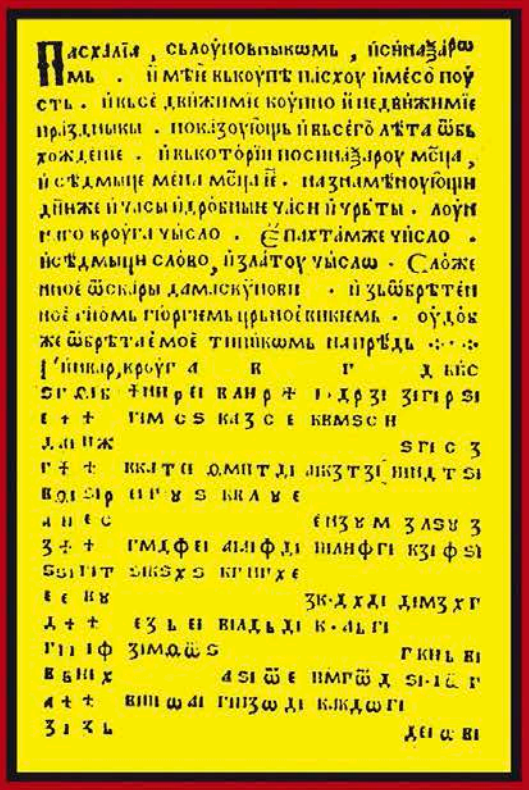

Mathematica Montisnigri

VOLUME XXXI-2014

The journal Mathematica Montisnigri is published by the Society of mathematicians and physicists of Montenegro and Department of Mathematics of The University of Montenegro.

At the front page there is a detail from the first known text in astronomy-mathematics that appeared in Montenegro. It was published in the book Psaltir in 1495. Psaltir was printed on September 22, 1495 in the printing shop of Djurdje Crnojević which was the first printing shop of South Slavs. In the book six, volume 23, Djurdje Crnojević, the sovereign of Montenegro, adapted the Tables of Jovan Damaskin and wrote the Paschalia with lunar calendar. He worked out a series of rules regarding the counting of days of Easter celebrations. Djurdje's Paschalia Tables can be found in numerous written and printed books of later period.

ДРУШТВО МАТЕМАТИЧАРА И ФИЗИЧАРА ЦРНЕ ГОРЕ
ПРИРОДНО-МАТЕМАТИЧКИ ФАКУЛТЕТ
УНИВЕРЗИТЕТА ЦРНЕ ГОРЕ

МАТЕМАТИКА ЦРНЕ ГОРЕ

КЊИГА XXXI

MATHEMATICA MONTISNIGRI

VOLUME XXXI

UDK 51 ISSN 0354 2238

ПОДГОРИЦА, 2014.

MATHEMATICA MONTISNIGRI
Vol XXXI (2014) 5-97

CONTENTS

Mathematics

Romeo Mestrovic and Zarko Pavicevic. A topological property of Privalov spaces on the unit disk…….…….. 5

Dušan S. Jokanović and Marina M. Zirojević. Automorphism groups of some classes of graphs ……..…… 16

Nikola Mihaljevich. Representation characteristic function of Sturm-Liuville type over the zeros …….……. 25

Radoslav Milošević. A logical Burbakies model program formalization of mathematics 38

Mathematical modeling

M. Zhukovskiy, M. Markov, S. Podolyako and R. Uskov. Hybrid parallelization of computing the electron fluxes produced by photon radiation ……. 43

A.E. Bondarev, E.A. Nesterenko. Approximate method for estimation of friction forces for axisymmetric bodies in viscous flows ……. 54

V.I. Mazhukin, A.V. Shapranov, O.N. Koroleva, A.V. Rudenko. Molecular dynamics simulation of critical point parameters for silicon …… 64

I.N. Zavestovskaya, A.P. Kanavin. Modeling of the laser metal nanoparticles fragmentation ……..…..... 78

MATHEMATICA MONTISNIGRI
Vol XXXI (2014)

A TOPOLOGICAL PROPERTY OF PRIVALOV SPACES ON THE UNIT DISK

ROMEO MEŠTROVIĆ* AND ŽARKO PAVIĆEVIĆ**

* Maritime Faculty
University of Montenegro
85330 Kotor, Montenegro
e-mail: romeo@ac.me

** Faculty of Science
University of Montenegro
81000 Podgorica, Montenegro
e-mail: zarkop@ac.me

Abstract. For $1 < p < \infty$, the Privalov class N^p consists of all holomorphic functions f on the open unit disk $\mathbb{D}$ of the complex plane $\mathbb{C}$ such that

$$\sup_{0\le r<1} \int_0^{2\pi} (\log^+ |f(re^{i\theta})|)^p \, \frac{d\theta}{2\pi} < +\infty.$$

M. Stoll [19] showed that the space N^p with the topology given by the metric d_p defined as

$$d_p(f,g) = \Big(\int_0^{2\pi} \big(\log(1 + |f^*(e^{i\theta}) - g^*(e^{i\theta})|) \big)^p \, \frac{d\theta}{2\pi} \Big)^{1/p}, \quad f, g \in N^p,$$

becomes an F-algebra, that is, an F-space (a complete metrizable topological vector space with the invariant metric) in which multiplication is continuous. In this paper we prove that for any $1 < p < \infty$ the space N^p is not locally bounded with respect to the topology induced by the metric d_p. The proof of this result is based on a characterization of multipliers from the spaces N^p $(1 < p < \infty)$ to the Hardy spaces $H^q (0 < q \le \infty)$.

1 INTRODUCTION AND THE MAIN RESULT

Let $\mathbb{D}$ denote the open unit disk in the complex plane and let $\mathbb{T}$ denote the boundary of $\mathbb{D}$. Let $L^p(\mathbb{T})$ $(0 < p \le \infty)$ be the familiar Lebesgue spaces on the unit circle $\mathbb{T}$. The

2010 Mathematics Subject Classification: 46E10, 30H10, 30H15, 30H50, 46J15.
Keywords and Phrases: Privalov class (space), Hardy space, F-algebra, multiplier, locally bounded topological vector space.

Privalov class N^p $(1 < p < \infty)$ consists of all holomorphic functions f on $\mathbb{D}$ for which

$$\sup_{0<r<1} \int_0^{2\pi} (\log^+ |f(re^{i\theta})|)^p \, \frac{d\theta}{2\pi} < +\infty,$$

where $\log^+ a = \max\{\log a, 0\}$ for $a > 0$ and $\log^+ 0 = 0$. These classes were first introduced by I.I. Privalov [17, p. 93], where N^p is denoted as A_q.

Notice that the above condition with $p = 1$ defines the *Nevanlinna class* N of holomorphic functions in $\mathbb{D}$ (see, e.g., [3]). Furthermore, the *Smirnov class* N^+ is the set of all functions f holomorphic on $\mathbb{D}$ such that

$$\lim_{r\to 1} \int_0^{2\pi} \log^+ |f(re^{i\theta})| \, \frac{d\theta}{2\pi} = \int_0^{2\pi} \log^+ |f^*(e^{i\theta})| \, \frac{d\theta}{2\pi} < +\infty,$$

where f^* is the boundary function of f on T, i.e.,

$$f^*(e^{i\theta}) = \lim_{r\to 1} f(re^{i\theta})$$

is the radial limit of f which exists for almost every $e^{i\theta}$.

Recall that we denote by H^q $(0 < q \le \infty)$ the classical *Hardy space* on $\mathbb{D}$, defined as the set of all holomorphic functions f on $\mathbb{D}$ for which

$$\|f\|_q^{\max\{1,q\}} := \sup_{0<r<1} \int_0^{2\pi} |f(re^{i\theta})|^q \, \frac{d\theta}{2\pi} < +\infty.$$

Further, H^∞ is the *space of all bounded holomorphic functions* on $\mathbb{D}$ with the supremum norm $\|\cdot\|_\infty$ defined as

$$\|f\|_\infty = \sup_{z\in\mathbb{D}} |f(z)|, \quad f \in H^\infty.$$

We refer [3] for a good reference on the spaces H^q and N^+.

It is known (see [16]) that

$$N^q \subset N^p \ (q > p), \quad \cup_{p>0} H^p \subset \cap_{p>1} N^p, \quad \text{and} \quad \cup_{p>1} N^p \subset N^+,$$

where the above containment relations are proper.

The study of the spaces N^p $(1 < p < \infty)$ was continued in 1977 by M. Stoll [19] (with the notation $(\log^+ H)^\alpha$ in [19]). Further, the topological and functional properties of these spaces were studied by C.M. Eoff ([4] and [5]), N. Mochizuki [16], Y. Iida and N. Mochizuki [6], Y. Matsugu [7], J.S. Choa [1], J.S. Choa and H.O. Kim [2], A.K. Sharma and S.-I. Ueki [18], and in works [8]–[15] of authors of this paper; typically, the notation varied and Privalov was mentioned in [7], [13], [14], [15] and [18]. For example, it is proved in [9, Theorem] that the space N^p $(1 < p < \infty)$ does not have the Hahn-Banach approximation property, and hence it does not have the Hahn-Banach separation property. Furthermore, the spaces N^p are not locally convex [9, Corollary].

In particular, the functional, topological and algebraic properties of the spaces N^p and their Fréchet envelopes were recently investigated in [10], [13] and [15].

Stoll [19, Theorem 4.2] showed that the space N^p (with the notation $(\log^+ H)^\alpha$ in [19]) with the topology given by the metric d_p defined by

$$d_p(f,g) = \Big(\int_0^{2\pi} \big(\log(1 + |f^*(e^{i\theta}) - g^*(e^{i\theta})|) \big)^p \, \frac{d\theta}{2\pi} \Big)^{1/p}, \quad f, g \in N^p, \tag{1}$$

becomes an F-algebra, that is, a topological vector space whose topology is given by a complete, translation invariant metric in which multiplication is continuous.

It was also investigated in [19] the containing Fréchet space $F_{1/p}$ for N^p with $p > 1$. It is proved in [19, Corollary 4.4] that the restriction of every continuous linear functional on $F_{1/p}$ to N^p forms a continuous linear functional on N^p. It is remained an open question whether the spaces N^p and $F_{1/p}$ have the same dual spaces, in the sense that every continuous linear functional on N^p is a restriction to one on $F_{1/p}$. In 1999 R. Meštrović and A.V. Subbotin [14, Theorem 2] gave a positive answer to this question. In order to prove a complete characterization of a *topological dual space* of N^p (the set of all linear functionals that are continuous with respect to the metric topology d_p) it was used a description of multipliers from the spaces N^p to the Hardy spaces H^q $(0 < q \leq \infty)$ established in [14, Theorem 1].

Let $p > 1$ and $0 < q \leq \infty$ be arbitrary fixed. A sequence $\{\lambda_n\}_{n=0}^\infty := \{\lambda_n\}$ of complex numbers is said to be a *multiplier* from the space N^p to the Hardy space H^q if for each function $f \in N^p$ with the Taylor expansion $f(z) = \sum_{n=0}^\infty a_n z^n$, the function g defined on $\mathbb{D}$ as $g(z) = \sum_{n=0}^\infty \lambda_n a_n z^n$ belongs to H^q. According to this definition, every multiplier $\{\lambda_n\}$ from N^p to H^q can be considered as an induced linear operator Λ from N^p to H^q defined as

$$\Lambda : \sum_{n=0}^\infty a_n z^n \longmapsto \sum_{n=0}^\infty \lambda_n a_n z^n. \tag{2}$$

Theorem A ([14, Theorem 1]; also see [8, Chapter 2, Section 2.2, Theorem 2.3]). *Suppose $\{\lambda_n\}$ is a multiplier from N^p to the Hardy space H^q $(0 < q \leq \infty)$. Then the linear operator Λ defined from N^p to H^q by (2) is continuous. Thus, Λ maps bounded subsets of N^p into bounded subsets of H^q.*

The characterization of multipliers from the spaces N^p to the spaces H^q given in [14] can be reformulated as follows.

Theorem B ([14, Theorem 1]). *Let $0 < q \leq \infty$ and $1 < p < \infty$. In order that a sequence $\{\lambda_k\}$ of complex numbers to be a multiplier from N^p into H^q, it is necessary and sufficient that*

$$\lambda_k = O\left(\exp(-ck^{1/(p+1)})\right) \tag{3}$$

for some positive constant c.

Remark. Note that the assumption of Theorem B contains q, but this is not the case for the growth estimate (3).

Notice that the proof of Theorem A given in [14] is based on Lemmas 1–3 from [14] by using Yanagigara's technique applied in [20] for characterizing multipliers from N^+ to the Hardy spaces H^q.

Recall that a subset L of a topological vector space X is *bounded* if for every neighborhood V of zero there is a $\alpha_0 > 0$ such that $\alpha L \subset V$ for all $\alpha \in \mathbb{C}$ such that $|\alpha| \leq \alpha_0$. Furthermore, a topological vector space X is *locally bounded* if it does not contain none base of neighborhood of zero consisting only bounded sets. Theorems A and B are used here to prove the following result (see [8, Chapter 2, Section 2.3, Corollary 3.1]).

Theorem 1.1. *The space N^p is not locally bounded. This means that none ball $B(c) = \{f \in N^p : d_p(f,0) < c\}$ is not bounded subset of N^p.*

2 PROOF OF THEOREM 1.1

Proof of Theorem 1.1 is based on the following six lemmas.

Lemma 2.1. *If a sequence of functions in N^p converges with respect to the metric d_p, then this sequence converges uniformly on each compact subset of the unit disk $\mathbb{D}$.*

Proof. The assertion immediately follows from the inequality (2) in [16] given for $f \in N^p$ by

$$\log(1 + |f(z)|) \leq 2^{1/p} d_p(f,0)(1 - |z|)^{-1/p} \quad (z \in \mathbb{D}).$$

□

Lemma 2.2. ([3, Theorem 6.4, p. 98]). *Suppose*

$$f(z) = \sum_{n=0}^{\infty} a_n z^n \in H^q, \quad 0 < q \leq 1.$$

Then

$$a_n = o(n^{1/q-1}), \tag{4}$$

as well as

$$|a_n| \leq C n^{1/q-1} \|f\|_q. \tag{5}$$

Lemma 2.3. *Suppose $\{\lambda_n\}$ is a multiplier from N^p to the Hardy space H^q $(0 < q \leq \infty)$. Then the linear operator Λ defined from N^p to H^q by (2) is continuous. Thus, Λ maps bounded subsets of N^p into bounded subsets of H^q.*

Proof. According to Lemma 2.1, if a sequence $\{f_n\}$ in N^p converges to some fubction $f \in N^p$ in N^p, then $\{f_n(z)\}$ converges uniformly to $f(z)$ on each compact subset $|z| \leq r < 1$. Hence, if $f_n(z) = \sum_{k=0}^{\infty} a_k^{(n)} z^k$ and $f(z) = \sum_{k=0}^{\infty} a_k z^k$, then

$$a_k^{(n)} \to a_k \ \ (k = 0, 1, \ldots), \ \text{ if } \ f_n \to f \ \text{ in } \ N^p \ \text{ as } \ n \to \infty. \tag{6}$$

Let $g_n(z) = \sum\limits_{k=0}^{\infty} b_k^{(n)} z^k$ be a sequence in H^q and let $g(z) = \sum\limits_{k=0}^{\infty} b_k z^k$ be a function in H^q such that $g_n \to g$ in H^q as $n \to \infty$. By [2, the inequality (9) in Theorem 6.4], we see that

$b_k^{(n)} \to b_k$ $(k = 0, 1, \ldots)$ as $n \to \infty$. This together with (6) immediately yields that Λ is a closed operator. Hence, by the Closed Graph Theorem, Λ is a continuous operator, and so Λ maps bounded subsets of N^p onto bounded subsets of H^q. □

Lemma 2.4. ([20, Lemma 2 and Remark 3]). *Let*

$$\exp\left(\frac{c}{2} \cdot \frac{1+z}{1-z}\right) = \sum_{n=0}^{\infty} a_n(c) z^n, \quad 0 < c \leq 1.$$

Then

$$\log |a_n(c)| \geq \sqrt{cn} + O(\log n) + O(\log c)$$

In particular, if $\{c_k^*\}$ is a sequence of positive numbers such that

$$\frac{1}{k^{1/(p+1)}} \leq c_k^* \leq 1,$$

then

$$\log |a_k(c_k^*)| \geq \sqrt{c_k^* k}(1 + o(1)). \tag{7}$$

Lemma 2.5. *Let $\{c_k\}$ and $\{r_k\}$ be sequences of positive numbers such that $c_k \downarrow 0$ and $r_k \uparrow 1$ as $k \to \infty$ and $r_k \geq 1/2$, $k = 1, 2, \ldots$. Define*

$$f_k(z) = \exp\left(c_k (1 - r_k)^{1-1/p} \frac{1 + r_k z}{1 - r_k z}\right), \quad z \in \mathbb{D},\ k = 1, 2, \ldots.$$

Then a sequence of functions $\{f_k\}$ $(k = 1, 2, \ldots)$, is a bounded subset of N^p.

Proof. Let $\{\varepsilon_k\}$ and $\{\delta_k\}$ be sequences of positive numbers such that $\varepsilon_k \downarrow 0$, $\delta_k \downarrow 0$ as $k \to \infty$ and

$$\frac{1 - r_k^2}{1 + r_k^2 - 2r\cos\theta} \leq 1 \quad \text{for} \quad |\theta| \geq \varepsilon_k \quad \text{and} \quad r \geq r_k, \quad \text{for all} \quad k = 1, 2, \ldots. \tag{8}$$

For given neighborhood

$$V = \{g \in N^p : d_p(g, 0) < \eta\}$$

of zero in N^p, choose $m \in \mathbb{N}$ for which

$$\log^p(1 + \delta_m) + 2^p \pi^{-1} \varepsilon_m \log^p 2 + 2^{p-1} C c_m^p < \eta^p, \tag{9}$$

where C is a positive constant also satisfying (11). Next assume α_0, $0 < \alpha_0 < 1$, such that

$$\alpha_0 \exp\frac{1 + r_m}{1 - r_m} \leq \delta_m, \quad \text{and thus} \quad \alpha_0 e \leq \delta_m. \tag{10}$$

Then for all $k \in \mathbb{N}$ with $k \leq m$ holds

$$|\alpha_0 f_k^*(e^{i\theta})| \leq \alpha_0 \exp\frac{1 + r_k}{1 - r_k} \leq \delta_m,$$

whence by (10) and (9), for $0 < \alpha \leq \alpha_0$ and $k \leq m$ we obtain

$$d_p(\alpha f_k, 0) \leq \log(1 + \delta_m) < \eta.$$

Therefore, $\alpha f_k \in V$ for all $k \le m$ and $0 < \alpha \le \alpha_0$. By the inequality $\sin x \ge (2/\pi)x$ for $0 \le x \le \pi/2$, we have

$$\begin{aligned} 1 - 2r\cos\theta + r^2 &= (1-r)^2 + 4r\sin^2\frac{\theta}{2} \\ &\ge (1-r)^2 + (4r/\pi^2)\theta^2. \end{aligned}$$

Hence, for $r_k \ge 1/2$ we obtain

$$\begin{aligned} &\int\limits_{|\theta|<\varepsilon_k} \left(\log^+ |f_k^*(e^{i\theta})|\right)^p \frac{d\theta}{2\pi} \\ &= c_k^p (1-r_k)^{p-1} \int\limits_{|\theta|<\varepsilon_k} \left(\frac{1-r_k^2}{1+r_k^2-2r_k\cos\theta}\right)^p \frac{d\theta}{2\pi} \\ &< 2^p \pi^{-1} c_k^p \int\limits_0^\infty \frac{dt}{(1+2\pi^{-2}t^2)^p} \qquad \left(t = \frac{\theta}{1-r_k}\right) \qquad (11) \\ &= C c_k^p, \end{aligned}$$

where the constant C does not depend on k. Now from (8), (9), (11) and the inequality $\log^p(1+|x|) \le 2^{p-1}\left((\log 2)^p + (\log^+|x|)^p\right)$, we find that for all $k > m$ and $0 < \alpha \le \alpha_0$

$$\begin{aligned} \left(d_p(\alpha f_k, 0)\right)^p &= \int\limits_0^{2\pi} \log^p\left(1 + |\alpha f_k^*(e^{i\theta})|\right) \frac{d\theta}{2\pi} \\ &= \int\limits_{|\theta|\ge\varepsilon_k} + \int\limits_{|\theta|<\varepsilon_k} \\ &\le \log^p(1+\alpha e) + 2^{p-1} \int\limits_{|\theta|<\varepsilon_k} \left(\log^p 2 + \left(\log^+|f_k^*(e^{i\theta})|\right)^p\right) \frac{d\theta}{2\pi} \\ &\le \log^p(1+\delta_m) + 2^p\pi^{-1}\varepsilon_m \log^p 2 + 2^{p-1} C c_m^p \\ &< \eta^p. \end{aligned}$$

Therefore, $\{\alpha f_k\} \subset V$ for every $0 < \alpha < \alpha_0$. This shows that the sequence $\{f_k\}$ forms a bounded set in N^p. □

Remark. Similarly, we can prove the converse of Lemma 2.5, i.e., if a sequence $\{f_k\}$ is a bounded subset of N^p and $r_k \uparrow 1$ as $k \to \infty$ and $c_k > 0$, then $c_k \to 0$ as $k \to \infty$.

Lemma 2.6. *Let $0 < q \le \infty$ and $1 < p < \infty$. Let $\{c_k\}$ and $\{r_k\}$ be sequences of positive numbers such that $c_k \downarrow 0$ and $r_k \uparrow 1$ as $k \to \infty$ and $r_k \ge 1/2$ fo all $k = 1, 2, \ldots$. Let $\{f_k\}$*

be a sequence of functions defined as

$$\begin{aligned} f_k(z) &= \exp\left(c_k(1-r_k)^{1-1/p}\frac{1+r_kz}{1-r_kz}\right) \\ &= \sum_{n=0}^{\infty} a_n^{(k)} r_k^n z^n, \quad k=1,2,\dots. \end{aligned}$$

Suppose that $\{\lambda_k\}$ is a multiplier from N^p into H^q, and let Λ be a linear operator from N^p to H^q defined by (2). If a sequence $\{\Lambda(f_k)\}$ is a bounded set in H^q by a constant L, then for all $n=1,2,\dots$

$$|\lambda_n a_n^{(k)}| r_k^n \le \begin{cases} C_q L n^{-1+1/q} & \text{for } 0<q<1, \\ C_q L & \text{for } 1\le q\le\infty, \end{cases} \tag{12}$$

where C_q is a positive constant depending only on q.

Proof. Under conditions on sequences $\{c_k\}$ and $\{r_k\}$ from Lemma 2.6, it follows by Lemma 2.5 that the sequence of functions $\{f_k\}$ defined as

$$\begin{aligned} f_k(z) &= \exp\left(c_k(1-r_k)^{1-1/p}\frac{1+r_kz}{1-r_kz}\right) \\ &= \sum_{n=0}^{\infty} a_n^{(k)} r_k^n z^n, \quad k=1,2,\dots. \end{aligned}$$

forms a bounded subset of N^p. Since by Lemma 2.3, the operator Λ is continuous, we conclude that the sequence $\{\Lambda(f_k)\}$ must be a bounded set in H^q. Assume that the sequence $\{\Lambda(f_k)\}$ is a bounded set in the space H^q by a constant L. As

$$\Lambda(f_k) = \sum_{n=0}^{\infty} \lambda_n a_n^{(k)} r_k^n z^n,$$

from Lemma 2.2 and ([3, Theorem 6.1, p. 94]), for all $n=0,1,2\dots$ we obtain

$$|\lambda_n a_n^{(k)}| r_k^n \le \begin{cases} C_q L n^{-1+1/q} & \text{for } 0<q<1, \\ C_q L & \text{for } 1\le q\le\infty, \end{cases}$$

where C_q is a positive constant depending only on q. The above inequality is in fact the desired inequality (12). □

We are now ready to prove Theorem 1.1.

Proof of Theorem 1.1. From the proof of the inequality (11) of Lemma 2.5 it follows that there is a positive constant b depending only on p, such that for the Poisson kernel $P_r(\theta,t) = (1-r^2)/(1+r^2-2r\cos(\theta-t))$ holds

$$\int_0^{2\pi} (P_r(\theta,t))^p \, \frac{d\theta}{2\pi} \le \frac{b}{(1-r)^{p-1}}\,. \tag{13}$$

Suppose that a ball $B(c)$ with radius c is bounded in N^p. Then choose numbers $\varepsilon > 0$, $\delta > 0$ and $a > 0$ such that

$$0 < \varepsilon^p + 2^{p-1}(\log 2)^p \varepsilon \pi^{-1}(1 + 2^{p-1}) + 4^{p-1}a^{2p}b < c^p, \tag{14}$$

$$|e^{\xi} - 1| < \varepsilon \quad \text{whenever} \quad |\xi| < \delta, \tag{15}$$

and

$$\frac{2a^2}{\sin \varepsilon} < \delta. \tag{16}$$

Define the function f_r on $\mathbb{D}$ as

$$f_r(z) = \exp\left(a^2(1-r)^{\frac{p-1}{p}} \frac{1+rz}{1-rz}\right) - 1 \quad \text{for each} \quad 0 < r < 1. \tag{17}$$

It is obvious that each function f_r with $0 < r < 1$ is a bounded holomorphic function on $\mathbb{D}$, and hence f_r belongs to N^p. Moreover, if $z = \rho e^{i\theta}$ for $|\theta| \geq \varepsilon$, then $|1 - rz| \geq \sin|\theta| \geq \sin \varepsilon$. From this together with (15) we obtain

$$a^2(1-r)^{\frac{p-1}{p}} \left|\frac{1+rz}{1-rz}\right| < \frac{2a^2}{|1-rz|} \leq \frac{2a^2}{\sin \varepsilon} < \delta. \tag{18}$$

Using the inequality $(\log^+|x-1|)^p \leq 2^{p-1}((\log^+|x|)^p + (\log 2)^p)$ and the fact that

$$\begin{aligned} \operatorname{Re}\left(\frac{1+re^{i\theta}}{1-re^{i\theta}}\right) &= \frac{1-r^2}{1-2r\cos\theta + r^2} \\ &= P_r(\theta, 0), \end{aligned}$$

we find that

$$(\log^+|f_r(e^{i\theta})|)^p \leq 2^{p-1}\left(a^{2p}(1-r)^{p-1}\left(P_r(\theta,0)\right)^p + (\log 2)^p\right). \tag{19}$$

Further, by (13)–(19) and the inequality

$$\log^p(1+|x|) \leq 2^{p-1}\left((\log 2)^p + (\log^+|x|)^p\right),$$

we obtain

$$\begin{aligned}
(d_p(f_r,0))^p &= \int_0^{2\pi} \log^p\left(1+|f_r(e^{i\theta})\right)\,\frac{d\theta}{2\pi} \\
&= \int_{|\theta|\geq\varepsilon} + \int_{|\theta|<\varepsilon} \\
&< \log^p(1+\varepsilon) \\
&\quad +2^{p-1}\times\left(\int_{|\theta|<\varepsilon}(\log 2)^p\,\frac{d\theta}{2\pi}+\int_{|\theta|<\varepsilon}(\log^+|f_r(e^{i\theta})|)^p\,\frac{d\theta}{2\pi}\right) \\
&\leq \varepsilon^p + 2^{p-1}(\log 2)^p\varepsilon\pi^{-1}+2^{p-1}2^{p-1} \\
&\quad \times\left(a^{2p}(1-r)^{p-1}\int_{|\theta|<\varepsilon}(P_r(\theta,0))^p\,\frac{d\theta}{2\pi}+\int_{|\theta|<\varepsilon}(\log 2)^p\,\frac{d\theta}{2\pi}\right) \\
&\leq \varepsilon^p + 2^{p-1}(\log 2)^p\varepsilon\pi^{-1}(1+2^{p-1})+4^{p-1}a^{2p}b<c^p.
\end{aligned}$$

From the above inequality we see that $\{f_r : 0\leq r<1\}\subset B(c)$. Therefore, the assumption that the ball $B(c)$ is bounded in N^p, by Lemma 2.3, it follows that every multiplier $\Lambda=\{\lambda_n\}$ maps the set $\{f_r : 0\leq r<1\}$ to some bounded subset of H^∞. Hence, if $f_r(z)=\sum_{n=0}^\infty a_n r^n z^n$, $z\in\mathbb{D}$, then the estimate (12) yields

$$|\lambda_n a_n r^n|\leq L=L(\Lambda) \tag{20}$$

for each r with $0\leq r<1$, where L is a positive constant depending on Λ. Using the notations from Lemma 2.4, by this lemma we have

$$|a_n|=a_n\left(2a^2(1-r)^{\frac{p-1}{p}}\right)\geq\exp\left(a(1-r)^{\frac{p-1}{2p}}\sqrt{2n}\,(1+o(1))\right) \tag{21}$$

for a constant a satisfying the conditions (13)–(15). Therefore, (20) and (21) immediately imply that

$$|\lambda_n|\leq Lr^{-n}\exp\left(-a(1-r)^{\frac{p-1}{2p}}\sqrt{2n}(1+o(1))\right)\quad\text{for each}\quad 0\leq r<1.$$

By setting $r = 1 - a^2/n^{\frac{p}{p+1}}$, from the previous inequality we obtain

$$\begin{aligned}
|\lambda_n| &\leq L\left(1-\frac{a^2}{n^{\frac{p}{p+1}}}\right)^{-n}\exp\left(-a\frac{a\sqrt{2}}{n^{\frac{p-1}{2(p+1)}}}\sqrt{n}(1+o(1))\right)\\
&\leq L\left(\left(1-\frac{a^2}{n^{\frac{p}{p+1}}}\right)^{-\frac{n^{\frac{p}{p+1}}}{a^2}}\right)^{a^2n^{\frac{1}{p+1}}}\exp\left(-a^2\sqrt{2}n^{\frac{1}{p+1}}\right)\\
&\leq L\exp\left(a^2n^{\frac{1}{p+1}(1+o(1))}\right)\exp\left(-a^2\sqrt{2}n^{\frac{1}{p+1}}\right)\\
&= L\exp\left(-a^2(\sqrt{2}-1)n^{\frac{1}{p+1}}(1+o(1))\right)\\
&< L\exp\left(-0.3a^2n^{\frac{1}{p+1}}\right).
\end{aligned}$$

This shows that every multiplier $\Lambda = \{\lambda_n\}$ from N^p into H^q satisfies the condition

$$\lambda_n = O\left(\exp\left(-0.3a^2n^{\frac{1}{p+1}}\right)\right). \tag{22}$$

On the other hand, the sequence $\Lambda^* = \{\lambda_n^*\}$ defined as $\lambda_n^* = \exp\left(-0.2a^2n^{\frac{1}{p+1}}\right)$ $(n = 0, 1, 2, \ldots)$ is by Theorem B, also a multiplier from N^p into H^q. This contradicts (22), and the proof of Theorem 1.1 is now complete. □

References

[1] J.S. Choa, Composition operators between Nevanlinna-type spaces, *J. Math. Anal. Appl.* **257**, 378–402 (2001).

[2] J.S. Choa and H.O. Kim, Composition operators on some F-algebras of holomorphic functions, *Nihonkai Math. J.* **7**, 29–39 (1996).

[3] P. L. Duren, *Theory of H^p spaces*, Academic Press, New York, (1970).

[4] C.M. Eoff, Fréchet envelopes of certain algebras of analytic functions, *Michigan Math. J.* **35**, 413–426 (1988).

[5] C.M. Eoff, A representation of N_α^+ as a union of weighted Hardy spaces, *Complex Var. Theory Appl.* **23**, 189–199 (1993).

[6] Y. Iida and N. Mochizuki, Isometries of some F-algebras of holomorphic functions, *Arch. Math. (Basel)* **71**, 297–300 (1998).

[7] Y. Matsugu, Invariant subspaces of the Privalov spaces, *Far East J. Math. Sci.* **2**, 633-643 (2000).

[8] R. Meštrović, *Topological and F-algebras of holomorphic functions*, Ph.D. Thesis, University of Montenegro, Podgorica, (1999).

[9] R. Meštrović, The failure of the Hahn Banach properties in Privalov spaces of holomorphic functions, *Math. Montisnigri* **17**, 27–36 (2004).

[10] R. Meštrović, F-algebras M^p $(1 < p < \infty)$ of holomorphic functions, *The Scientific World Journal* (*subject area: Mathematical Analysis*) Vol. **2014**, Article ID 901726, 10 pages (2014).

[11] R. Meštrović and Ž. Pavićević, Remarks on some classes of holomorphic functions, *Math. Montisnigri* **6**, 27–37 (1996).

[12] R. Meštrović and Ž. Pavićević, Topologies on some subclasses of the Smirnov class, *Acta Sci. Math. (Szeged)* **69**, 99–108 (2003).

[13] R. Meštrović and Ž. Pavićević, Weakly dense ideals in Privalov spaces of holomorphic functions, *J. Korean Math. Soc.* **48**, 397-420 (2011).

[14] R. Meštrović and A.V. Subbotin, Multipliers and linear functionals in Privalov's spaces of holomorphic functions on the disk, *Dokl. Akad. Nauk* **365**, no. 4,, 452–454 (1999) (in Russian).
[15] R. Meštrović and J. Šušić, Interpolation in the spaces N^p $(1 < p < \infty)$, *Filomat* **27**, 293-301 (2013).
[16] N. Mochizuki, Algebras of holomorphic functions between H^p and N_*, *Proc. Amer. Math. Soc.* **105**, 898–902 (1989).
[17] I.I. Privalov, *Boundary properties of singled-valued analytic functions*, Izdat. Moskov. Univ., Moscow, (1941) (in Russian).
[18] A.K. Sharma and S.-I. Ueki, Composition operators from Nevanlinna type spaces to Bloch type spaces, *Banach J. Math. Anal.* **6**, 112–123 (2012).
[19] M. Stoll, Mean growth and Taylor coefficients of some topological algebras of analytic functions, *Ann. Polon. Math.* **35**, 139–158 (1977).
[20] N. Yanagihara, Multipliers and linear functionals for the class N^+, *Trans. Amer. Math. Soc.* **180**, 449–461 (1973).

Received December 6, 2012

MATHEMATICA MONTISNIGRI
Vol XXXI (2014)

AUTOMORPHISM GROUPS OF SOME CLASSES OF GRAPHS

DUŠAN S. JOKANOVIĆ[*] AND MARINA M. ZIROJEVIĆ[†]

[*]University of East Sarajevo
Production and Management Faculty Trebinje
Stepe Stepanovića bb, 89 101 Trebinje, Republic of Srpska, BiH
e-mail: dusanjok@yahoo.com, web page: http://www.fpmtrebinje.com

[†]University of East Sarajevo
Production and Management Faculty Trebinje
Stepe Stepanovića bb, 89 101 Trebinje, Republic of Srpska, BiH
e-mail: marina.zirojevic@live.com, web page: http://www.fpmtrebinje.com

Summary. There is a natural connection between the fields of algebra and graph theory. Both provide interesting ways of studing relationships among elements of a given set. An algebraic approach to graph theory can be useful in numerous ways. These arise from two algebraic objects associated with a graph: its adjacency matrix and its automorphism group. In this paper we investigate automorphism groups of common graphs and introduce a celebrated theorem of Sabidussi. Beside, by finding a graph of a given group, we can define an extremely important family of vertex-transitive graphs. The paper discusses algebraic aspects of Cayley graphs and its group of automorphism. We also give a short presentation of tools which are developed in "Wolfram Mathematica 10.0." to represent finite groups, to perform various group operations.

1 INTRODUCTION

The automorphism group of graph can be naturally defined as a group of permutations of its vertices, and so presents some basic information about permutation group.

A permutation of a set Ω is a bijective mapping $\pi:\Omega\to\Omega$. The composition $\pi_1\pi_2$ of two permutation π_1 and π_2 is the permutation obtained by applying π_1 and then π_2, thus is:

$$v(\pi_1\pi_2)=(v\pi_1)\pi_2 \text{ for each } v\in\Omega. \tag{1}$$

A permutation group on Ω is a set S of permutations of Ω satisfying the following conditions:

- S is closed under composition: if $\pi_1,\pi_2\in S$ than $\pi_1\pi_2\in S$;
- S contains the identity permautation 1 defined by $v1=v$ for $v\in\Omega$.
- S is closed under inversion, where the inverse of π is the permutation π^{-1} defined by the rule that $v\pi^{-1}=w$ if $w\pi=v$.

In this paper $\mathrm{Sym}(\Omega)$ denotes the set of all permutations of Ω, S_n denotes the symmetric group $\mathrm{Sym}(\{1,2,\ldots,n\})$.

Let S be a permutation group on Ω. The relation $\sim$ on Ω, defined by

$$v\sim w \text{ if } w=v\pi \text{ for some } \pi\in S, \tag{2}$$

2010 Mathematics Subject Classification: 11H56, 18A10, 68R10.
Key words and Phrases: Automorphism groups of graphs, Cayley graphs.

is an equivalence relation, and its equivalence classes are the orbits of S. S is transitive if it has just one orbit, thus, S is transitive if, for any $v, w \in \Omega$ there exists $\pi \in \Omega$ such that $v\pi = w$.

The stabilizer S_v of a point $v \in \Omega$ is the set

$$H = \{\pi \in S : v\pi = v\}; \tag{3}$$

it is a subgroup of S. Moreover, if w is a point in the same orbit as v, then the set

$$\{\pi \in S : v\pi = w\} \tag{4}$$

is a right coset of H in S.

2 AUTOMORPHISMS OF TYPICAL GRAPHS

Let $\Gamma := (V, E)$ be a simple, undirected graph. An automorphism of a graph is a permutation of the vertex set that preserves adjacency. The set of all automorphisms of a graph Γ, with the operation of composition of permutations, is a permutation group on vertex set that preserve adjacency. This is the automorphism group of graph Γ denoted by

$$A(\Gamma) := \{\pi \in Sym(V) : \pi(E) = E\}. \tag{5}$$

The automorphism group is an algebraic invariant of a graph. Here are some simple properties (see [1]).

Theorem 1.

(a) A graph and its complement have the same automorphism group.

(b) The automorphism group of *n* disjoint copies of graph Γ is $A(n\Gamma) = S_n[A(\Gamma)]$.

(c) $A(K_n) = S_n$.

Every graph has the trivial automorphism $id : V \to V$ defined by $id(v) = v$. Most graphs have no other automorphisms than, but many interesting graphs have many automorphisms. Erdös and Rényi [3] showed:

Theorem 2. Almost all graphs have no non-trivial automorphisms.

The smallest graph, apart from the one-vertex graph, whose automorphism group is trivial is shown in Figure 1.

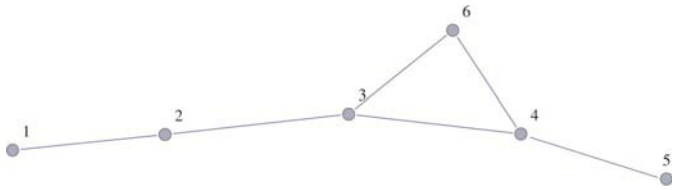

Figure 1: A graph Γ for which $|A(\Gamma)| = 1$

Cyclic graph C_4 is the opposite case, because it has 8 automorphisms. In order to define the possible automorphisms α of C_4, we will define $Z_4 := \{1,2,3,4\}$. First, $\alpha(v_1) = v_i$ for

some $i \in Z_4$. Then $\alpha(v_2)$ has to be a neighbour of v_i, so it is either v_{i+1} or v_{i-1}. Now $\alpha(v_4)$ has to be the neighbour of v_i that isn't $\alpha(v_2)$, so it is v_{i-1} or v_{i+1}, whichever one is not $\alpha(v_2)$. Finally, v_{i+2} is the only remaining vertex not yet in the image of α, so it must be equal to $\alpha(v_2)$. We had 4 choices for i, and then we had to choose either $\mathrm{i}+1$ or $\mathrm{i}-1$, which is 2 further choices. That gives us $4 \times 2 = 8$ ways to choose an automorphism of C_4; thus $|\mathrm{A}(\mathrm{C}_4)| = 8$.

Example 1. Let Γ be the octahedron graph. The octahedron graph are shown on next Figure. The complement graph of the octahedron graph is $3\mathrm{K}_2$. We can easily calculate that $|\mathrm{A}(3\mathrm{K}_2)| = 2^3 3! = 48$ since there are 3! ways to permute edges and on each edge we can either switch vertices on that edge or leave them fixed what yields another 2^3 automorphisms. Because every automorphism preserves adjacency as well as non-adjacency, a graph and its complement have the same automorphism group, so we have $|\mathrm{A}(\Gamma)| = 2^3 3! = 48$.

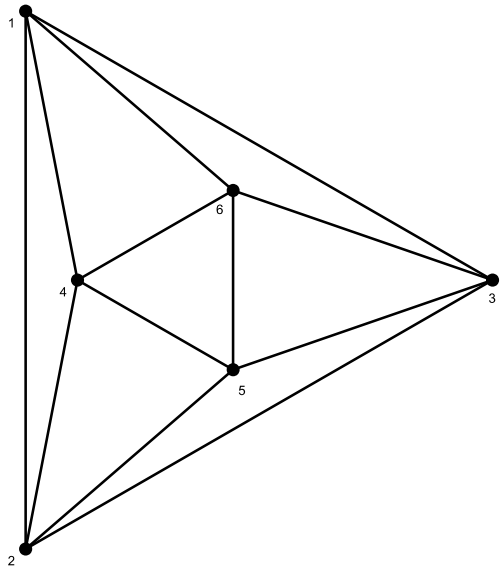

Figure 2: The Octahedron graph

Graph which has more automorphism than any other graph, relative to its size is Petersen graph P. Let $Z_5 = \{1,2,3,4,5\}$ and let $\mathrm{P}_2(Z_5)$ be the set of all unordered pairs of elements of Z_5. Then $\mathrm{V}(\mathrm{P}) = \{\mathrm{v}_{\mathrm{ij}} : \{\mathrm{i},\mathrm{j}\} \in \mathrm{P}_2(Z_5)\}$. The vertices v_{ji} and v_{ij} are the same vertex. Two vertices in P are adjacent if and only if their labels are disjoint sets, ie $\mathrm{E}(\mathrm{P}) = \{\mathrm{v}_{\mathrm{ij}}\mathrm{v}_{\mathrm{ji}} : \{\mathrm{i},\mathrm{j}\} \cap \{\mathrm{k},\mathrm{l}\} = \varnothing\}$. The Petersen graph with the 2-index vertex labelling are shown on the next Figure.

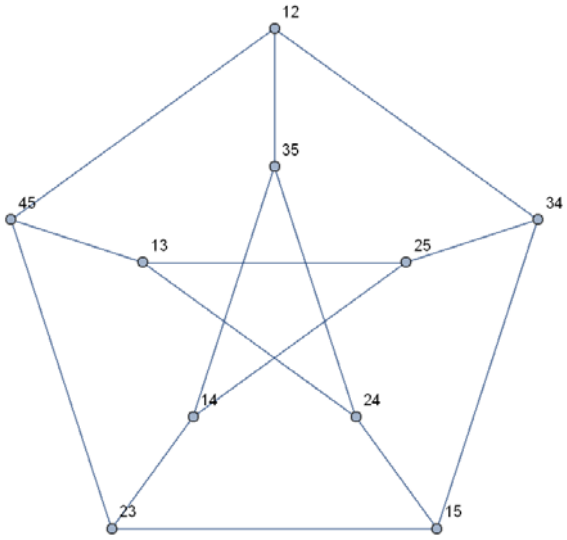

Figure 2: The Petersen graph

Any permutation of Z_5 gives an automorphism of P, and different permutations give different automorphisms. Because there are no other automorphisms of P we can say $\left|A(P)\right| = 120$.

Following results holds:

Theorem 3. The full automorphism group of the Petersen graph is isomorphic to S_5.

Proof: Let Γ be the Petersen graph. Every element $\pi \in S_5$ induces a permuatation $\hat{\pi}$ of Γ. Each of these permutations is an automorphism of Γ because for all $\pi \in S_5$, A, B are disjoint if and only if $\pi(A)$ and $\pi(B)$ are disjoint. Thus, the map $\phi : S_5 \mapsto V, \pi \mapsto \hat{\pi}$ is an injective group homomorphism into $A(\Gamma)$, and so $S_5 \cong \phi(S_5) \leq A(\Gamma)$.

If we want to show that there is no other automorphisms than $\phi(S_5)$ i.e. that $\phi(S_5)$ is a full automorphism group, it is sufficed to show that $A(\Gamma) \leq \phi(S_5)$. If π is any automorphism, then by composing with an appropriate permutation of {1,2,3,4,5} we may assume that the map fixes {1,2}; that means that the vertices adjacent to {1,2}, {3,4}, {3,5}, and {4,5}, must map to each other. To prove this, let $\pi \in A(\Gamma)$. We show that there exists $\hat{g} \in \phi(S_5)$ such that $\pi\hat{g} = 1$. This would imply that $\pi = \hat{g}^{-1} \in \phi(S_5)$.

Suppose $\pi : \{1,2\} \to \{a,b\}$. Let $g_1 \in S_5$ map $a \mapsto 1$, $b \mapsto 2$. Then $\pi\hat{g}_1$ fixes the vertex 12 and hence permutes its neighbors 34, 45 and 35. We consider a few cases:

1. Suppose $\pi\hat{g}_1$ fixes all three neighbors 34,45,35. So $\pi\hat{g}_1$ permutes the neighbors of 35, and hence fixes 14 and 24, or swaps 14 and 24.

1.1. If $\pi\hat{g}_1 : 14 \mapsto 14$, then 15 is sent to a vertex adjanced to 34 and not adjanced to 14, hence 15 is fixed. Similary, all the vertex are seen to be fixed, and so $\pi\hat{g}_1 = 1$, as was to be shown.

1.2. If $\pi\hat{g}_1 : 14 \mapsto 24$, then it swaps 14 and 24. 15 is sent to a neighbor of 24($\pi\hat{g}_1$)=14, and hence 15 is sent to 25. Thus, we see that $\pi\hat{g}_1$ swaps 14 and 24, 15 and 25, and also 13 and 23, and fixes the remaining vertices. But then $\pi\hat{g}_1 = \hat{g}_2$, where $g_2 = (1,2)$. So, $\pi \in \phi(S_5)$.

2. Suppose $\pi\hat{g}_1$ fixes exactly 2 of the 3 vertices 34, 45 and 35. But this case is not possible, because if it fixes 2 of the 3 vertices, it must also fix the third vertex.
3. Suppose $\pi\hat{g}_1$ fixes exactly 1 of 34, 45 and 35, say 34. So $\pi\hat{g}_1$ swaps 45 and 35. Let $\pi\hat{g}_1$ swaps 45 and 35. Let $g_2 = (3,4)$. Then $\pi\hat{g}_1\hat{g}_2$ satisfies the condition of case (1).
4. Suppose $\pi\hat{g}_1$ fixes none of 34, 45 and 35. Say it has (34, 45, 35) as a 3-cycle. Let $g_2 = (3,4)$. Then $\pi\hat{g}_1\hat{g}_2 = (34,35)(45)$, and we are back to case (3).

In all cases if $\pi \in \mathrm{Aut}(\Gamma)$, then for some nonnegative integer r, there exists $g_1,\ldots,g_r$ such that $\pi g_1,\ldots,g_r = 1$, implying that $\pi \in \phi(S_5)$. □

3 VERTEX-TRANSITIVE GRAPHS

A graph Γ is vertex-transitive if the automorphism group of Γ acts transitively on the vertex-set of Γ. Thus for any two distinct vertices of Γ there is an automorphism mapping one to other.

Common example of vertex-transitive graphs is k-cubes Q_k. The vertex-set of Q_k is the set of all 2^k binary k-tules, with two being adjacent if they differ in precisely one coordinate position.

Theorem 4. The k-cone Q_k is vertex-transitive.

Proof. If we fixed k-tuple, then the mapping $\rho_v : x \mapsto x + v$ is a permutation of the vertices of Q_k. This mapping is an automorphism bacause the k-tuples x and y differ in precisely one coordinate position if and only if x+v and y+v differ in precisely one coordinate position. There are 2^k such permutations, and they form a subgroup H of the automorhism group of Q_k. This subgroup acts transitively on $V(Q_k)$ bacause for any two vertices x and y, the automorhism ρ_{y-x} maps x to y. □

Another example of vertex-transitive graph are circulant graphs.

Definition 1. Let $\mathbb{Z}_n$ denote the additive group of integers modulo n. If C is a subset of $\mathbb{Z}_n \setminus 0$, then construct a direct graph $\Gamma(\mathbb{Z}_n, C)$ as follows. The vertices of Γ are the elements

of $\mathbb{Z}_n$ and (i,j) is an arc of Γ if and only if $j-i \in C$. The graph $\Gamma(\mathbb{Z}_n, C)$ is called a circulant graph of order n, and C is called its connection set.

The cycles are special cases of circulant grahs. The cycle C_n is a circulant graph of order n, with conection set $\{1,-1\}$. The complete and empty graphs are also circulant, with connection set $C = \mathbb{Z}_n$ and $C = 0$, respectively.

Let G be a group and let C be a subset of G that is closed under taking inverses and does not contain the identity. Then the Cayley graph $\Gamma(G,C)$ is the graph with vertex set G and edge set

$$E(\Gamma(G,C)) = \{gh : hg^{-1} \in C\}. \tag{6}$$

Theorem 5. The Cayley graph $\Gamma(G,C)$ is vertex transitive.

Proof. For each $g \in G$ the mapping

$$\rho_g : x \mapsto xg \tag{7}$$

is a permuatation of the elements of G. This is an automorphism of $\Gamma(G,C)$ because

$$(yg)(xg)^{-1} = ygg^{-1}x^{-1} = yx^{-1}, \tag{8}$$

and so $xg \sim yg$ if and only if $x \sim y$. The permutations ρ_g form a subgroup of the automorphism group of $\Gamma(G,C)$ isometric to G. This subgroup acts transitively on the vertices of $\Gamma(G,C)$ because for any two vertices g and h, the automorphism $\rho_{g^{-1}h}$ maps g to h.

4 CAYLEY GRAPHS

As we mentioned before, every Cayley graph is vertex-transitive. In fact, most small vertex transitive graphs are Cayley graphs, but there are also many families of vertex transitive graphs that are not Cayley graphs. One example of such graph is Petersen graph. He is vertex-transitive, but not Cayley graph.

Circulant graph on n vertices is a Cayley graph for the cyclic group of order n and k-cube is a Cayley graph for the elementary abelian group $\mathbb{Z}_2^k$.

Some Cayley grahs appear frequently in the literature.

The complete graphs and their complements are Cayley graphs. K_n is a Cayley graph on any group G or order n where connection set is the set of non-identity elements of the group.

The graph formed on the finite field $\mathbb{F}_q$, where $q = 1 \pmod 4$ and the connection set is the set od quadratic residues in $\mathbb{F}_q$, is also a Cayley graph, called a Paley graph.

Definition 2. Let p be a prime number and n be a positive integer such that $p^n \equiv 1 \pmod 4$. The graph $P = (V,E)$ with

$$V(P)=\mathbb{F}_{p^n} \text{ and } E(P)=\left\{\{x,y\}: x,y\in\mathbb{F}_{p^n}, x-y\in\left(\mathbb{F}_{p^n}^*\right)^2\right\} \tag{10}$$

is called a Paley graph.

The list of integers which can be considered as an order of the Paley graph starts with 5, 9, 13, 17, 25, 29, 37, 41, 49, 53, 61, 73, 81… . The Paley graph of oreder 5 is cycle C_5.

Answer to question whether the arbitrary graph is a Cayley graph gives the theorem of Sabidussi. Before the proceeding to the theorem, a definition is required.

Let G be a transitive permutation group acting on a finite set Ω. Folowing three conditions are equivalent:

1. The only element of G that fixes an element of Ω is the identity permutation;
2. $|G|=|\Omega|$;
3. For any $w_1, w_2\in\Omega$, there is a unique element $\pi\in G$ satisfying $w_1\pi=w_2$.

A transitive permutation group G that satisfies any of the these conditions is said to be regular. We now state the theorem of Sabidussi.

Theorem 6. A graph Γ is a Cayley graph if and only if A(Γ) contains a regular subgroup.

Some of the most interesting and extensively investigated problem connected with Cayley graph is trying to determine when two graphs are isomorphic.

Let p be a prime and let $\mathbb{Z}_p^*$ denote the multiplicative group of units of $\mathbb{Z}_p$. Define the permutation $T_{a,b}$ on $\mathbb{Z}_p$ for $a\in\mathbb{Z}_p^*$ and $b\in\mathbb{Z}_p$, by $xT_{a,b}=ax+b$. Denoting equivalent permutation group as $G\equiv H$, we state theorem of Burnside.

Theorem 7. A transitive permutation group G of prime degree p is either doubly transitive or $G\equiv\left\{T_{a,b}: a\in H<\mathbb{Z}_p^*, b\in\mathbb{Z}_p\right\}$.

Burnside's theorem has applications for circulant graphs of prime order. If $A(\Gamma)$ is doubly transitive for a graph Γ, then Γ is either complete or has no edges.

The most important result about isomorphism of Cayley graph is provided by theorem of Turner via next characterization.

Theorem 8. Let p be a prime. Two circulant graphs $\Gamma(p,C)$ and $\Gamma(p,C')$ of order p are isomorphic if and only if $C'=aC$ for some $a\in\mathbb{Z}_p^*$.

It is very difficult to determine the full automorphism group of Cayley graphs. The answer is complete known in special case od prime order circulants.

Suppose that p is a prime, and that we are given the circulant graph $\Gamma(p,C)$, which is Cayley graph on the additive group $\mathbb{Z}_p$. The graph is complete if and only if C is all of $\mathbb{Z}_p^*$ and it is empty graph if and only if C is $\varnothing$. The resulting automorphism group is symmetric group S_p.

When $\varnothing\subset C\subset\mathbb{Z}_p^*$ using Theorem 7 we obtain that $A(\Gamma)$ has the form $\left\{T_{a,b}: a\in H<\mathbb{Z}_p^*, b\in\mathbb{Z}_p\right\}$. This implies that the stabilizer of the vertex labelled 0 is $T_{a,0}$ with $a\in H<\mathbb{Z}_p$. Thus, if there is an edge joining 0 and k in Γ, than there is an edge joining 0 and all of kH, and so the connection set C is a union of cosets of the multiplicative subgroup H of

$\mathbb{Z}_p^*$. If C is a union of cosets of the subgroup H of $\mathbb{Z}_p^*$, but not an union of cosets of any supergroup of H, then the stabilizer of 0 is $\left\{T_{a,0} : a \in H < \mathbb{Z}_p^*\right\}$ and we know precisely what $A(\Gamma)$ is.

If graph Γ is a circulant graph $\Gamma(p,C)$ and $\varnothing \subset C \subset \mathbb{Z}_p^*$, then let $e(C)$ denote the maximum even order subgroup H of $\mathbb{Z}_p^*$ for which C is an union of cosets of H. We now state the folowing result.

Theorem 9. Let graph Γ be a circulant graph $\Gamma(p,C)$ of prime order. If $C = \varnothing$ or $\mathbb{Z}_p^*$, then $A(\Gamma) = S_p$. Otherwise, $A(\Gamma) = \left\{T_{a,b} : a \in e(C), b \in \mathbb{Z}_p\right\}$.

5 APLICATION OF "WOLFRAM MATHEMATICA 10.0" IN ALGEBRAIC GRAPH THEORY

In closing section we investigate „Wolfram Mathematica 10.0" which contains many constructors and tools relating to group theory and algebraic graph theory. The automorphisms group of graph Γ may be computed in Mathematica using GraphAutomorphismGroup[g]. Precomputed automorphisms for many named graphs can be obtained using GraphData[graph, "Automorphisms"]. Just a small part of Wolfram Mathematica utility and his package Combinatorica will be exemplified by the following example. The example shows graph constracting in Wolfram Mathematica, finding his group of automorphisms, group generating set, group orbits and Cayley graph.

Example 2.

```
Graph[{1, 2, 3, 4, 5, 6, 7}, {1 ↔ 5, 1 ↔ 2, 2 ↔ 5, 5 ↔ 3, 3 ↔ 4, 4 ↔ 5, 5 ↔ 6, 5 ↔ 7 }
 VertexLabels → "Name", ImagePadding → 10]
```

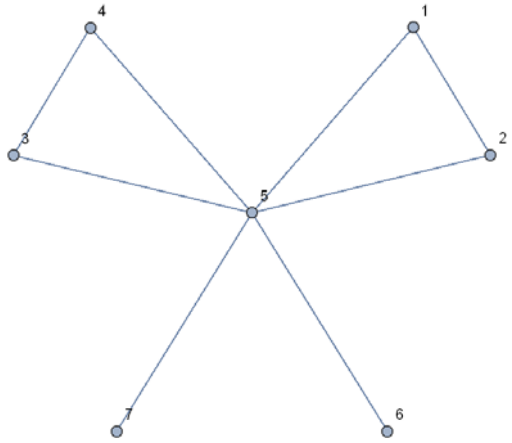


```
GraphAutomorphismGroup[%]
PermutationGroup[
 {Cycles[{{6, 7}}], Cycles[{{3, 4}}], Cycles[{{1, 2}}], Cycles[{{1, 3}, {2, 4}}]}
```

```
GroupGenerators[
 PermutationGroup[{System`Cycles[{{6, 7}}], System`Cycles[{{3, 4}}]
   System`Cycles[{{1, 2}}], System`Cycles[{{1, 3}, {2, 4}}]}]]
{System`Cycles[{{6, 7}}], System`Cycles[{{3, 4}}],
 System`Cycles[{{1, 2}}], System`Cycles[{{1, 3}, {2, 4}}]}
GroupOrbits[PermutationGroup[{Cycles[{{6, 7}}],
   Cycles[{{3, 4}}], Cycles[{{1, 2}}], Cycles[{{1, 3}, {2, 4}}]}]]
{{1, 2, 3, 4}, {5}, {6, 7}}
CayleyGraph[PermutationGroup[{Cycles[{{6, 7}}], Cycles[{{3, 4}}],
   Cycles[{{1, 2}}], Cycles[{{1, 3}, {2, 4}}]}], VertexLabels → "Name"]
```

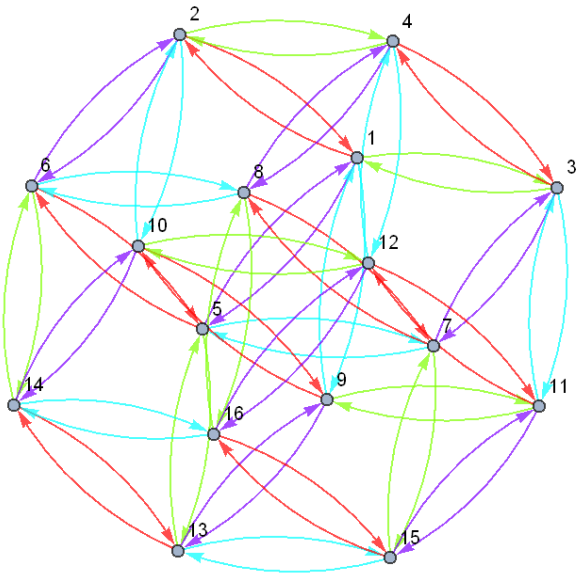

Acknowledgements: This research was supported under the grant by the Ministry of Science and Technology, Government of the Republic of Srpska.

REFERENCES

[1] L. Beineke, R. Wilson and P. Cameron, *Topics in Algebraic Graph Theory*,Cambridge University Press, (2004).
[2] C. Godsil and G. Royle, *Algebraic Graph Theory*, Springer-Verlag New York, (2001).
[3] P. Erdős and A. Rényi, *Asymmetric graphs*, Acta Math. Acad. Sci. Hungar, (1963).
[4] G. H. Fath-Tabar, *The automorphism group of finite graphs*, Iranian Journal of Mathematical Sciences and Informatics Vol.2, No.2 (2007).
[5] R. Jajcay, *The Structure of Automorphism Groups of Cayley Graphs and Maps*, Journal of Algebraic Combinatorics 12 (2000).
[6] A. N. Elsawy, *Paley Graphs and Their Generalizations*, A thesis submitted to Heinrich Heine University Düsseldorf, Germany for the Degree of Master of Science, (2009).

Received March, 20 2014

MATHEMATICA MONTISNIGRI
Vol XXXI (2014)

ПРЕДСТАВЛЕНИЕ ХАРАКТЕРИСТИЧЕСКОЙ ФУНКЦИИ ОПЕРАТОРА ТИПА ШТУРМ-ЛИУВИЛЛЯ ПО НУЛЯМ

НИКОЛА МИХАЛЕВИЧ

Университет Черногории, Морской факультет
Котор, Черногория
e-mail: nikolamih@ac.me

Ключевые слова: оператор, характеристическая функция, асимптотика, собственные значения.

Аннотация. В статье мы представляем асимптотику характеристической функции оператора $D^{(2)}$ по нулям, которые описаны в работах [1] и [13], т.е. в виде бесконечного произведения, в зависимости от уровия гладкости потенциала q и функции задержки α. В статье также рассчитан первый регуляризованный след оператора $D^{(2)}$.

REPRESENTATION CHARACTERISTIC FUNCTION OF STURM-LIUVILLE TYPE OVER THE ZEROS

NIKOLA MIHALJEVICH

University of Montenegro, Faculty of Marine
Kotor, Montenegro
e-mail: nikolamih@ac.me

Summary. In this paper, we present the asymptotic behavior of the characteristic functions operatora $D^{(2)}$ over the zeros, which are described in the works [1] and [13], that is in the form of an infinite product, depending on the smoothness potontsiala q and delay functions α. We also consider the first regularized trace of the operator $D^{(2)}$.

2010 Mathematics Subject Classification: 34B24, 35B05.
Key words and Phrases: Operator, characteristic function, asymptotic behavior, own values.

1 АНАЛИЗ БЕСКОНЕЧНОГО ПРОИЗВЕДЕНИЯ

В работе [13] мы получили асимптотику ноль характеристической функции F в зависимости от уровия гладкости потенциала q и функции задержки α. Следствием теоремы, доказанной в работе [13] является то, что собственные значения оператора $D^{(2)}$ имеют асимптотику

$$\lambda_{nij} = n^2 + \zeta_0 + \begin{cases} o(1), & q \in L_1[0,\pi] \\ \dfrac{\zeta_1(-1)^{n+1}\sin n\alpha(\pi)}{n} + o\left(\dfrac{1}{n}\right), & q \in AC[0,\pi] \\ \dfrac{\zeta_1(-1)^{n+1}\sin n\alpha(\pi)}{n} + \dfrac{\zeta_2^{(0)} + \zeta_2^{(1)}(-1)^{n+1}\cos n\alpha(\pi)}{n^2} + o\left(\dfrac{1}{n^2}\right), & q' \in AC[0,\pi] \end{cases} \quad (1)$$

при $n = 1,2,...,\ j = 1,2,$ где $\zeta_0 = 2C_1$, $\zeta_1 = 2C_2$, $\zeta_2^{(0)} = 2C_3^{(0)} + \dfrac{(h+H)^2}{\pi^2}$ и $\zeta_2^{(1)} = 2C_3^{(1)}$.

Мы подчеркнули, что характеристическая функция F оператора $D^{(2)}$ является целой функцией, экспоненциального типа и полвины степени роста по переменной λ. Кроме того, это счетная функция. Что означает, если z_n, $n \in N$ является нулем функции F, то и $-z_n$ также является нулем этой функции. Опираясь на классическую теорию представления таких функций к виду бесконечного произведения, что аналогично факторизации полинома, мы можем написать

$$F(z) = A \cdot \prod_{n=0}^{\infty}\left(1 - \frac{z^2}{\lambda_n}\right) \quad (2)$$

В (2) коефициент A является неопределенным, но его значение впоследствие устанавливается. А именно, (1) из работы [13] и (2) являются двумя различными представления одной и той же функции. Асимптотическое разложение этих различных представлений, при $z \to \infty$, вдоль произвольной прямой, проходящей через начало координат, может устанавливать различные отношения между параметрами оператора $D^{(2)}$, такими как h, H и значениями функций q и α в концов отрезка $[0,\pi]$ и параметрами асимптотического разложения собственныйх значений этого оператора. Мы обычно используем это разложение вдоль действительной или мнимой оси в комплексной z - плоскости.

Лемма 1.

$$A = \pi\lambda_0 \prod_{n=1}^{\infty}\frac{\lambda_n}{n^2}. \quad (3)$$

Доказательство. Рассмотрим асимптотику функции F при $z \to \infty$, $z \in R$. На основе формулы (1) имеем

$$\lambda_n = n^2 + \zeta_0 + o(1),$$

где главный член асимптотического выражения $o(1)$ на самом деле

$$\frac{1}{2}\int_0^{\pi} q(t_1)\cos n(\pi - t_1 + \alpha(t_1))dt_1 + \frac{1}{2}\int_0^{\pi} q(t_1)\cos n(\pi - t_1 - \alpha(t_1))dt_1 .$$

Далее, вместо (2) запишем

$$F(z) = A\prod_{n=0}^{\infty}\left(1 - \frac{z^2}{\lambda_n}\right) = A\left(1 - \frac{z^2}{\lambda_0}\right)\prod_{n=1}^{\infty}\left(1 - \frac{z^2}{\lambda_n}\right).$$

Так как (см. [14], с. 272)

$$\sin \pi z = \pi z\prod_{n=1}^{\infty}\left(1 - \frac{z^2}{n^2}\right),$$

имеем

$$\frac{F(z)}{-z\sin \pi z} = \frac{A\left(1 - \frac{z^2}{\lambda_0}\right)\prod_{n=1}^{\infty}\left(1 - \frac{z^2}{\lambda_n}\right)}{-\pi z^2\prod_{n=1}^{\infty}\left(1 - \frac{z^2}{n^2}\right)} =$$

$$= \frac{A}{\pi}\left(\frac{1}{\lambda_0} - \frac{1}{z^2}\right)\prod_{n=1}^{\infty}\frac{n^2}{\lambda_n}\prod_{n=1}^{\infty}\frac{\lambda_n - z^2}{n^2 - z^2} =$$

$$= \frac{A}{\pi\lambda_0}\left(1 - \frac{\lambda_0}{z^2}\right)\prod_{n=1}^{\infty}\frac{n^2}{\lambda_n}\prod_{n=1}^{\infty}\left(\frac{\lambda_n - n^2 + n^2 - z^2}{n^2 - z^2}\right) =$$

$$= \frac{A}{\pi\lambda_0}\prod_{n=1}^{\infty}\frac{n^2}{\lambda_n}\left(1 - \frac{\lambda_0}{z^2}\right)\prod_{n=1}^{\infty}\left(1 + \frac{\lambda_n - n^2}{n^2 - z^2}\right).$$

Пусть

$$\frac{A}{\pi\lambda_0}\prod_{n=1}^{\infty}\frac{n^2}{\lambda_n} = b .$$

Тогда у нас есть

$$\frac{F(z)}{-z\sin \pi z} = b\cdot\left(1 - \frac{\lambda_0}{z^2}\right)\prod_{n=1}^{\infty}\left(1 + \frac{\zeta_0 + o(1)}{n^2 - z^2}\right) =$$

$$= b\left(1 - \frac{\lambda_0}{z^2}\right)\left(1 + O\left(\frac{1}{z}\right)\right). \qquad z \to \infty,\ z \in R .$$

Здесь

$$F(z) = -bz\sin\pi z + O(\sin\pi z), \quad (z \to \infty) \tag{4}$$

С другой стороны, из (1), работа [13] непосредственно следует

$$F(z) = -z\sin\pi z + O(\sin\pi z) \quad (z \to \infty) \tag{5}$$

Из (4) и (5) следует (2).

2 ПРЕДСТАВЛЕНИЕ ФУНКЦИИ F, КОГДА ПОТЕНЦИАЛ q ЯВЛЯЕТСЯ АБСОЛЮТНО НЕПРЕРЫВНОЙ ФУНКЦИЕЙ

Точное асимптотическое разложение функции F из произведения, возможно только, если предположить, что q абсолютно непрерывная функция. Затем, в соотвествии с формулой (1) имеем

$$\lambda_{nij} = n^2 + \zeta_0 + \frac{\zeta_1(-1)^{n+1}\sin n\alpha(\pi)}{n} + o\left(\frac{1}{n}\right). \tag{6}$$

Теорема 1. Пусть q абсолютно непрерывная функция. Тогда характеристическая функция F на основе собственных значения (6) имеет следующее асимптотическое представление

$$F(z) = \left[-z + \frac{1}{z}\left(\lambda_0 - \frac{\zeta_0}{2} + s_1 + \frac{\pi}{8}\zeta_0^2 + \frac{\zeta_1\pi\alpha(\pi)}{2}\right)\right]\sin\pi z +$$

$$+ \frac{\pi}{2}\zeta_0\cos\pi z - \frac{\zeta_1\pi}{2z}\sin z\alpha(\pi) + O\left(\frac{\sin\pi z}{z^2}\right), \tag{7}$$

где s_1 первый регуляризованный след оператора $D^{(2)}$.

Доказательство.

$$\frac{F(z)}{-z\sin\pi z} = \left(1 - \frac{\lambda_0}{z^2}\right)\prod_{n=1}^{\infty}\left(1 + \frac{\lambda_n - n^2}{n^2 - z^2}\right) =$$

$$\left(1 - \frac{\lambda_0}{z^2}\right)\left(1 + \sigma_0(z) + \frac{1}{2}\sigma_1(z)\right) + R(z) \tag{8}$$

где

$$\sigma_0(z) = \sum_{n=1}^{\infty}\frac{\lambda_n - n^2}{n^2 - z^2},$$

и

$$\sigma_1(z)=\left(\sum_{n=1}^{\infty}\frac{\lambda_n-n^2}{n^2-z^2}\right)^2-\sum_{n=1}^{\infty}\left(\frac{\lambda_n-n^2}{n^2-z^2}\right)^2.$$

Используя известные суммы

$$\sum_{n=1}^{\infty}\frac{(-1)^n\cos n\alpha(\pi)}{n^2-z^2}=\frac{\pi}{2z}\cdot\frac{\cos z\alpha(\pi)}{\sin z\pi}-\frac{1}{2z^2},\ \sum_{n=1}^{\infty}\frac{(-1)^{n+1}\sin nx}{n}=\frac{\pi}{2},\ (-\pi<x<\pi)$$

и

$$\sum_{n=1}^{\infty}\frac{1}{n^2-z^2}=\frac{1}{2z^2}-\frac{\pi}{2z}\operatorname{ctg}z\pi \tag{9}$$

получается

$$\sum_{n=1}^{\infty}\frac{(-1)^{n+1}\sin n\alpha(\pi)}{n\left(n^2-z^2\right)}=\frac{\pi}{2z^2}\left(\frac{\sin z\alpha(\pi)}{\sin\pi z}-\alpha(\pi)\right). \tag{10}$$

Далее

$$\sigma_0(z)=\sum_{n=1}^{\infty}\frac{\lambda_n-n^2}{n^2-z^2}=\sum_{n=1}^{\infty}\frac{\lambda_n-n^2-\zeta_0-\dfrac{\zeta_1(-1)^{n+1}\sin n\alpha(\pi)}{n}}{n^2-z^2}+$$

$$+\sum_{n=1}^{\infty}\frac{\zeta_0}{n^2-z^2}+\sum_{n=1}^{\infty}\frac{\zeta_1(-1)^{n+1}\sin n\alpha(\pi)}{n\left(n^2-z^2\right)}=$$

$$=\zeta_0\sum_{n=1}^{\infty}\frac{1}{n^2-z^2}+\zeta_1\sum_{n=1}^{\infty}\frac{(-1)^{n+1}\sin n\alpha(\pi)}{n\left(n^2-z^2\right)}-$$

$$-\frac{1}{z^2}\sum_{n=1}^{\infty}\left(\lambda_n-n^2-\zeta_0-\zeta_1\frac{(-1)^{n+1}\sin n\alpha(\pi)}{n}\right)+$$

$$+\frac{1}{z^2}\sum_{n=1}^{\infty}\left(\lambda_n-n^2-\zeta_0-\zeta_1\frac{(-1)^{n+1}\sin n\alpha(\pi)}{n}\right)\cdot\frac{n^2}{n^2-z^2}=$$

$$=\zeta_0\left(\frac{1}{2z^2}-\frac{\pi}{2z}\operatorname{ctg}\pi z\right)+\frac{\zeta_1\pi}{2z^2}\left(\frac{\sin z\alpha(\pi)}{\sin\pi z}-\alpha(\pi)\right)-\frac{1}{z^2}s_1+o\left(\frac{1}{z^2}\right), \tag{11}$$

где

$$s_1=\sum_{n=1}^{\infty}\left(\lambda_n-n^2-\zeta_0-\zeta_1\frac{(-1)^{n+1}\sin n\alpha(\pi)}{n}\right).$$

Для $\sigma_1(z)$ получаем

$$\sigma_1(z)=\left(\sum_{n=1}^{\infty}\frac{\zeta_0+\frac{\zeta_1(-1)^{n+1}\sin n\alpha(\pi)}{n}}{n^2-z^2}\right)-\sum_{n=1}^{\infty}\frac{\zeta_1^2}{\left(n^2-z^2\right)^2}-$$

$$-2\sum_{n=1}^{\infty}\frac{\zeta_0\zeta_1(-1)^{n+1}\sin n\alpha(\pi)}{n\left(n^2-z^2\right)^2}-\sum_{n=1}^{\infty}\zeta_1\frac{1-\cos 2n\alpha(\pi)}{2n^2\left(n^2-z^2\right)}=$$

$$=\zeta_0^2\left(\frac{1}{4z^2}-\frac{\pi}{2z^3}\operatorname{ctg}\pi z+\frac{\pi}{4z^2}\operatorname{ctg}^2\pi z\right)+$$

$$+2\zeta_0\zeta_1\left(\frac{1}{2z^2}-\frac{\pi}{2z}\operatorname{ctg}\pi z\right)\left[\frac{\pi}{2z^2}\left(\frac{\sin z\alpha(\pi)}{\sin\pi z}-\alpha(\pi)\right)\right]-$$

$$-\zeta_0^2\left(-\frac{1}{2z^4}+\frac{\pi^2}{4z^2\sin^2\pi z}+\frac{\pi\operatorname{ctg}\pi z}{4z^3}\right)-$$

$$-2\zeta_0\zeta_1\sum_{n=1}^{\infty}\left[\frac{(-1)^{n+1}\sin n\alpha(\pi)}{n\left(n^2-z^2\right)^2}-\frac{1}{2}\zeta_1^2\frac{1-\cos 2n\alpha(\pi)}{2n^2\left(n^2-z^2\right)^2}\right]+O\left(\frac{\sin\pi z}{z^3}\right).$$

Легко проверить, что $R(z)=O\left(\frac{\sin\pi z}{z^3}\right)$.

При отделении членов, которые были с $\frac{1}{z^2}$ получаем

$$\sigma_1(z)=\zeta_0^2\frac{\pi}{4z^2}\operatorname{ctg}^2\pi z-\zeta_0^2\frac{\pi}{4z^2}\cdot\frac{1}{\sin^2\pi z}+o\left(\frac{1}{z^2}\right)=$$

$$=\zeta_0^2\frac{\pi}{4z^2}\cdot\frac{\cos^2\pi z-1}{\sin^2\pi z}+o\left(\frac{1}{z^2}\right)=-\zeta_0^2\frac{\pi}{4z^2}+o\left(\frac{1}{z^2}\right). \qquad (12)$$

Из равенства (8), (11) и (12) следует утверждение теоремы.

Легко установить и следующее.

Теорема 2. На отрицательной часты мнимой оси характеристическая функция F имеет следующую асимптотику

а) от произведения

$$F\left(-i\sqrt{\mu}\right)=e^{\pi\sqrt{\mu}}\left(\frac{\sqrt{\mu}}{2}+\frac{\pi}{4}\zeta_0+\frac{\xi}{2\sqrt{\mu}}+o\left(\frac{1}{\sqrt{\mu}}\right)\right), \qquad (13)$$

где

$$\xi = \lambda_0 - \frac{1}{2}\zeta_0 + s_1 + \frac{1}{2}\zeta_1\pi\alpha(\pi) - \frac{\pi}{8}\zeta_0^2,$$

б) от оператора

$$F\left(-i\sqrt{\mu}\right) = e^{\pi\sqrt{\mu}}\left(\frac{\sqrt{\mu}}{2} + \frac{h+H}{2} + \frac{hH}{2\sqrt{\mu}} + o\left(\frac{1}{\sqrt{\mu}}\right)\right). \qquad (14)$$

Теорема 3. Первый спектральный след s_1 оператора $D^{(2)}$ имеет вид

$$s_1 = 2hH - \lambda_0 + \frac{1}{2}\left(h^2 + H^2\right) + \frac{h+H}{\pi} - \frac{1}{2}\pi\alpha(\pi)\zeta_1.$$

Доказательство. Доказательство непосредственно следует выравниванием соответствующих значений из (13) и (14).

3 ПРЕДСТАВЛЕНИЕ ФУНКЦИИ F, КОГДА ПЕРВАЯ ПРОИЗВОДНАЯ ПОТЕНЦИАЛА q' АБСОЛЮТНО НЕПРЕРЫВНАЯ ФУНКЦИЯ

Точнее асимптотическое разложение функций F от произведения возможно только если предположить, что q' абсолютно непрерывная функция. Тогда в соответствим с формулой (1) имеем

$$\lambda_{nij} = n^2 + \zeta_0 + \frac{\zeta_1(-1)^{n+1}\sin n\alpha(\pi)}{n} + \frac{\zeta_2^{(0)} + \zeta_2^{(1)}(-1)^{n+1}\cos n\alpha(\pi)}{n^2} + o\left(\frac{1}{n^2}\right) \qquad (15)$$

Теорема 4. Пусть q' абсолютно непрерывная функция. Тогда характеристическая функция F на основе собственных значений (15) имеет следующее асимптотическое представление

$$F(z) = -z\sin\pi z + \frac{\pi}{2}\zeta_0\cos\pi z + \frac{1}{z}\left(\lambda_0\sin\pi z - \frac{\zeta_0}{2}\sin\pi z + s_1\sin\pi z + \right.$$

$$\left. + \frac{\zeta_1\pi\alpha(\pi)}{2}\sin\pi z - \frac{\zeta_1\pi}{2}\sin z\alpha(\pi) + \frac{\pi}{8}\zeta_0^2\sin\pi z\right) +$$

$$+ \frac{1}{z^2}\left(\frac{\pi\zeta_0\lambda_0}{2}\cos\pi z + \frac{\zeta_2^{(0)}\pi}{2}\cos\pi z + \frac{\zeta_2^{(1)}\pi}{2}\cos z\alpha(\pi) + \right.$$

$$+\frac{3}{8}\pi\zeta_0^2\cos\pi z-\frac{\pi^2}{4}\zeta_0\zeta_1\alpha(\pi)\cos\pi z+\frac{\pi}{4}\zeta_0\zeta_1\alpha(\pi)\cos z\alpha(\pi)\Big)-$$

$$-\frac{\pi^3\zeta_0^3}{48z^2}\cos\pi z+o\left(\frac{\sin\pi z}{z^2}\right), \tag{16}$$

где s_1 первый регуляризованный след оператора $D^{(2)}$.

Доказательство. Мы будем иметь

$$\frac{F(z)}{-z\sin\pi z}=\left(1-\frac{\lambda_0}{z^2}\right)\prod_{n=1}^{\infty}\left(1+\frac{\lambda_n-n^2}{n^2-z^2}\right)=$$

$$\left(1-\frac{\lambda_0}{z^2}\right)\left(1+\sigma_0(z)+\frac{1}{2}\sigma_1(z)+\frac{1}{6}\sigma_2(z)\right)+R_n(z), \tag{17}$$

где

$$\sigma_0(z)=\sum_{n=1}^{\infty}\frac{\lambda_n-n^2}{n^2-z^2},$$

$$\sigma_1(z)=\left(\sum_{n=1}^{\infty}\frac{\lambda_n-n^2}{n^2-z^2}\right)^2-\sum_{n=1}^{\infty}\left(\frac{\lambda_n-n^2}{n^2-z^2}\right)^2,$$

и

$$\sigma_2(z)=\left(\sum_{n=1}^{\infty}\frac{\lambda_n-n^2}{n^2-z^2}\right)^3+2\sum_{n=1}^{\infty}\left(\frac{\lambda_n-n^2}{n^2-z^2}\right)^2-3\sum_{n=1}^{\infty}\left(\frac{\lambda_n-n^2}{n^2-z^2}\right)\cdot\sum_{n=1}^{\infty}\frac{\lambda_n-n^2}{n^2-z^2}.$$

Далее

$$\sigma_0(z)=\sum_{n=1}^{\infty}\frac{\lambda_n-n^2}{n^2-z^2}=\sum_{n=1}^{\infty}\frac{\lambda_n-n^2-\zeta_0-\dfrac{\zeta_1(-1)^{n+1}\sin n\alpha(\pi)}{n}}{n^2-z^2}+$$

$$+\sum_{n=1}^{\infty}\frac{\zeta_0}{n^2-z^2}+\sum_{n=1}^{\infty}\frac{\zeta_1(-1)^{n+1}\sin n\alpha(\pi)}{n(n^2-z^2)}=$$

$$=\zeta_0\sum_{n=1}^{\infty}\frac{1}{n^2-z^2}+\zeta_1\sum_{n=1}^{\infty}\frac{(-1)^{n+1}\sin n\alpha(\pi)}{n(n^2-z^2)}-$$

$$-\frac{1}{z^2}\sum_{n=1}^{\infty}\left(\lambda_n-n^2-\zeta_0-\zeta_1\frac{(-1)^{n+1}\sin n\alpha(\pi)}{n}\right)+\frac{1}{z^2}\zeta_2^{(0)}\sum_{n=1}^{\infty}\frac{1}{n^2-z^2}+$$

$$+\frac{1}{z^2}\zeta_2^{(1)}\sum_{n=1}^{\infty}\frac{(-1)^{n+1}\cos n\alpha(\pi)}{n^2-z^2}+\frac{1}{z^2}\sum_{n=1}^{\infty}\frac{o(1)}{n^2-z^2}=$$

$$=\zeta_0\left(\frac{1}{2z^2}-\frac{\pi}{2z}\operatorname{ctg}\pi z\right)+\frac{\zeta_1\pi}{2z^2}\left(\frac{\sin z\alpha(\pi)}{\sin\pi z}-\alpha(\pi)\right)-\frac{1}{z^2}s_1-$$

$$-\frac{\pi}{2z^3}\zeta_2^{(0)}\operatorname{ctg}\pi z-\frac{\pi}{2z^3}\zeta_2^{(1)}\frac{\cos z\alpha(\pi)}{\sin\pi z}+O\left(\frac{\sin z\alpha(\pi)}{z^4\sin\pi z}\right)=$$

$$=\frac{\zeta_0}{2z^2}-\frac{\pi\zeta_0}{2z}\operatorname{ctg}\pi z+\frac{\zeta_1\pi}{2z^2}\cdot\frac{\sin z\alpha(\pi)}{\sin\pi z}-\frac{\zeta_1\pi}{2z^2}\alpha(\pi)-\frac{1}{z^2}s_1-$$

$$-\frac{\pi}{2z^3}\zeta_2^{(0)}\operatorname{ctg}\pi z-\frac{\pi}{2z^3}\zeta_2^{(1)}\frac{\cos z\alpha(\pi)}{\sin\pi z}+O\left(\frac{\sin z\alpha(\pi)}{z^4\sin\pi z}\right). \qquad (18)$$

где

$$s_1=\sum_{n=1}^{\infty}\left(\lambda_n-n^2-\zeta_0-\zeta_1\frac{(-1)^{n+1}\sin n\alpha(\pi)}{n}\right).$$

Для $\sigma_1(z)$ получим

$$\sigma_1(z)=\left(\sum_{n=1}^{\infty}\frac{\zeta_0+\dfrac{\zeta_1(-1)^{n+1}\sin n\alpha(\pi)}{n}}{n^2-z^2}\right)-\sum_{n=1}^{\infty}\left(\frac{\lambda_n-n^2}{n^2-z^2}\right)^2=$$

$$=\zeta_0^2\left(\frac{1}{4z^2}-\frac{\pi}{2z^3}\operatorname{ctg}\pi z+\frac{\pi}{2z^2}\operatorname{ctg}^2\pi z\right)+$$

$$+\frac{1}{z^3}\left(-\frac{1}{2}\zeta_0\zeta_1\pi^2\frac{\cos\pi z\sin z\alpha(\pi)}{\sin^2\pi z}+\frac{1}{2}\zeta_0\zeta_1\pi^2\alpha(\pi)\operatorname{ctg}\pi z\right)-$$

$$-\zeta_0^2\sum_{n=1}^{\infty}\frac{1}{\left(n^2-z^2\right)^2}-2\zeta_0\zeta_1\sum_{n=1}^{\infty}\frac{(-1)^{n+1}\sin n\alpha(\pi)}{n\left(n^2-z^2\right)^2}-\zeta_1^{\,2}\sum_{n=1}^{\infty}\frac{1-\cos 2n\alpha(\pi)}{2n^2\left(n^2-z^2\right)^2}+$$

$$+O\left(\frac{\sin z\alpha(\pi)}{z^4\sin\pi z}\right).$$

Дифференцируем по z левую и правую часть равенства

$$\sum_{n=1}^{\infty}\frac{1}{n^2-z^2}=\frac{1}{2z^2}-\frac{\pi}{2z}\operatorname{ctg}z\pi\,,$$

получаем

$$\sum_{n=1}^{\infty}\frac{1}{\left(n^2-z^2\right)^2}=\frac{\pi\operatorname{ctg}\pi z}{4z^3}+\frac{\pi^2}{4z^2\sin^2\pi z}+O\left(\frac{1}{z^4}\right).$$

Так, как

$$\sum_{n=1}^{\infty}\frac{(-1)^{n+1}\sin n\alpha(\pi)}{n\left(n^2-z^2\right)}=\frac{\pi}{2z^2}\left(\frac{\sin z\alpha(\pi)}{\sin\pi z}-\alpha(\pi)\right),$$

то дифференцируя по z левую и правую части этого последнего равенства получаем

$$\sum_{n=1}^{\infty}\frac{(-1)^{n+1}\sin n\alpha(\pi)}{n\left(n^2-z^2\right)^2}=-\frac{\pi}{2z^4}\left(\frac{\sin z\alpha(\pi)}{\sin\pi z}-\alpha(\pi)\right)+$$

$$+\frac{\pi}{4z^3}\cdot\frac{\alpha(\pi)\cos z\alpha(\pi)\sin\pi z-\pi\cos\pi z\sin z\alpha(\pi)}{\sin^2\pi z}.$$

Если, в известного равенства

$$\sum_{n=1}^{\infty}\frac{\cos nx}{n^2+\mu}=\frac{\pi}{2\sqrt{\mu}}\cdot\frac{\operatorname{ch}(\pi-x)\sqrt{\mu}}{\operatorname{sh}\pi\sqrt{\mu}}-\frac{1}{2\mu},$$

положим $\sqrt{\mu}=iz$, тогда получаем

$$\sum_{n=1}^{\infty}\frac{\cos nx}{n^2-z^2}=\frac{1}{2z^2}+\frac{\pi}{2iz}\cdot\frac{\operatorname{ch}(\pi-x)iz}{\operatorname{sh}\pi iz}=\frac{1}{2z^2}-\frac{\pi}{2z}\cdot\frac{\cos(\pi-x)z}{\sin\pi z}.$$

Интегрируем последнее выражение (по x) в пределах от 0 до x, получаем

$$\sum_{n=1}^{\infty}\frac{\sin nx}{n\left(n^2-z^2\right)}=\frac{x-\pi}{2z^2}+\frac{\pi\sin(\pi-x)z}{2z^2\sin\pi z}.$$

При повторном интегрировании в тех же пределах, получаем

$$\sum_{n=1}^{\infty}\frac{1-\cos nx}{n^2\left(n^2-z^2\right)}=\frac{x(x-2\pi)}{4z^2}+\frac{\pi}{2z^2\sin\pi z}\left[\cos z(\pi-x)-\cos\pi z\right].$$

Дифференцируя по z последнее равенство, мы получаем

$$\sum_{n=1}^{\infty}\frac{1-\cos nx}{n^2\left(n^2-z^2\right)^2}=O\left(\frac{\operatorname{ctg}\pi z}{z^4}\right),$$

и

$$\sum_{n=1}^{\infty}\frac{1-\cos 2n\alpha(\pi)}{2n^2\left(n^2-z^2\right)^2}=O\left(\frac{\operatorname{ctg}\pi z}{z^4}\right).$$

Далее

$$\sigma_1(z)=\zeta_0^2\left(\frac{1}{z^4}-\frac{\pi}{2z^3}\operatorname{ctg}\pi z+\frac{\pi^2}{4z^2}\operatorname{ctg}^2\pi z\right)-\frac{1}{2}\zeta_0\zeta_1\pi^2\frac{\cos\pi z\sin z\alpha(\pi)}{z^3\sin^2\pi z}+$$

$$+\frac{1}{2}\zeta_0\zeta_1\frac{\pi^2\alpha(\pi)\operatorname{ctg}\pi z}{z^3}-\zeta_0^2\left(\frac{\pi\operatorname{ctg}\pi z}{4z^3}+\frac{\pi^2}{4z^2\sin^2\pi z}\right)-$$

$$-2\zeta_0\zeta_1\left(-\frac{\pi}{2z^4}\left(\frac{\sin z\alpha(\pi)}{\sin\pi z}-\alpha(\pi)\right)\right)+\frac{\pi}{4z^3}\cdot\frac{\alpha(\pi)\cos z\alpha(\pi)\sin\pi z-\pi\cos\pi z\sin z\alpha(\pi)}{\sin^2\pi z}+$$

$$+O\left(\frac{\sin z\alpha(\pi)}{z^4\sin\pi z}\right).$$

Когда мы отделяем члены, которые были с $\frac{1}{z^2}$ и $\frac{1}{z^3}$, получаем

$$\sigma_1(z)=-\frac{\pi^2}{4z^2}\zeta_0^2+\frac{1}{z^3}\left(-\frac{\pi\zeta_0^2}{2}\operatorname{ctg}\pi z+\frac{\pi^2}{2}\zeta_0\zeta_1\alpha(\pi)\operatorname{ctg}\pi z-\right.$$

$$\left.-\frac{\zeta_0^2\pi}{4}\operatorname{ctg}\pi z-\frac{\pi\zeta_0\zeta_1\alpha(\pi)\cos z\alpha(\pi)}{2\sin\pi z}-\frac{\zeta_1^2\alpha(\pi)(\alpha(\pi)-\pi)}{4}\right)+$$

$$+O\left(\frac{\sin z\alpha(\pi)}{z^4\sin\pi z}\right)=-\frac{\pi^2}{4z^2}\zeta_0^2+\frac{1}{z^3}\left(-\frac{3}{4}\zeta_0^2\pi\operatorname{ctg}\pi z+\right.$$

$$\left.+\frac{\pi^2}{2}\zeta_0\zeta_1\alpha(\pi)\operatorname{ctg}\pi z-\frac{\pi\zeta_0\zeta_1\alpha(\pi)\cos z\alpha(\pi)}{2\sin\pi z}\right)+$$

$$+O\left(\frac{\sin z\alpha(\pi)}{z^4\sin\pi z}\right). \qquad (19)$$

Дважды дифференцируя по z следующее равенство

$$\sum_{n=1}^{\infty}\frac{1}{n^2-z^2}=\frac{1}{2z^2}-\frac{\pi}{2z}\operatorname{ctg}z\pi$$

получаем

$$\sum_{n=1}^{\infty}\frac{1}{\left(n^2-z^2\right)^3}=\frac{-\pi^3\cos\pi z}{8z^3\sin^3\pi z}+o\left(\frac{1}{z^3}\right),$$

далее для $\sigma_2(z)$ имеем

$$\sigma_2(z)=\left(\sum_{n=1}^{\infty}\frac{\zeta_0+\frac{\zeta_1(-1)^{n+1}\sin n\alpha(\pi)}{n}}{n^2-z^2}\right)^3+2\sum_{n=1}^{\infty}\left(\frac{\zeta_0+\frac{\zeta_1(-1)^{n+1}\sin n\alpha(\pi)}{n}}{n^2-z^2}\right)^3-$$

$$-3\sum_{n=1}^{\infty}\left(\frac{\zeta_0+\frac{\zeta_1(-1)^{n+1}\sin n\alpha(\pi)}{n}}{n^2-z^2}\right)^2\cdot\sum_{n=1}^{\infty}\frac{\zeta_0+\frac{\zeta_1(-1)^{n+1}\sin n\alpha(\pi)}{n}}{n^2-z^2}=$$

$$=-\frac{\pi^3}{8z^3}\zeta_0^3\operatorname{ctg}^3\pi z+2\zeta_0^3\sum_{n=1}^{\infty}\frac{1}{\left(n^2-z^2\right)}+o\left(\frac{1}{z^3}\right)=$$

$$=-\frac{\pi^3}{8z^3}\zeta_0^3\operatorname{ctg}^3\pi z-\zeta_0^3\frac{\pi^3\cos\pi z}{4z^3\sin^3\pi z}+3\zeta_0^3\pi^3\frac{\operatorname{ctg}\pi z}{8z^3\sin^2\pi z}+o\left(\frac{1}{z^2}\right)=$$

$$=\frac{\pi^3\zeta_0^3}{8}\cdot\frac{\cos\pi z}{z^3\sin\pi z}+O\left(\frac{\sin z\alpha(\pi)}{z^4\sin\pi z}\right) \qquad (20)$$

Из равенств (17), (18), (19) и (20) следует утврерждение теоремы.

REFERENCES

[1] N.Mihaљeviћ, M.Pikula, *Karakteristichna funktcija operatora tipa Shturm-Leeuvila sa promenљivim kashњenjem*, Zbornik Fakulteta za pomorstvo u Kotoru, **20**, 403-410, (2003).

[2] S.B. Norkin, *Differentcial`ny`e uravneniia vtorogo poriadka s zapazdy`vaiushchim argumentom*, Nauka, Moskva, (1965).

[3] I.M. Gel`fand, B.M.Levitan, "Ob opredelenii differentcial`nogo uravneniia po ego spektral`noi` funktcii", *Izv. AN SSSR, Ser. Mat*., **15**, S. 309-360, (1951).

[4] L.E`. E`l`sgol`tc, S.B. Norkin, *Vvedenie v teoriiu differentcial`ny`kh uravnenii` s otcloniaiushchimsia argumentom*, Nauka, Moskva, (1971).

[5] R.Lazović, M.Pikula, "Regularized trace of the operator applied to solving inverse problems", *Radovi matematički*, 2002. Lazović R., "Pikula M. Regularized trace of the operator applied to solving to inverse problem", *Radovi matematički*, **11**, pp. 49-57, (2002)

[6] M. Pikula, "Ob opredelenii differentcial`nogo uravneniia s peremenny`m zapazdy`vaniem", *Mathematica Montisnigri*, **VI**, 71-91, (1996).

[7] M. Pikula, "Opredelenie differentcial`nogo operatora Shturma-Leeuvillia s zapazdy`vaiushchim argumentom po dvum spektram", *Matematicheskii` vestneyk*, **43**, 159-171, (1991).

[8] R.Lazoviћ, *Doktorska disertatcija*, Beograd (1998).

[9] N.Mihaljevich, "A reconstruction of the operator by using given spectral characteristic", *Mathematica Montisnigri*, **XX-XXI**, 15-34, (2007-2008).

[10] N.Mihaljevich, M.Pikula, "The inverse Sturm-Liouville problem with changeable delay", *Mathematica Montisnigri*, **XVI**, 41-68, (2003).

[11] V.A. Sadovnichii`, *Teoriia operatorov*, Moskva, MGU, (1979).
[12] N.Levinson, “The inverse Sturm-Liouville problem”, *Math. Tidsskr*. **13**, 25-30, (1949).
[13] N.Mihaљevich, “Asimptotika soobstvenny`kh znachenii` operatora tipa Shturm-Leeuvilia s peremenny`m zapazdy`vaniem”, *Mathematica Montisnigri*, **XXVIII**, (2013)
[14] B.V.Shabat, *Vvedenie v kompleksny`i` analiz*, Nauka, Moskva (1985).

Поступила в редакцию 20 января 2014 года.

MATHEMATICA MONTISNIGRI
Vol XXXI (2014)

A LOGICAL BURBAKIES MODEL PROGRAM FORMALIZATION OF MATHEMATICS

RADOSLAV MILOŠEVIĆ

University of East Sarajevo, Faculty of Philosophy Pale Aleksa Santic 1,
Republic of Srpska, Bosnia and Herzegovina
e-mail: radoslav_milosevic@yahoo.com

Summary. Gate mathematical theory requires special model axiomatic formalization of the mathematical theory. Classic formal mathematical theories, such as number theory, function theory, group theory, game theory, information theory, theory of surfaces, probability theory, and others have each individually own logical model construction. Each of these theories must satisfy the requirements uncontradictions, independence and thoroughness of his axiomatic system. Similarly in this paper we will present a logical model Burbakies program of formalization of mathematics. As an illustration of a solution that is technically in detail (especially for example. Introduction in how objects) quite different from the above theory of classical mathematics, with a tendency to be as adaptable to formalize a number of specific mathematical theory, we outline in brief strokes (tentative) program of formalization mathematics to Burbaki (Nicolas Bourbaki). Next, we will show how to Burbaki so by the program develops (or sketch) the formalization of some logical and mathematical theory: the logic of the statement, predicate logic, predicate logic with equality, set theory (etc., at least in principle).

1 INTRODUCTION

The philosophical orientation of Mathematics of the 20th century began with the reconstruction of all three programs of classical mathematics, where there are three program reimbursement basis of mathematics, namely: logicism (founder Bretnard Russell), formalism (founder of David Hilbert) and intuitionism (founder Brauer). As the criticism that followed the development of these programs created a new philosophical trends in contemporary mathematics that time, from which follows a series of founder intuitionistic - constructivist school, which belongs Brauer, Heitinga, Troelstra, Van Dalen (holansdski intiucionizam), then Markov, Kushner, Bishop, Majnes, Rajhman (American pragmatic constructivism) and Johanston, Staples (englesni sophisticated constructivism).

Along with these projects, the philosophical orientation in mathematics in France, appeared a group of mathematicians under the name Burbakisti who offered his program of reconstruction of mathematics.

Burbaki Nicholas alias group of French mathematicians of the younger generation, which was formed in 1937., and has set itself the task to realize the establishment's fundamental axiomatic mathematics, providing that the fundamental role of the structures. Revealed that they were among the founders of the group A. Kartan, A. Bale, Z. Djedone and K. Chevalier. Under the name Burbaki the beginning of 1939. Published scientific papers and a large series of monographs Elements des Mathematique.

2010 Mathematics Subject Classification: 03C55, 03C62, 03C65, 03C70.
Key words and Phrases: Logic, model, Burbaki, program, formalization.

Burbakisti, mathematicians gathered in a group or Burbaki about these groups, also those who accept and implement the notion of the group were in science or in teaching mathematics.

This paper presents a sketch of the logical model Burbakijevog program of formalization of mathematics.

2 LOGICAL INTERPRETATION OF PROGRAM BURBAKIES FORMALIZATION OF MATHEMATICS

We assume that the choice of the structure of a formalized mathematical theory there is a lot of freedom and that decisions about it are not only mathematically and logically motivated. As an illustration of a solution that is technically in detail (especially for example. Way of introducing the objects that correspond to bound variables), and is designed, among other things, with a tendency to be more adaptable to the formalization of a large number of specific mathematical theory, we outline in brief strokes (tentative) program of formalization of mathematics to Burbaki (Nicolas Bourbaki).

Signs and words ("assemblages"). Signs of a mathematical theory T are these: Logical 1 means: □ , □ , ¬ .

The letters 2, which are introduced as required; It will regularly be sensitive of the Latin alphabet, possibly with accents, for example: A, A', A", ...

Specific means 3, which depend on the considered theory. (Eg. for set theory to the = sign, □, □).

Word of the theory T strings of T are written next to each other, some characters (but not the letters) can be connected in pairs moves above characters that call-ups. For example: in set theory question.

Exclusive printing words, effective as they are, would lead quickly to virtually insurmountable difficulties (because of their often large lengths of tens of thousands of characters, and more), and therefore for them to introduce abbreviations, among other things, the words of ordinary speech - which, of course, not belong to the formal mathematics and theory are urgently needed. For example: □ stands for ¬ and O is an abbreviation for (empty set).

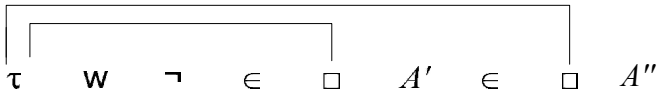

Some do mathematical (meta) theory, less theory contains rules that allow you to say certain words that are terms or relations theory, and other rules that allow you to say certain words that are theorems of the theory. Description of the rules (below) does not belong to itself (formal) theory; it is frequently used abbreviations and various substitute word or parts thereof, the meaning of which is usually clear from the context. Regularly, for brevity, will mean that these abbreviations words, instead of indicating them. (For example: if A, V word, AV will be the word that comes concatenating character of V, in order to come behind the signs of A, in the order they come).

Let A be a word, a letter h□h(A) will mark the word that gets this in words □A Connect to

tie each h wherever you come in and □ to the left of A and then replace h wherever you come in and with □ (It □h(A) therefore does not contain h). Eg: □ h (xy□) meaning of the word.

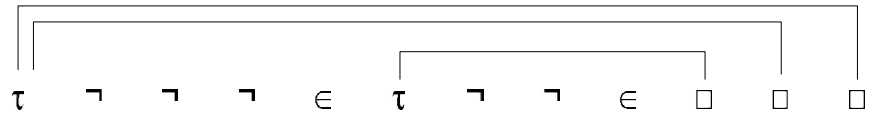

Let A, V word, and the letter h. Word that result from replacing By changing h wherever comes with a V means the following: (V| h)A.

For example: with A ≡ □ xy = xx, V ≡ □ being (V | h) A ≡ □ □ □ □ = y.

If we want to point out one or two different letters, for example h and h, and in which can (but need not) coming to A, writing the Ax{A} or {x, y}. In such a case, for example A{V} is the same as (V|h)A; analogous to A{V, S} with simultaneous replacement of h with a V, with the S in A. The possibility of confusion to avoid the most common (in abbreviation) additional brackets. For example: replacing R□Q for N and M□N received word it shall be indicated with M□(R□Q).

Criteria substitutions. Formal mathematics contains only the explicit written word. Practically, however, are required (theoretically not required) criteria for certain manipulations with the words - of course, they belong to the proper meta. Thus, the criteria of substitution are obtained. Among them, for example:

CS 1. Let A, V words, h, h' case. If h' is not an A, then (V|H) ≡ A (V|h')(h'|h)A.

CS 2. Let A, V field, and h the (codes for) various letters. If x out of the V, then (V|u)□h(A)≡□h(A'), where A' is ≡ (V|u)A.

Formative structures. Among the specific character of each is called relational, others substantive. Each specific sign associated with its weight; it is an integer, usually 2.

The word is called the first kind it starts with □ or substantive character, or if it consists of only one letter; Otherwise called the other species.

Formative design theory T is a sequence of words with this feature: for every word A series filled with one of the following characteristics:

a) A letter is.
b) In the series there in front of a word other types of V such that A ≡ ¬ V.
c) In the front row there are a word other types B, C such that A ≡ ¬ VS.
g) there is a row in front of the other types and the word V, so that for a letter Ahh≡ □(V).
d) There is a specific sign of the weight n8 benzyl and n the words of the first type A1, A2,
e) . . . an outside A, such that A is A1 A2 s ≡ . . , An.

Terme (or relations) of T are the words of the first kind (or other species) to come among the members of the formative structure of T. For example in set theory is □ relational character of weight 2, and the following series of formative structures:

A, A', A"□A, A', □A, A", ¬ □ A, A', ¬ □ A, A' □ A, A",

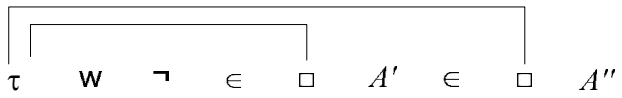

Its members are, for example: last, thermal theory.

Intuitive Talaso corresponding objects (the classical theory that should be formally "cover"), and the relations between relations such facilities. In particular, for example in g) if V is a proposition which expresses a property of the object h, then h□(V) corresponds to a"privileged" object that owns the property, if it exists, otherwise it represents an object about which nothing can be said.

Formative criteria allow the words you already know that the spa or relationships concluded for such a word. For example: let A be a relation (or term) of a theory T, h letter, a term T of T. Then (T| h)A relation (or term) of T.

Axioms. Setting its specific character and defines the thermal relations of a theory T. To conclude construction of T, should be :

1) Print a certain relation of T to be called explicit axioms of T; letters that come in explicit axioms are called constants of T.
2) Set the one or more rules which are referred to the scheme of the T and which must have the properties of:
   a) the application of such a rule R gives a relation of T;
   b) If T is a terma of T, the letter h, R relation of T is constructed using the scheme R, then the relation (T| h)R can be obtained by applying R.

Any relation obtained by applying a scheme of T is called the implicit axiom of T.

Intuitively, an axiom is any obvious claims, any hypothesis that is accepted to be of consequence, they withdrew; Constants are some specific objects, which are assumed to possess properties making them explicit axioms express. On the contrary, if the letter h is not constant, it is a completely indeterminate object; If an axiom assumes that the object x has a particular characteristic, such is necessarily implicit axiom, so this feature then truth of whatever object T.

Demonstrations. Each demonstration text of a theory T contains:

1. Auxiliary formatted structure of some relation and the baths of T.
2. Some of the demonstration of T, ie. a set of relations of T to come in the formative auxiliary structure, such that for every relation R of the array filled with at least one of these conditions:

a1) R is an explicit axiom of T.

a2) R result of applying some diagrams of T on thermal or relationships that come in the auxiliary formative structure.

b) In a series of R are in front of the relation S, T, such that T S ≡ ¬ R.

Theorem of T is a relation of T that comes in a demonstrations of T.

The notion of a theorem relative to the state of the construction discussed theories; a relation of T becomes a theorem when he managed to get involved in a demonstration of T.

Let R be a relation of T, h letter, a term T of T; if (T|h)R theorem of T, says that T(a) solution of R in T.

For a theory T is said to be contradictory if (when) found a relation R of T for which it was shown that the R and ¬ R theorem of T.

Deductive criteria are mathematical rules that allow shortening the conclusion of the demonstration, for example:

S1. Let A theorem of a theory T, T theorem of T, and the letter h is not a constant of T. Then (T|h)A theorem of T.

Comparison theory. The theory T' is called stronger than theory T if you are all trademarks of T and signs of T', all explicit axioms of T theorem of T' and all the schemes of the T schema of T'.

S2. If the theory T' is stronger than the theory T, all theorems of T are theorems of T'.

3 INSTEAD OF CONCLUSION

Burbaki to set this program develops (or sketch) the formalization of some logical and mathematical theory: the logic of the statement, predicate logic, predicate logic with equality, set theory (etc. at least in principle) - in which is not discussed. At the end of the note, and that is a critical note on intuitionism in the preface Burbakijevog description of the formalization of mathematics in a review of that work in one of the world's leading mathematical journals of reference experienced (maybe a little pointedly, but perhaps justified) "opponent" Burbakijevog entire program of formalization of mathematics.

REFERENCES

[1] Ansolet Holgben, *Creation of Mathematics*, (translation: D . Zibanovic), Belgrade: IP "Vuk Karadzic", (1972).

[2] N. Burbaki, *Sets theory,* Moscow, Fizmagis, (1965).

[3] N. Bourbaki, *Theorie des Ensembles,* Paris: Livre I. ASI 1212, (1954). [4] M. Gros, A. Lanten, *Theory of formal grammars,* Moscow: Mir. (1971).

[5] D. Vladimir, *Mathematical logic*, Beograd (Part I: Classical logic vessels), (1964).

[6] K. Doets, *Basic model theory*, CSLI Publications, (1996).

[7] Prešić, *Elements of mathematical logic*, Belgrade: Institute for Textbooks SR, Serbia, (1968).

[8] C. C. Chang, J. H. Keisler, *Model THEORI*, North - Holland, Amsterdam, (1997).

[9] Z. Sikic, *It is very real new age math*, Zagreb: School books, (1989).

Received March, 15 2014.

MATHEMATICA MONTISNIGRI
Vol XXXI (2014)

HYBRID PARALLELIZATION OF COMPUTING THE ELECTRON FLUXES PRODUCED BY PHOTON RADIATION

M. ZHUKOVSKIY[*], M. MARKOV[*], S.PODOLYAKO[*] AND R. USKOV[*]

[*] Keldysh Institute for Applied mathematics of RAS
Moscow, Russia
e-mail: zhuk@kiam.ru, web page: http://www.keldysh.ru

Summary. Principles of Monte Carlo simulating the radiative electron emission by use of supercomputers having the heterogeneous architecture are considered. Questions of calculation parallelization with application of graphical processors as arithmetical co-processors are discussed. A technique of effective distribution of calculation between central processor and graphical one is worked out. Developed weight modification of Monte Carlo method meant for computing by use of NVIDIA© CUDA is described. Some results of modeling of electron emission from aluminum plate being under photon radiation are represented.

Keywords. Mathematical modeling, electron transport, CUDA technology, hybrid parallelization

2010 Mathematics Subject Classification: 97M50, 93A30.
Key words and Phrases: Mathematical Modeling, Bremsstrahlung, Hybrid Parallelization.

1 INTRODUCTION

The photon propagation through matter produces fast electron fluxes. These electrons can leave an object being under photon radiation. As a result the processes of radiative electron emission occur outside and in interior cavities of the investigated object. Accounting the electron emission is significant when carrying out different experiments with ionizing radiation, for instance during non-destructive testing of materials. Modeling of perspective X-ray sources and development of modern detectors of radiation is impossible without correct taking into account the radiative electron emission.

Investigation of electron emission processes requires solving the complex boundary tasks of radiation transport in 3D problem statements. The Monte Carlo method is effective method of solution of the mentioned problems. However application of this method for modeling radiation transport in objects with complex geometrical structure requires huge computational burden and presupposes the use of multiprocessors computers including hybrid supercomputers as well. Modeling of the electron emission is more complex because of the small parameter of the task. Namely, the photon path up to its absorption is much bigger than electron path up to its thermalization.

The algorithms of radiative electron emission modeling on hybrid computers with use of NVIDIA© CUDA technology are considered in the paper.

2 CONCEPT OF MODELING OF RADIATIVE ELECTRON EMISSION

Physical models of electron transport are developed usually on the basis of complex theories describing the average characteristics of investigated processes, for instance, theory of multiple scattering[1], Landau theory of energy losses[2] etc. Implementation of such models implies working up the algorithms with complex logic stipulated by necessity of applicable conditions control of the used approximations when computing. In addition it is often required to carry out iteration procedures when the choice of model parameters is impossible a priori. It should be noted that these models are hardly fit hybrid computers architecture because of their own complex inner logic.

On the other hand computing systems with traditional architecture do not allow detail studying the physical processes under enough full models developed without conventional statements. These models taking into account every interaction between particle and matter give possibility to investigate processes under study in detail.

Therefore the modeling of particle transport is carried out by authors of the paper within the bounds of the model of individual collisions[3] (MIC). This model has simple inner logic and it is much more effective when it is implemented for hybrid computers in comparison with widely used models based on the embedded trajectories idea[4,5].

The basis of the MIC is a distribution of particles parameters changing in the course of the processes being simulated. The distribution is determined in the following way.

Let x be the values of ξ characterizing the state of the particle (e.g. energy loss or angle of scattering). If the distribution density of this value in the current physical process (normalized by 1) $f(x)$ is known, then, the distribution of this value $F(x)$ is determined by the integral $F(x) = \int_{-\infty}^{x} f(t)\,dt$. The value $F(x)$ is equal to the probability of inequality $\xi < x$. In order to

simulate (play) the random value ξ the inverse function technique[6] is used. Namely: $x = F^{-1}(\gamma), \gamma \in (0,1)$, $F^{-1}(\gamma)$ is the function inverse to $F(x)$, γ is uniformly distributed in $(0,1)$.

The probability distribution density $f(x)$ is constructed by cross-section data[7] handling: $f(x) = \frac{1}{\sigma}\frac{\partial\sigma}{\partial x}$; where σ and $\frac{\partial\sigma}{\partial x}$ are the cross-section and differential cross-section of the processes in question.

Modeling of radiative electron emission includes next stages:

- Simulating the photon transport in the objects of complex inner structure with accounting the processes of elastic and inelastic interaction between X-rays and matter;
- Modeling of generation of fast electron fluxes produced due to photo absorption and Compton scattering of X- rays in the object;
- Simulating the electron transport in matter with taking into account the various collision processes up to leaving the electron from the object or up to the fast electron thermalization. The base feature of the electron transport is the significant difference between range photon path and electron distance (up to three orders);
- Modeling of registration of emitted electrons by detecting system.

The algorithms of statistical simulation of electron emission processes are created by developing the weight versions of the Monte Carlo method. As mentioned above the photon path up to its absorption is much bigger than electron path up to its thermalization. A direct statistical simulation of electron emission is ineffective under these conditions as far as the fraction of electrons able to reach boundary surfaces of the object is very low.

The following way is worked out for increasing the photon trajectory worth. First of all, energy E_e of photo or Compton electrons produced by current photon is played. Secondly, the stopping path $L_e(E_e)$ of the electron is calculated. Then a segment of possible electron appearance is constructed so that the electron can leave object. It is supposed that an electron can leave the object if the distance between it and bound of the object is not bigger than L_e. Length of the segment is chosen in agreement with beforehand calculated L_e as shown on the fig.1 (segment AC).

A point of photo absorption or Compton scattering is then played according to formula:

$$x = \frac{1}{\mu_{ph}} \ln\left[1 - \gamma\left(1 - \exp\left\{-\mu_{ph}\left|AC\right|\right\}\right)\right], \qquad (1)$$

in (1): x is the distance between A and point of the photon interaction; γ is uniformly distributed in $(0,1)$ random number; $\mu_{ph}(E_{ph})$ is the total attenuation coefficient (total macroscopic cross section) of the photon.

Initial statistical weight w_e^0 of produced electron is defined as $w_e^0 = w_{ph} \cdot p_{\text{int}}(E_{ph}) \cdot p_e(L_e)$, where: w_{ph} is current weight of photon; $p_{\text{int}}(E_{ph})$ is

probability of producing the electron by the photon of energy E_{ph}; $p_e(L_e)$ is probability of the electron production on the segment AC. The probability $p_e(L_e)$ is equal to

$$p_e(L_e) = \exp(-\mu_{ph} OA) - \exp(-\mu_{ph} OC) = \exp(-\mu_{ph} OA)(1 - \exp(-\mu_{ph} AC)). \quad (2)$$

First factor in right part of (2) is the probability of photon to reach the point A. Second one is the probability of electron production on segment AC under the condition that the photon has reached the point A.

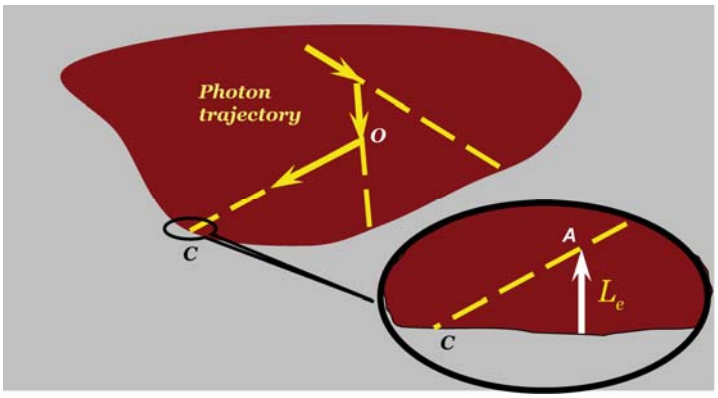

Fig.1. Scheme of modeling of radiative electron emission

The processes of both electrons production are considered on every section of every photon trajectory. Thus, the rare event of production of electron capable to leave the object is simulated by the developed weight algorithm considerably decreasing the results variance. The trajectory of produced electron is computed up to its leaving the object or up to its thermalization by use of the Monte Carlo method coupled with MIC being mentioned above.

After two electron trajectories completion the photon trajectory is continued from the point O. The new point O' of interaction is played and then new direction and energy of the photon are played. The following way is applied in order to increase the information value of the photon trajectory.

It is stated that the photon does not leave an object during a priori defined number n_{coll} of collisions. After every scattering its statistical weight is decreased by the probability p_{rm} of the remaining in the object: $w'_{ph} = w_{ph} \cdot \left[1 - \exp(-\mu_{ph} s)\right]$; w_{ph}, w'_{ph} are weights of the photon before and after scattering respectively; s is the distance from the point of interaction up to the object boundary ($s = OC$ on the fig.1). Moreover, it is supposed that the photon is not absorbed by the matter of the object. The photon weight is decreased in that case by the survival probability $p_{sr} = 1 - p_{ab}$; $w''_{ph} = w'_{ph} \cdot p_{sr}$; p_{ab} is the probability of the photo absorption. After n_{coll} collisions the photon trajectory is simulated via the analog computation. Number n_{coll} can be specified for instance in agreement with the criterion of the weight smallness.

It is important to note that the electrons produced at the point O' are ignored even through O' belong to corresponding segment $A'C'$ (see above).

The developed methods are sufficiently homogeneous. Therefore they can be easy parallelized including the application of graphical processors due to independence of particle trajectories.

The main features of the described algorithm implementation for hybrid computers are considered in the paper below.

3 IMPLEMENTATION OF DEVELOPED ALGORITHM FOR HYBRID COMPUTERS

It is necessary to take into account a number of features of using the graphical processors as arithmetical co-processors.

1. Graphical processor (GPU) is very useable for performing the huge number of arithmetical calculations. A lot of logical operations can sufficiently decrease performance of the graphical processor though.
2. The RAM memory space available to GPU is not large. The NVIDIA© CUDA technology 4.0 gives possibility to use RAM of central processor (CPU). However it leads to significant decrease of the graphical processor speed.
3. Load balancing between CPU and GPU is the key for effective usage of hybrid computer.

Algorithms of simulating the radiation transport in matter based on the Monte Carlo method have large number of independent threads. Such algorithms can be well parallelized by use any parallel computational architecture including the computer having poor data access synchronization techniques (hybrid computers with nodes including CPU and graphical processors as well). At the same time the algorithms in question require huge amount of arithmetical calculations. These circumstances make well suitability of the algorithms for implementation for hybrid computers.

Approaches to application of NVIDIA© CUDA technology for solving the problems of X-ray transport through the multicomponent objects[8] are developed by the authors of this paper. Algorithms of statistical modeling of electron transport for carrying out the numerical experiment on hybrid computers using NVIDIA© CUDA technology[9] are worked out as well. The effectiveness of mentioned implementation is caused by relatively uniform density of calculations on any stage of the algorithms.

Radiative electron emission modeling method has not the calculation density homogeneity. Therefore it is impossible to develop effective direct application of the parallelization ways[8,9]. It is necessary to distribute calculation charge between CPU and GPU and to carry out load balancing for optimization of computing.

Let us consider the computational scheme of the emission modeling (fig.2). The sequence of stages is the following.

- The tracing of object (finding of intersection points of a ray along current motion direction of a photon with boundaries of the object homogeneous parts) is carried out in compliance with ray-tracer algorithm[10].
- Modeling of Compton and photo electrons production inside the corresponding segment AC (see fig.1).
- Simulation of the electron trajectory up to its leaving the object or up to its thermalization.

- Registration of the electron if it reaches boundary of the object.
- Continuation of the photon trajectory.

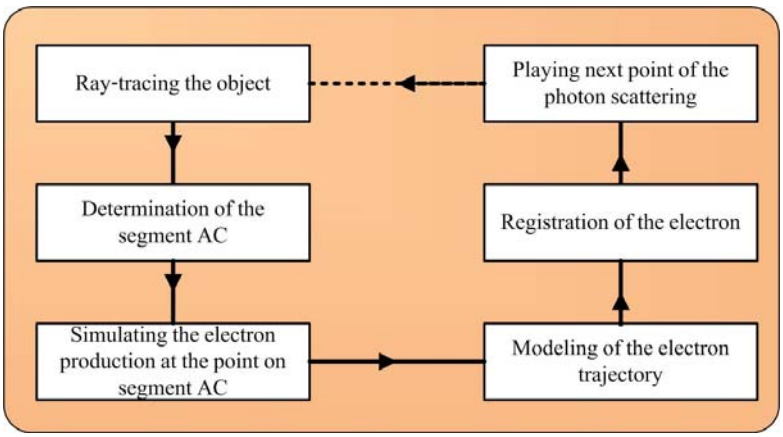

Fig.2. Calculation scheme of the electron emission modeling

Different parts of the computing scheme have different calculation density. Therefore it is necessary in some parts of the algorithm to rely on GPU and for remainder - on CPU. Namely, parts of high computational density are executed on GPU and parts of relatively low computational density are executed on CPU.

Investigations of the computing load on every stage of the electron emission modeling allow estimating the relative calculation density of different parts of the algorithm. Analysis of developed method has shown that simultaneous modeling of the photon trajectories and produced electrons leads to strongly nonuniform computational density on different stages of algorithm. Parts of low density (simulating the interaction between photons and matter, electron production processes) alternate with parts of high density (tracing the object, simulating the electron trajectories).

Results of the analysis have allowed distributing the computational load among the central processors and the graphical ones.

3.1 Ray-tracing the object

The goal of tracing the multicomponent object is to compute points of intersection of the ray along the photon motion direction with homogeneous parts of the object. Corresponding task is solved in two stages.

- Calculation of points coordinates of the intersection of the photon ray with envelopes bounding the homogeneous components of the object;
- Determination of optical thickness of intersected component along the ray.

The triangulation model is used for description of the complex objects having the piecewise homogeneous structures[10]. In practice the envelopes of homogeneous parts are defined by hundreds of thousand triangles. Therefore the problem of determination of intersection points coordinates requires huge number of arithmetical operations. Counting for mentioned above features of using the hybrid computers this stage is carried out on GPU.

It is known that a computational job for GPU (kernel) consists of group of calculation threads collated to blocks. Blocks are collated to grid.

Two computing kernels are used for executing the first stage of ray tracing. First kernel performs transformation of triangle vertexes to local coordinate system defined by the motion direction of current photon. Grid of this kernel consists of $N_{ph} \times M_v$ array of blocks. Every block is one-dimensional array of 512 threads. Total number of vertexes is $512 \cdot M_v$. Structure of the kernel is represented on figure 3.

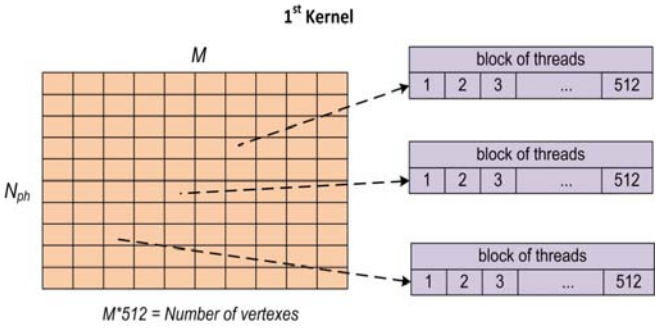

Fig.3. Configuration of first kernel.

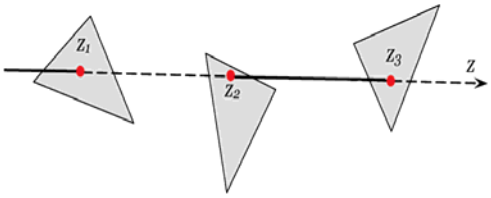

Fig.4. Intersection of triangles by photon ray.

Thus, the pair "photon-vertex" is corresponded to one thread.

Second kernel computes intersection point coordinates along the motion direction of current photons. It is assumed that polar axis z of local coordinate system is coaxial to the photon motion direction (fig.4).

Grid of 2nd kernel consists of N_{ph} blocks. Every block is array of 512 threads. A thread computes array of z by exhaustive searching all of the triangles in accordance with algorithm[10]. Result of 2nd kernel work is N_{ph} of array enclosing the intersection point coordinates. Increasing the computation speed is attained by allocating the desired arrays in shared memory of the blocks. Atomic operations excluding the simultaneous access to the memory are used for synchronization of access to array elements.

The 2nd stage of object tracing is to determine the set of optical thicknesses homogeneous parts of object intersecting by the photon ray. This stage requires substantially executing the logical operations of comparison and rearrangement. Therefore this stage is carried out by use of CPU.

3.2 Modeling of the electron emission

Firstly the segment AC is determined. As mentioned above it is equal to stopping path of electron (production and transport of photo electron is modeled at first and of Compton electron after that or vice-versa).

Using the results of the object tracing and $L_e\left(E_e\right)$ the segment AC is constructed (fig.1). The point of electron production is played according to conditional probability (1). The electron initial motion direction is played then. This part of algorithm is carried out on CPU.

Then trajectories of two produced electrons are followed up to its thermalization or up to leaving the object. Modeling the electron trajectory is computed on GPU by use of MIC[3].

Modeling the electron transport requires reconfiguration of GPU memory (roll-out of object geometry data; roll-in of electron interaction data). Therefore running this modeling of every step of photon trajectory is not effective. The next approach is used for increasing the

effectiveness of calculations. Characteristics of produced electrons are saved in electron pool and trajectories of all electrons of the pool are computing all together after filling of the pool.

Electron trajectory modeling is carried out on graphical processor and registration of electron is computed on CPU because of big dimension of electron sample and the GPU memory is not enough for saving the sample.

After finishing the electron transport simulating the photon trajectory is continued from the point O (fig.1). Next point of photon interaction is played and modeling of interaction between photon and matter in the point is computing. Algorithms of solving the corresponding tasks have complex logical structure and therefore are carrying out on CPU.

An analysis of calculation density of different steps of electron emission modeling has allowed distributing the parts of algorithm between central processor and graphical one of a node of hybrid computing system. The distribution of different parts calculation scheme is shown on the figure 5.

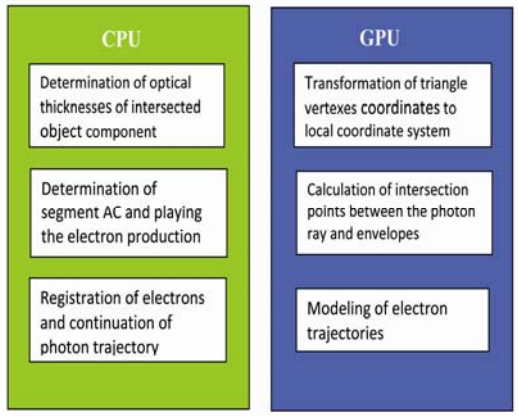

Fig.5. Distribution of parts of computing scheme between CPU and GPU.

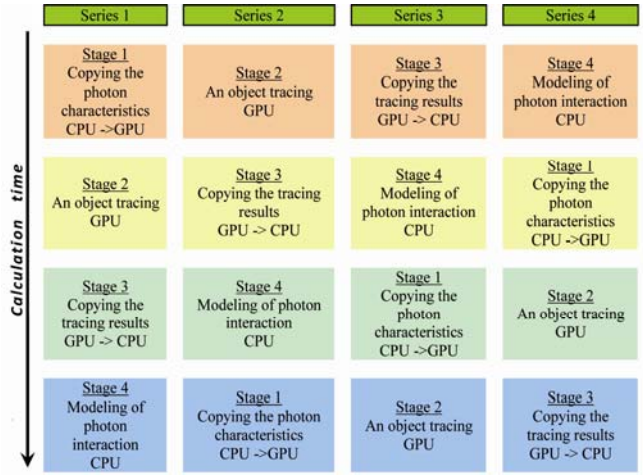

Fig.6. An example of organization computing series for simultaneous loading of CPU and GPU.

The iteration of the computational algorithm (modeling the next step of photon trajectory) is a sequence of calculation stages carrying out either on CPU or on GPU. Independence of photon trajectory modeling gives possibility to compute simultaneously calculations of different series. At that different calculations of the series are on the different stages. Thus, computing is carried out at the same time on both CPU and GPU. The fact allows increasing the effectiveness of hybrid computers application. An example of simultaneous loading of central processor and graphical one is represented on figure 6.

4 RESULTS OF MODELING

Two experiments were carried out for analysis of developed method capabilities: computational experiment with aluminum plate irradiated by X-ray (and its comparison with MCNP[11]) and natural experiment with aluminum plate irradiated by ^{137}Cs source of gamma rays.

4.1 Computational experiment

Configuration of the experiment is next. The photon flux is falling normally on aluminum plate. Energy of incident photons is E_0, thickness of the plate is h. Energy spectra of emitted from irradiated surface of the plate and from rear one are measured.

Calculations are carried out for two variants. Electron emission modeling results are represented on figures 7-10. Results of MCNP computing are shown for comparison.

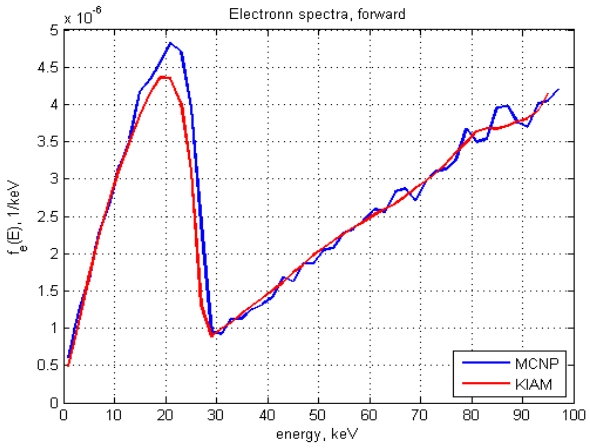

Fig.7. Spectra of electrons emitted from rear surface of the aluminum sample

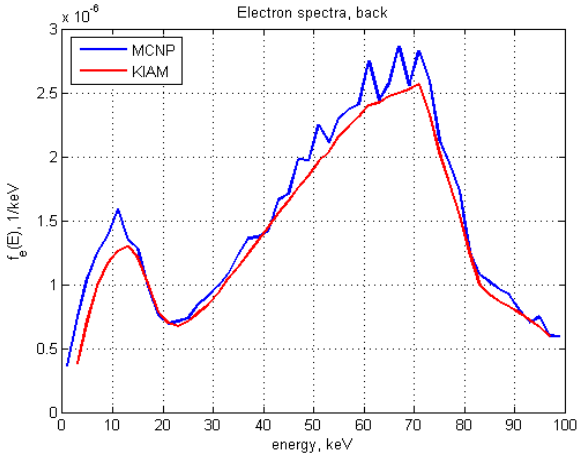

Fig.8. Spectra of electrons emitted from irradiated surface of the aluminum sample

Electron spectra on fig. 7 and 8 are obtained for $E_0 = 100\,keV$ and $h = 1cm$. Red line - results computed by described in the paper method (KIAM – Keldysh Institute for Applied Mathematics), blue line – by MCNP.

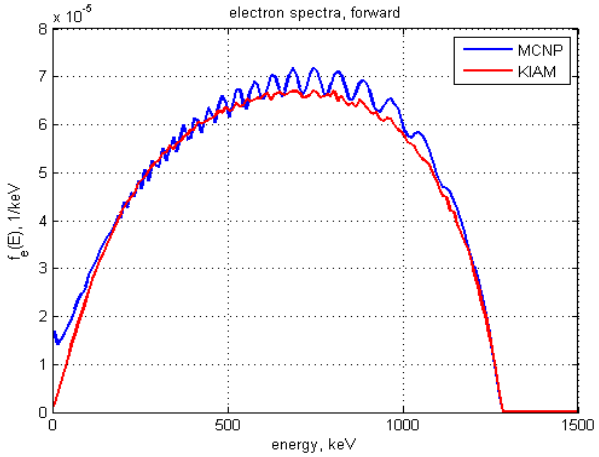

Fig.9. Spectra of electrons emitted from rear surface of the aluminum sample

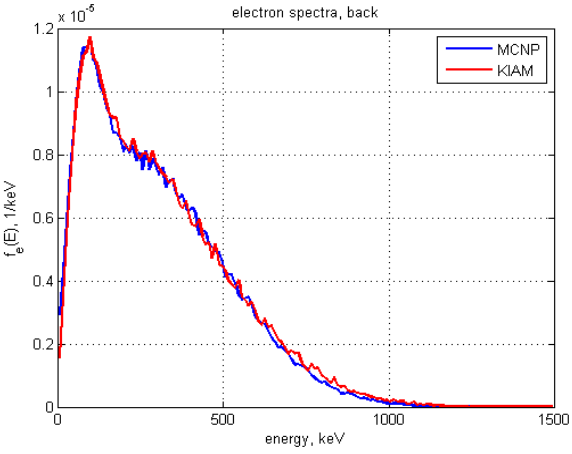

Fig.10. Spectra of electrons emitted from irradiated surface of the aluminum sample

Electron spectra pictured on fig. 9 and 10 are obtained for $E_0 = 1500\,keV$ and $h = 4cm$. Represented figures demonstrate satisfactory fit of results.

4.2 Modeling of experiment with ^{137}Cs source

Scheme of experiment is shown on fig. 11. An aluminum plate is irradiated by photons emitted from ^{137}Cs source. Measurements of radiation are carried out with use of silicon detector. Measured value is number of pulses $F(E)$, E is radiation energy deposit in detector.

It is obvious that a contribution in the measured value is made by emitted electrons and transmitted photons as well.

Next experimental technique is used for obtaining the emitted electrons contribution $F_e(E)$. Firstly the photon contribution $F_{ph}(E)$ is measured by performing the experiment without sample. Then the experiment with sample is carried out (measured value $F(E)$). Thus, $F_e(E)$ is calculated as:

$$F_e(E) = F(E) - F_{ph}(E). \quad (3)$$

Suggested experimental technique is reasonable when next conditions are fulfilled:

1. Gamma-radiation attenuation when passing through the sample is insignificant;
2. Contribution of scattered gamma-radiation is negligible in comparison with electron one;
3. Relative electron distribution in detector is appreciably larger than measurement error.

As shown in the paper[12] the conditions 1 – 3 are satisfied for ^{137}Cs as source and for the sample of 2 mm Al.

The comparison of computed data and experimental measurements are represented on the figure 12.

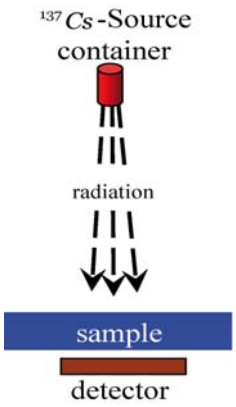

Fig.11. Scheme of the experiment

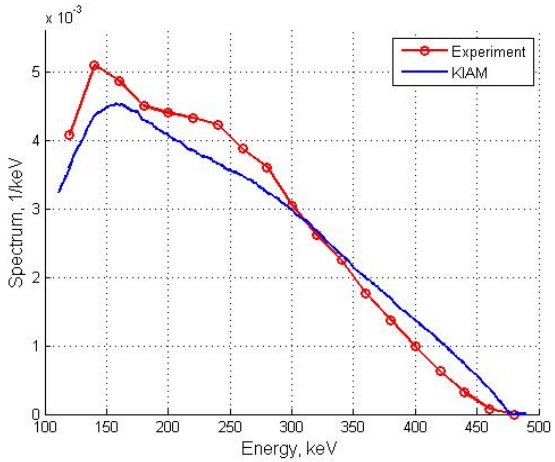

Fig.12. Energy deposit distribution. Red line – experiment; blue one – calculations.

5 CONCLUSION

Developed method is applicable for computing the characteristics of electron fluxes emitted from surfaces of objects being under radiation by use of hybrid supercomputers.

Constructed algorithms based on the Monte Carlo method modifications are effective for mathematical modeling of X-ray and electron transport on calculating systems with heterogeneous architecture. The significant feature of the method is the effective distribution of calculation between central processor and graphical one.

Acknowledgement. The work was partially supported by RFBR grant No 14-01-00350.

REFERENCES

[1] S. Goudsmit and J.L. Saunderson, "Multiple scattering of electrons. II", *Phys. Rev.*, **58**, 36-42 (1940).

[2] L.D. Landau, *On ionization energy losses of fast electrons*, Collected works, **1**, Moscow, "Nauka", (1969) (in Russian).

[3] M.E. Zhukovskiy, S.V. Podoliako, and R.V. Uskov, "Model of individual collisions for description of electron transport in matter", *Mathematical Models and Computer Simulations*, **4**, 1, 101-109, DOI: 10.1134/S2070048212010140 (2012).

[4] Stephen M. Seltzer, *An Overview of ETRAN Monte Carlo Methods*, in "Monte Carlo Transport of Electrons and Photons", edited by Theodore M. Jenkins, Walter R. Nelson, and Alessandro Rindi, Plenum Press, New York, **153**, (1988).

[5] M. Vilches, S. Garcia-Pareja, R. Guerrero, M. Anguiano, A.M. Lallena, "Monte Carlo simulation of the electron transport through thin slabs: A comparative study of PENELOPE, GEANT3, GEANT4, EGSnrc and MCNPX", *Nucl. Instrum. Meth.*, **B254**, 219-230 (2007).

[6] I.M. Sobol', *Numerical Monte Carlo Methods*, Moscow, "Nauka" (1973) (in Russian).

[7] http://www.nndc.bnl.gov/sigma/index.jsp?as=Elemental&lib=endfb7.0&nsub=113

[8] M.E. Zhukovskiy, R.V. Uskov, "Modeling of interaction gamma-radiation with matter on hybrid calculation systems", *Mathematical modeling*, **23**, 7, 20-32 (2011) (in Russian).

[9] M.E. Zhukovskiy, G.-R. Jaenisch, A. Deresch, R.V. Uskov, "Monte Carlo modeling of electron transport using CUDA technology", *Beitrag zu einem Tagungsband: 18th WCNDT - World conference on nondestructive testing (Proceedings)*, **89**, 1-8 ISBN 978-0-620-52872-6 (2012).

[10] M.E. Zhukovskiy, V.P. Zagonov, S.V. Podoliako, et al., "The application of surface oriented description of objects for modeling of transformation of X-rays in tasks of computational diagnostics", *Mathematical modeling*, **16**, 5, 103-116 (2004) (in Russian).

[11] J.F. Briesmeister (ed.), "MCNP – A General Monte Carlo N-Particle Transport Code", *LANL Report LA-13709-M*, Los Alamos, (2000).

[12] S.O. Vyazmin, A.G. Zhogov, M.E. Zhukovskiy, et al., "Modeling of experiment for research of radiative electron emission", *Mathematical modeling*, **24**, 6, 45-56 (2012) (in Russian).

Received March, 15 2014

MATHEMATICA MONTISNIGRI
Vol XXXI (2014)

ПРИБЛИЖЕННАЯ МЕТОДИКА ОЦЕНКИ СОПРОТИВЛЕНИЯ ТРЕНИЯ НА ТЕЛАХ ВРАЩЕНИЯ В ВЯЗКОМ ПОТОКЕ

А.Е. БОНДАРЕВ[1], Е.А. НЕСТЕРЕНКО[1, 2]

[1] Институт прикладной математики им. М.В. Келдыша РАН
Москва, Россия
[2] Московский государственный технический университет имени Н.Э. Баумана
Москва, Россия
e-mail: bond@keldysh.ru web page: http://www.keldysh.ru
e-mail: nesterenko_ea@bk.ru web page: http://www.keldysh.ru

Ключевые слова: вязкие течения, ламинарный и турбулентный режимы, верификация

Аннотация. Рассмотрен метод верификации численных расчетов вязких течений на основе приближенного полуэмпирического подхода. Приближенный подход основан на экспериментальных результатах для течения на пластине и методе эффективной длины. Методика используется для оценки коэффициента сопротивления трения и характерных толщин пограничного слоя в задачах обтекания осесимметричных тел вязким потоком. Описаны практические аспекты реализации метода и приведены результаты расчетов. Описанный подход может быть использован для отладки моделей и вычислительных кодов в случае отсутствия экспериментальных данных.

APPROXIMATE METHOD FOR ESTIMATION OF FRICTION FORCES FOR AXISYMMETRIC BODIES IN VISCOUS FLOWS

A.E. BONDAREV[1], E.A. NESTERENKO[1, 2]

[1] Keldysh Institute of Applied Mathematics Russian Academy of Sciences
Moscow, Russia
[2] Bauman Moscow State Technical University
Moscow, Russia
e-mail: bond@keldysh.ru web page: http://www.keldysh.ru
e-mail: nesterenko_ea@bk.ru - web page: http://www.keldysh.ru

Summary. The paper considers verification method for numerical modelling of bodies in viscous flow. The verification is based on approximate semi-empirical approach. The approach uses experimental data for flat plate and "effective length" method. One can apply approximate approach to estimate friction coefficient and specific thicknesses of boundary layer for axisymmetric objects placed in viscous flow. Practical aspects of approximate approach and numerical results are described. Described approach can be used for verification and improving of numerical models in the case of lack of experimental data.

2010 Mathematics Subject Classification: 76F40, 76F65.
Key words and Phrases: Viscous Flows, Laminar and Turbulent Regimes, Verification

1 ВВЕДЕНИЕ

В задачах численного моделирования обтекания тел потоком вязкого газа особое значение приобретает проблема верификации численных результатов. Это связано в общем и целом с тем, что моделирование вязких течений с использованием уравнений Навье-Стокса приводит к добавлению схемной вязкости к моделируемой физической вязкости исследуемой задачи. Исследователь должен иметь четкое представление о том, какая вязкость в итоге определяет численное решение: моделируемая физическая или добавляемая схемная, являющаяся свойством той или иной применяемой разностной схемы. Если для случая ламинарных течений возможно сравнение с известными решениями для пограничного слоя[1-3], то для турбулентных течений задача верификации становится еще более важной, так как применение той или иной модели турбулентности полностью определяет турбулентную вязкость задачи. Турбулентная вязкость на порядки превышает ламинарную и оказывает существенное влияние на итоговые аэродинамические характеристики тела в потоке газа.

Выбор модели турбулентности во многом определяет численное решение. Моделей существует большое количество, и при выборе конкретной модели и ее применении необходимо проведение верификационных процедур. Особенную важность это приобретает при использовании моделей турбулентности, объединяющих в себе свойства модели пристеночного типа и модели слоя смешения.

Наилучшей процедурой верификации является сравнение с натурным физическим экспериментом. Однако проведение подобного сравнения не всегда возможно ввиду отсутствия экспериментальной базы для конкретной исследуемой задачи. Для подобных случаев была разработана приближенная полуэмпирическая методика оценки коэффициента сопротивления трения тела в потоке и характерных толщин пограничного слоя. Под характерными толщинами пограничного слоя имеется в виду, как сама толщина пограничного слоя, так и характерные интегральные толщины: толщина вытеснения и толщина потери импульса.

Приближенная полуэмпирическая методика основана на экспериментальных работах Л.В. Козлова[4-6] и теоретических работах В.С. Авдуевского[7,8]. В работах Козлова описан и обобщен ряд экспериментальных исследований течения в турбулентном пограничном слое на плоской пластине. В этих экспериментах с помощью плавающего датчика проводились одновременные измерения напряжения поверхностного трения и тепловых потоков в турбулентном пограничном слое для различных значений чисел Маха и Рейнольдса и температурного фактора. В результате этих исследований стало возможным обобщение экспериментальных результатов для сопротивления трения и характерных толщин пограничного слоя в виде степенных зависимостей.

В.С. Авдуевский в своих работах[7,8] ввел понятие эффективной длины. Эффективная длина – это длина плоской пластины, на которой при внешнем течении с такими же параметрами, как и в рассматриваемой точке обтекаемого тела, нарастает такой же пограничный слой с аналогичными свойствами. Введение этого понятия позволило применить степенные зависимости Л.В. Козлова к телам вращения с криволинейной образующей.

Этот подход был модифицирован и широко применялся в начале 1990-х годов для оценки параметров пограничного слоя при моделировании вязкого обтекания тел вращения в практических расчетах. Следует заметить, что в те годы расчеты с

использованием полной системы уравнений Навье-Стокса и введением модели турбулентности были не столь распространены как сейчас. Методика использовалась для организации расчетов следующим образом. Моделирование обтекания тела проводилось невязким потоком с использованием системы уравнений Эйлера. Полученное распределение газодинамических функций на поверхности обтекаемого тела использовалось для оценки коэффициента сопротивления трения по приближенной методике. Далее формировался суммарный коэффициент сопротивления тела. Проводимые таким образом расчеты позволяли достигать погрешности при сравнении с натурным экспериментом не превышающей 3%.

В настоящее время описываемый приближенный подход к оценке сопротивления трения может оказаться также весьма полезным. Так, например, при расчетах обтекания тела вращения вязким потоком на основе использования полной системы уравнений Навье-Стокса для моделирования турбулентных режимов течения перед исследователем встает задача выбора модели турбулентности. А после выбора модели возникает следующая задача – надо провести «тонкую настройку» выбранной модели к исследуемому классу задач. При отсутствии экспериментальных данных приближенная методика, позволяющая по газодинамическим параметрам на границе пограничного слоя, получать оценочное значение коэффициента сопротивления трения, становится эффективным средством верификации.

2 ОПИСАНИЕ ПРИБЛИЖЕННОЙ МЕТОДИКИ

Рассмотрим обтекание осесимметричного тела вязким потоком сжимаемого газа под нулевым углом атаки (Рис.1)

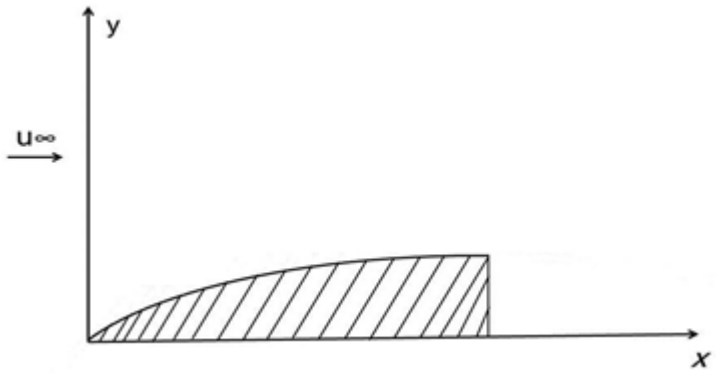

Рис. 1. Обтекание осесимметричного тела.

Суммарный коэффициент трения C_τ можно представить следующим образом[2]:

$$C_\tau = \frac{W}{\frac{\rho_\infty {u_\infty}^2}{2} S} = \frac{\int_0^S \tau_w dS \cos\alpha}{\frac{\rho_\infty {u_\infty}^2}{2} S} = \frac{\int_0^S C_f dS \cos\alpha}{S}.$$

Здесь ρ_∞ и u_∞ - плотность и скорость в набегающем потоке соответственно; S –

характерная площадь (площадь миделя тела или площадь боковой поверхности); W – суммарная сила трения; C_f – местный коэффициент трения; α – угол между осью OX и касательной к поверхности рассматриваемого тела.

Задача ставится, как нахождение в каждой точке осесимметричного тела местного коэффициента трения и дальнейшее нахождение суммарного коэффициента трения путем интегрирования местного коэффициента по всей поверхности тела.

Будем считать пограничный слой на теле турбулентным. Для плоской пластины, помещенной в вязкий поток, обладающий аналогичными свойствами, экспериментальные исследования Козлова[1-3] и других авторов позволяют находить местный коэффициент трения с помощью общей аппроксимирующей зависимости:

$$C_f = C_{f0}\left(1 + r\frac{\gamma - 1}{2}\mathrm{M}_w^2\right)^{-0.55},$$

где $r \approx 0.88$; $\gamma = C_p/C_v$ – соотношение удельных теплоемкостей; $\mathrm{M}_w = \frac{u_w}{a_w}$ - местное число Маха на теле.

Значение C_{f0} может быть вычислено с помощью целого ряда эмпирических зависимостей, приводимых в работах[1-3,7,8]. Например,

$$C_{f0} = (2\lg(\mathrm{Re}_x) - 0.65)^{-2.3};$$
$$C_{f0} = 0.085\,\mathrm{Re}_x{}^{-0.29+0.01 lg Re_x};$$
$$C_{f0} = 0.059\,\mathrm{Re}_x{}^{-0.2}.$$

Последняя зависимость дает наиболее приемлемые результаты в рассматриваемом диапазоне чисел Маха $0 \le M \le 10$, что подтверждено многочисленными расчетами. Она получила наибольшее распространение при использовании в диапазоне значений числа Рейнольдса от 10^6 до 10^8. Здесь число $\mathrm{Re}_x = \rho u x/\mu$ - это местное число Рейнольдса, вычисляемое по длине пластины *x* в каждой точке пластины.

Также при малых скоростях и отсутствии теплового потока в стенку может быть применен следующий подход[2]. Для наиболее интересного с точки зрения моделирования турбулентных течений диапазона чисел Рейнольдса от 10^5 до 10^{10} можно применять различные простые формулы для определения местного коэффициента трения C_{f0} в зависимости от местного числа Рейнольдса:

$$10^5 \le \mathrm{Re}_x \le 10^6; \quad C_{f0} = 0.042\,\mathrm{Re}_x{}^{-0.18};$$
$$10^6 \le \mathrm{Re}_x \le 10^7; \quad C_{f0} = 0.0322\,\mathrm{Re}_x{}^{-0.16};$$
$$10^7 \le \mathrm{Re}_x \le 10^8; \quad C_{f0} = 0.023\,\mathrm{Re}_x{}^{-0.14};$$
$$10^8 \le \mathrm{Re}_x \le 10^9; \quad C_{f0} = 0.016\,\mathrm{Re}_x{}^{-0.12};$$
$$10^9 \le \mathrm{Re}_x \le 10^{10}; \quad C_{f0} = 0.011\,\mathrm{Re}_x{}^{-0.10}.$$

Применение данного подхода в ряде случаев весьма полезно и позволяет получать более точный результат оценки.

Для того, чтобы применить эти зависимости для нахождения местного коэффициента трения на осесимметричном теле с криволинейной образующей, следует использовать метод эффективной длины, разработанный В.С. Авдуевским[4,5], который вкратце можно представить следующим образом.

Рассмотрим применение метода эффективной длины применительно к осесимметричному телу в некоторой точке с декартовой координатой x^* и радиусом R (Рис.2). Здесь l^* - длина дуги образующей от начал тела до рассматриваемой точки.

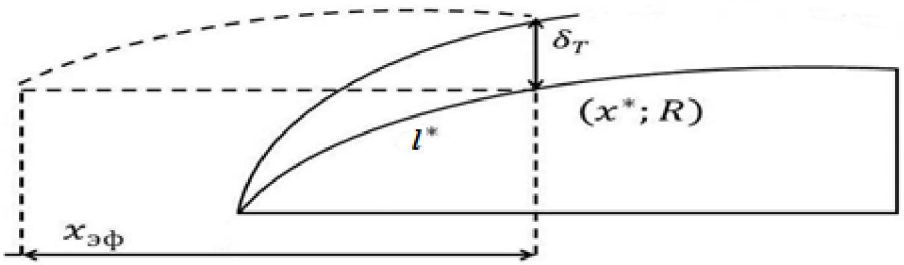

Рис.2. Применение метода эффективной длины.

Считаем, что в точке (x^*, R) на теле сформировался тепловой пограничный слой толщиной δ_T. Эффективной длиной $x_{эф}$ называют длину плоской пластины на которой при внешнем течении с такими же параметрами как в рассматриваемой точке тела нарастает такой же пограничный слой как и на длине l^* рассматриваемого тела. Для осесимметричного случая $x_{эф}$ будет длиной некоего цилиндра с радиусом равным радиусу R.

Согласно[7,8] для турбулентного случая эффективную длину в точке тела можно определить с помощью соотношения

$$x_{эф} = \frac{\int_0^{l^*} \rho_w u_w R^{1.25} dl}{\rho_w u_w R^{1.25}}.$$

Здесь ρ_w, u_w – значения плотности и скорости на внешней границе пограничного слоя. Теперь можно использовать вышеприведенные формулы для вычисления местного коэффициента трения, если во входящее в них число Рейнольдса вместо длины пластины x подставить вычисленную эффективную длину $x_{эф}$, вычисляя таким образом эффективное число Рейнольдса

$$\mathrm{Re}_{эф} = \frac{\rho_w u_w x_{эф}}{\mu_w}.$$

Здесь μ_w – значение коэффициента вязкости на теле, которое вычисляется, например, с помощью формулы Сазерленда или ее упрощенного представления:

$$\frac{\mu_w}{\mu_\infty} = \left(\frac{T_w}{T_\infty}\right)^{0.7}.$$

Для ламинарного случая процедура оценки проводится по аналогичной схеме с изменением ряда соотношений.

$$C_f = C_{f0}\left(1 + 0.72r\frac{\gamma - 1}{2}\mathrm{M}_w^2\right)^{-0.15};$$
$$C_{f0} = 0.646\,\mathrm{Re}_x{}^{-0.5}.$$

Кроме оценки коэффициента сопротивления трения на теле в рамках приближенного полуэмпирического подхода, представленного выше, можно определять в каждой конкретно взятой точке на образующей тела характерные параметры пограничного слоя, такие как толщина пограничного слоя δ и интегральные толщины пограничного слоя: толщина вытеснения δ* и толщина потери импульса δ**.

Толщина вытеснения δ* является мерой уменьшения расхода через сечение вследствие уменьшения скорости потока в пограничном слое. Толщина потери импульса δ** характеризует уменьшение импульса в сечении за счет торможения потока в пограничном слое.

Схема вычисления характерных толщин пограничного слоя в точке на теле для случая турбулентного пограничного слоя выглядит следующим образом: для каждой точки тела вычисляется эффективная длина $x_{эф}$. Далее по расчетным значениям определяется эффективное число Рейнольдса $\mathrm{Re}_{эф.}$. Далее определяются следующие величины для несжимаемого случая:

$$\delta_н = 0.37\,\mathrm{Re}_{эф}{}^{-0.2} x_{эф};$$
$$\delta^*{}_н = 0.125\,\delta_н;$$
$$\delta^{**}{}_н = 0.097\,\delta_н.$$

После их определения вычисляются характерные толщины для турбулентного сжимаемого пограничного слоя с помощью следующих соотношений[1-3].

$$\delta_{сж} = \delta_н \left(1 + 0.72r\frac{\gamma-1}{2}\mathrm{M}_w{}^2\right)^{0.34};$$
$$\delta^*{}_{сж} = \delta^*{}_н \left(1 + 0.72r\frac{\gamma-1}{2}\mathrm{M}_w{}^2\right)^{0.34};$$
$$\delta^{**}{}_{сж} = \delta^{**}{}_н \left(1 + 0.72r\frac{\gamma-1}{2}\mathrm{M}_w{}^2\right)^{-0.66}.$$

Для случая ламинарного течения используется аналогичный подход с заменой соответствующих соотношений. Для ламинарного пограничного слоя величины для несжимаемого случая $\delta_н$, $\delta^*{}_н$, $\delta^{**}{}_н$ определяются с помощью соотношений

$$\delta_н = 4.64\,\mathrm{Re}_{эф}{}^{-0.5} x_{эф};$$
$$\delta^*{}_н = 0.376\,\delta_{нсж};$$
$$\delta^{**}{}_н = 0.14\,\delta_{нсж}.$$

Набор характерных толщин для ламинарного пограничного слоя в сжимаемом потоке газа может быть вычислен с помощью следующих соотношений:

$$\delta_{сж} = \delta_н \left(1 + 0.72r\frac{\gamma-1}{2}\mathrm{M}_w{}^2\right)^{0.85};$$
$$\delta^*{}_{сж} = \delta^*{}_н \left(1 + 0.72r\frac{\gamma-1}{2}\mathrm{M}_w{}^2\right)^{0.85};$$
$$\delta^{**}{}_{сж} = \delta^{**}{}_н \left(1 + 0.72r\frac{\gamma-1}{2}\mathrm{M}_w{}^2\right)^{-0.15}.$$

3 ПРАКТИЧЕСКАЯ РЕАЛИЗАЦИЯ И ПРИМЕНЕНИЕ

Представленная в предыдущих разделах методика была реализована в виде двух самостоятельных программных модулей на C и Fortran90. Верификация программных модулей проводилась на данных расчета невязкого обтекания осесимметричного тела и сравнивалась с известными результатами работы[9], полученными с помощью численного решения уравнений Прандтля для двух чисел Маха. Результаты сравнения представлены ниже (C_τ^* – данные расчета, C_τ^{**} – данные работы[9]):

$$M_\infty = 1.5; \quad C_\tau^* = 0.0356; \; C_\tau^{**} = 0.03944;$$
$$M_\infty = 3.0; \quad C_\tau^* = 0.0281; \; C_\tau^{**} = 0.024.$$

Реализованные программные модули могут применяться пользователем автономно, а также могут достаточно просто подключаться к основным программам моделирования течений.

Разработанные программные модули применялись для оценки и отладки реализации модели турбулентности в двумерном программном комплексе, предназначенном для моделирования плоских течений и обтекания осесимметричных тел. Ниже приводится пример оценки толщины пограничного слоя на пластине для турбулентного случая. С помощью программного комплекса был проведен тестовый расчет течения на пластине при числе Маха набегающего потока $\mathrm{M} = 1.9$, температуре набегающего потока $T = 3000\,\mathrm{K}$ для турбулентного случая. Для моделирования турбулентности использовалась известная модель Смагоринского. На рисунке 3 приведена часть турбулентного профиля скорости.

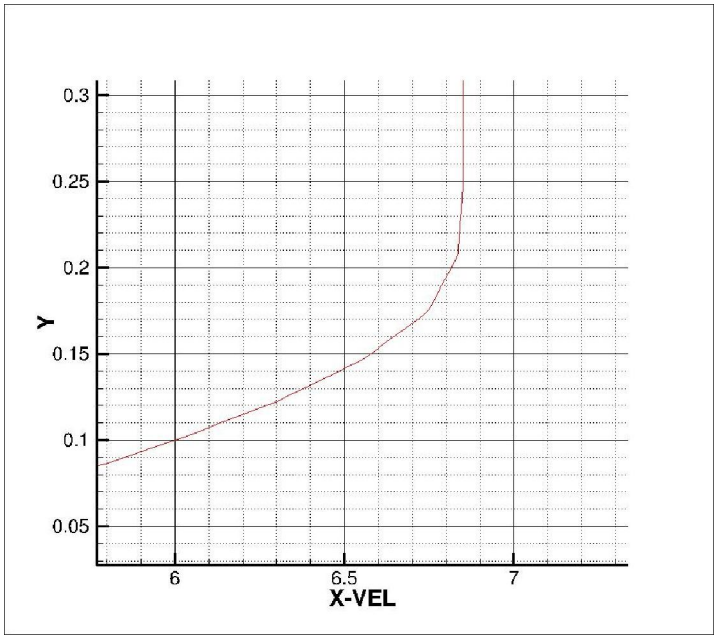

Рис.3 Профиль скорости для турбулентного расчета течения на пластине.

При практической оценке толщины пограничного слоя по расчетным результатам за толщину пограничного слоя обычно принимают толщину при значении скорости

равном $0.99U_\infty$, где U_∞ – скорость на внешней границе пограничного слоя.

Для данного сечения $U_\delta = 0.99U_\infty = 6.78$. Тогда для данного профиля расчетная толщина пограничного слоя $\delta_p = 0.18$. Проведение оценки по вышеприведенной методике Авдуевского-Козлова позволяет получить оценочное значение, равное $\delta_o = 0.173$. Расхождение расчетного результата с оценкой составляет 3.89 %. При этом необходимые газодинамические величины берутся из результатов основного расчета по внешней границе пограничного слоя.

Данное совпадение следует считать достаточно хорошим. Улучшение совпадения может быть достигнуто за счет изменения параметров используемой модели турбулентности.

Другой пример использования данной методики реализован для расчетов турбулентного обтекания осесимметричного тела, представленного на рисунке 4. Здесь показано тело вращения и изолинии скорости при обтекании тела турбулентным потоком при числе Маха, равном 2.08. Входные параметры для реализации приближенной методики оценки коэффициента сопротивления трения и характерных толщин пограничного слоя брались с внешней границы пограничного слоя (Рис.5).

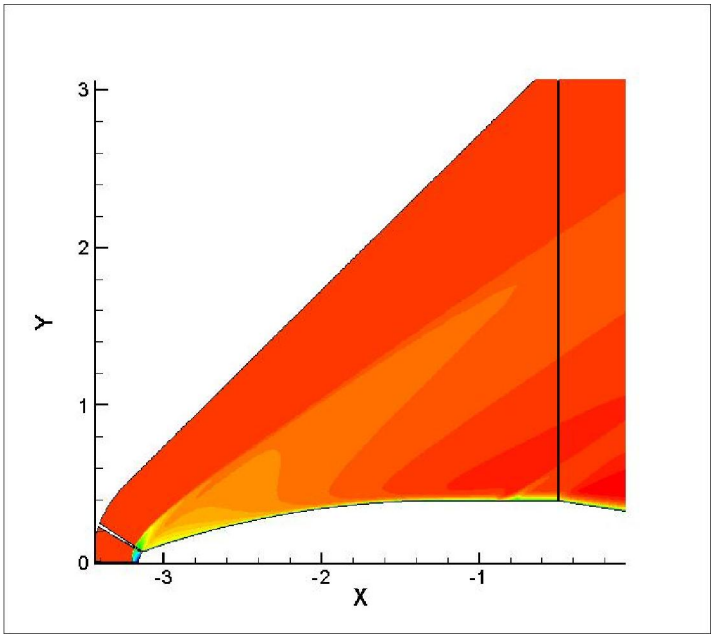

Рис.4. Распределение скорости при обтекании тела вращения.

В результате были получено следующее значение коэффициента сопротивления трения $C_\tau^* = 3.7382 \cdot 10^{-3}$. В качестве характерной площади при определении C_τ^* использовалась площадь боковой поверхности тела $S = 6.6614 \cdot 10^{-4}$ м^2. Соответственно, значение силы трения получалось равным $F = 0.7474$ Н. Данные значения были использованы в дальнейшем для отладки организации расчета и настройки параметров модели турбулентности.

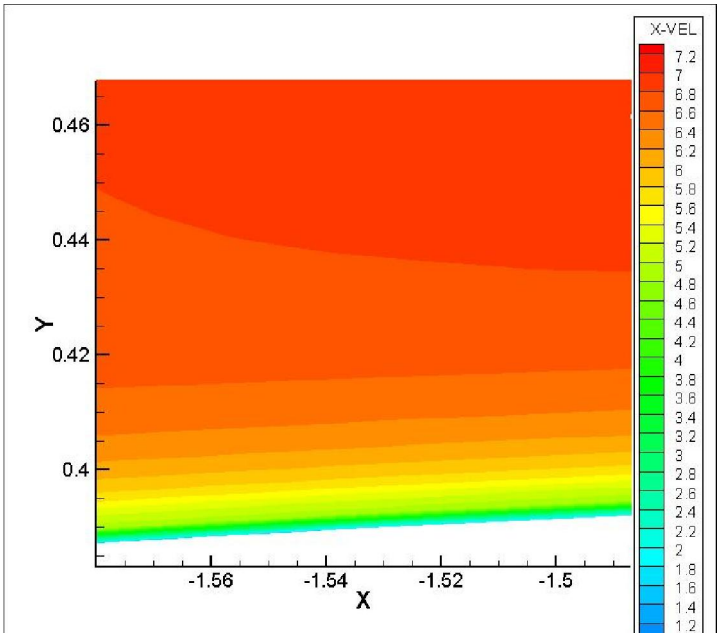

Рис.5. Распределение скорости в пограничном слое.

Следует заметить, что описанный подход в настоящей реализации обладает рядом существенных ограничений. Так по своей сути он не предполагает возможности отрыва пограничного слоя. Следовательно, течения с отрывом выпадают из рассмотрения. Далее, описанный подход не учитывает возможности перехода пограничного слоя из ламинарного режима в турбулентный. Описанный подход реализован лишь для тел в потоке под нулевым углом атаки. Тем не менее, для достаточно большого количества задач он позволяет получать оценки, которые могут служить определенными ориентирами для отладки моделей и методов расчета при отсутствии результатов натурных экспериментов и точных решений.

Для трехмерных задач, т.е. задач обтекания под ненулевым углом атаки, существует возможность применения описанного подхода вдоль линий тока, получение распределения местного коэффициента сопротивления трения по телу и последующее интегрирование его по поверхности (при условии безотрывного течения). Подобная реализация подхода предполагается при дальнейшей разработке. Также предполагается реализация учета явления перехода от ламинарного режима течения к турбулентному.

4 ЗАКЛЮЧЕНИЕ

Рассмотрена практическая реализация приближенного полуэмпирического подхода оценки коэффициента сопротивления трения и характерных толщин пограничного слоя при обтекании осесимметричных тел вязким потоком газа. Данный подход позволяет получать оценочные величины, которые могут быть полезны в задачах верификации моделей и численных методов. При отсутствии экспериментальных данных для конкретных практических задач данный подход может использоваться для отладки и настройки численных методов, организации расчетов, используемых моделей

турбулентности.

REFERENCES

[1] Krasnov N.F. *Aerodinamica*. M.: Visshaya shkola, (1976).

[2] Bondarev E.N., Dubasov V.T., Ryzhov Y.A. i dr. *Aerigidromeckanika*. M.: Mashinostroenie, (1993)

[3] Schlichting H. *Teoriya pogranichnogo sloya*. M.: Nauka, (1974)

[4] Kozlov L.V. ”Experimentalnoe issledovanie poverhnostnogo treniya na ploskoy plastine v sverhzvukovom potoke pri nalichii teploobmena“. *Izvestiya AN SSSR, OTN, Mekhanika i mashinostroenie*, **2**, (1963).

[5] Kozlov L.V. *Experimentalnoe opredelenie zakona teploobmena dlya turbulentnogo pogranichnogo sloya v sverhzvukovom potoke. Issledovanie teploobmena v potokah zhidkosti i gaza.* M.: Mashinostroenie, (1965).

[6] Kozlov L.V. i dr. *Modelirovanie teplovyh rezhimov kosmicheskogo apparata i okruzhayushey ego sredy*. M.: Mashinostroenie, (1971).

[7] Avduevskiy V.S. ”Metod rascheta prostranstvennogo turbulentnogo pogranichnogo sloya v szhimaemom gaze“. *Izvestiya AN SSSR, OTN, Mekhanika i mashinostroenie*, **4**, 3 (1962)

[8] Avduevskiy V.S. i dr. Pod red. prof. V.K. Koshkina. *Osnovy teploperedachi v aviatsionnoy i raketnoy tekhnike*. M.: Oborongiz, (1960).

[9] Kolina N.P., Pyatnova A.I., Solodkin E.E. ”Materialy dlya rascheta kharakteristik turbulentnogo pogranichnogo sloya na linii rastekaniya pri konicheskom vneshnem techenii“. *Trudi TSAGI*, (1979).

Поступила в редакцию 1 февраля 2014 года.

MATHEMATICA MONTISNIGRI
Vol XXXI (2014)

MOLECULAR DYNAMICS SIMULATION OF CRITICAL POINT PARAMETERS FOR SILICON

V.I. MAZHUKIN[1,2], A. V. SHAPRANOV[1,2], O.N.KOROLEVA[1,2], A.V. RUDENKO[3]

[1]Keldysh Institute of Applied Mathematics, RAS, Moscow, Russia
e-mail: vim@modhef.ru
[2] National Research Nuclear University MIPhI (Moscow Engineering Physics Institute)
Moscow, Russia
[3]Moscow Institute of Physics and Technology, State University (MIPT)
Moscow, Russia

Summary. On the basis of nine semi-empirical potentials: Stillinger-Weber (SW), Stillinger-Weber modification (SWM), Tersoff (T-C, T-D), EDIP, Erhart-Albe (EA-1, EA-2), KIHS and MIX using molecular dynamics modeling the critical parameters of silicon was determined. Analysis of simulation results and then comparing with calculations of other authors allowed us to determine the interaction potentials (EA-1, EA-2, KIHS and MIX) for which there is the greatest alignment with critical parameters of silicon used in practice.

1 INTRODUCTION

One of the fundamental problems in materials science is research of critical phenomena and determination of the critical parameters in the liquid - gas system for a wide range of pure metallic and nonmetallic materials [1,2]. Investigation of the behavior of matter in the vicinity of the critical point is a component of a more general problem - investigation of the properties of materials based on the equations of state [3-6]. However, up to the present for the vast majority elements parameters of the critical point has not been experimentally determined. The development of theoretical propositions is based on phenomenological [7, 8] and microscopic approaches [9, 10]. The use of phenomenological theory allowed us to obtain parameter estimates for a large number of elements [11]. The importance of determining the parameters of the critical point and its incompleteness are marked in [12].

During the last decades keen practical interest to critical phenomena has appeared and associated with wide application of concentrated energy flows (laser and electron beams, streams of fast particles), the power of which is sufficient to achieve near-critical and supercritical states [13,14]. In this field there are a number of unsolved problems relating to the behavior of nonequilibrium states, in particular, features of the behavior of superheated liquid phase during rapid heating of substance. Theoretical analysis of these problems can now be performed by means of mathematical modeling within the atomistic approach, in which the behavior of matter is described by molecular - dynamic (MD) models [15].

This work is devoted to the theoretical description, including determining the critical parameters such as pressure p_{cr}, density ρ_{cr} and temperature T_{cr} of silicon carried out by means of computational experiments (CEs) based on the molecular dynamics models.

2010 Mathematics Subject Classification: 82B26, 82B30, 82C27.
Key words and Phrases: Molecular dynamic, Interaction potentials, Critical parameters, Critical point, Silicon.

2 THE PROPOSED METHODS AND APPROACHES

Investigations of the behavior of matter in the vicinity of the critical point is traditionally generate an increased interest associated with a wide variety of physical properties and the unusual behavior of critical phenomena in the liquid - vapor system. Many critical phenomena experimentally were observed 50-100 years ago. From generalization of the experimental data it is known that the equation of state of condensed medium defines a surface in 3 dimensional space with coordinates: temperature T, density ρ, pressure p. Each of the points of this surface corresponds to the equilibrium state of the system. The surface projection on plane pT makes 3 separate areas corresponding to 3 aggregate states of matter: solid, liquid and gaseous. Solid and gaseous phases are in equilibrium along the curve of sublimation, solid and liquid - along the melting (hardening) curve and liquid and gaseous - along boiling (condensation) curve. Each point on these curves corresponds to the equilibrium state in which two phases can coexist. There is only one point, in which may coexist all three phases - the so-called triple point. On a plane pT the curve of sublimation from the triple point continues down to low temperatures, the melting (hardening) curve from the triple point goes to infinity, the boiling (condensation) curve in contrast to the melting curve is cut off at a certain point, called the critical point with coordinates $p_{cr}, \rho_{cr}, T_{cr}$. The fact that the boiling (condensation) curve terminates at the critical point means that the liquid (along the binodal curve) can be transformed into gas continuously without crossing the line of the phase transition, what is typical for phase transitions of the 2nd kind. The critical point is the only one point on the curve of phase equilibrium of liquid-gas - binodal, which coincides with the boundary of stability - the spinodal.

The critical state (as well as phase transitions of the second kind) on the phase equilibrium curve liquid-gas is a special singular point of the thermodynamic potential. Other points on this curve (binodal) do not consist any features of the thermodynamic potential . On the curve of phase equilibrium potentials of both phases are equal and each of them, with some reservations, can be extended into the metastable region. In the case of the critical point, the function of thermodynamic potential in a "foreign" temperature region does not correspond to any, even a metastable state. At the critical point the curve of phase transitions of the first kind of goes into a curve of phase transitions of the second kind. In the vicinity of the critical point phase transitions of the first kind are similar to the second order phase transitions. Thermodynamic quantities that depend on the first derivative of thermodynamic potential: entropy, specific volume, and others have small jumps of these derivatives, with simultaneous anomalous behavior of thermodynamic quantities that depend on the second derivative of thermodynamic potential: heat capacity, isothermal compressibility, thermal expansion coefficient, and others.

Phase transitions and related critical phenomena, vastly complicate the problem of their investigation both as physically and as mathematically. From a physical point of view of the complexity of critical phenomena is reduced to the necessity of explicit taking account of statistical fluctuations in the vicinity of the phase transition. Their existence and anomalous large value leads to an anomalous features a number of thermodynamic quantities. All physical difficulties inevitably manifested in attempts to make correct mathematical description of critical phenomena. At creation of corresponding mathematical models are used phenomenological [16,17] and atomistic approaches [18,19]. MD models describe a collection

of interacting particles (atoms, ions, molecules), and represent a system of differential equations. When using the MD models for the investigation of various properties of materials, including to determine the critical parameters $p_{cr}, \rho_{cr}, T_{cr}$ crucial role played by the choice of the interaction potentials between particles, since the accuracy of the results is directly dependent on it.

Therefore, despite the wide opportunities of MD models, their usage requires a careful test calculations to determine the suitability of the selected interaction potentials in certain specific circumstances. This problem is especially acute in material with covalent bonds, which include silicon.

Interatomic interaction in silicon is more complicated than in metals. Silicon refers to materials with covalent binding and has a number of structural features. So, under normal conditions, the silicon has a diamond structure, characterized by a small compactedness with the coordinate number of 4, which is much less than that of metals (8-12). As the pressure increases in silicon formed new structures - simple cubic, face-centered cubic with increasing coordination number, but differ little in energy. After melting liquid silicon becomes a metal with a coordination number of about 6 and with density greater than the density of the solid phase. The presence of these features makes the problem of constructing the interatomic interaction potential for silicon is not a simple task. At present there are several approaches to the construction of interatomic potentials for materials with covalent bonds. The best known and frequently used are the potentials Stillinger-Weber, (SW) [20], modification of Stillinger-Weber (SWM) [21], Tersoff, (T-C, T-D) [22 - 24], Erhart-Albe, (EA -1, EA-2) [25, 26] and KIHS [27], EDIP [28-30]. Comparative analysis of interatomic interaction potentials for crystalline silicon, made in [31] shows that in the aggregate of mechanical and thermophysical parameters and characteristics the results of calculations with any of the potential does not satisfy the required accuracy of coincidence with the referenced and experimental data. The smallest number of poorly matching parameters and characteristics in a wide range of temperature and pressure for monocrystalline silicon has showed by potentials SW, KIHS, EA-2 and MIX (MIX = (31KIHS + SWM)/32) - a linear combination of two potentials: SWM and KIHS). This fact should be taken into account when determining the parameters of the critical point. Therefore, by analogy with [31] simulation was carried out with the same interaction potentials, supplemented potential MIX [31]. Comparison of simulation results among themselves, with the experimental estimates and calculations of other authors will allow to estimate in the aggregate of characteristics the most appropriate interaction potential suitable for describing processes in the near-critical region.

To determine the critical parameters, there are several methods: of saturated vapor, of the heat of vaporization and of the average cluster size in the critical region, as well as meniscus, Cailletet - Mathias and isotherms methods (Van der Waals criteria) [7, 9, 32,33] that never used together and did not analyzed for their applicability. Statement of computational experiment allows for all of these methods to perform research for a wide class of interaction potentials on a single methodological basis and from a comparative analysis of simulation results to determine the most reliable values of the critical parameters of silicon.

3 STATEMENT OF THE PROBLEM, MATHEMATICAL MODEL AND COMPUTATIONAL ALGORITHM

Mathematical model. The basis of the method of molecular dynamics (MD) is a model representation of a multi-atomic molecular system in which the particles are represented by material points, each of which has a mass, radius vector and velocity, respectively $m_i, \vec{r}_i, \vec{\upsilon}_i$, where $i = 1 \ldots N$. Interaction between the particles is carried out by forces $\vec{F}_i = -\frac{\partial U(\vec{r}_1 \ldots \vec{r}_N)}{\partial \vec{r}_i}$, where $U(\vec{r}_1 \ldots \vec{r}_N)$ is the potential energy of interaction of the system of N particles; interaction with the external field occurs through the of force $\vec{F}_i^{ext}$. In the classical case, the movement of an ensemble of particles is described by the Newton equations.

As a result, the mathematical formulation of the problem consists of a system of ordinary differential equations, their difference analogue (difference scheme), the interatomic interaction potential and specifically defined initial and boundary conditions. The evolution of an ensemble of particles is described by the system of 2N ordinary differential equations of motion:

$$\begin{cases} m_i \dfrac{d\vec{\upsilon}_i}{dt} = \vec{F}_i + \vec{F}_i^{ext} \\ \dfrac{d\vec{r}_i}{dt} = \vec{\upsilon}_i \qquad i = 1 \ldots N \end{cases} \tag{1}$$

Initial conditions. Integration of the system of equations (1) requires the knowledge of the coordinates and velocities $(\vec{r}_i, \vec{\upsilon}_i)\big|_{t=0}$ for all N particles at the initial time t=0. At the initial time, the simulated environment is a crystal, polycrystal or liquid. To specify the initial values of macroscopic parameters more accurately as well as to ensure the sustainability of the system, a relaxation of the simulated ensemble is performed after setting the coordinates and velocities.

Combined use of a thermostat and barostat that returns energy to the chaotic component of the particle motion to hold a given temperature T and pressure allows to quickly bring the system to a steady state. After bringing the system to such state, certain modified values of the lattice constant, taking into account the influence of the boundaries of the object will be reached automatically.

Boundary conditions. In the case of an infinite domain with respect to one, two or three spatial directions *X, Y, Z*, the modeling of the processes is performed in the finite computational domain with the dimensions $L_x \times L_y \times L_z$ along *X*, *Y*, *Z* axes correspondingly. Periodic boundary conditions are used along *X*, *Y*, *Z* axes with the periods of L_x, L_y, L_z correspondingly.

Periodic boundary conditions along *X* assume that the particles with the coordinate *x* within the range of $0 \le x < L_x$ exactly represent the particles within $kL_x \le x < (k+1)L_x$ for any

integer $k \neq 0$. That is, the particle leaving the computational domain from the upper boundary $x = L_x$ is replaced by a new particle with the same value of velocity but entering the computational domain from the bottom boundary $x = 0$. If the accent marks the quantities relating to the new particle then:

$$\begin{cases} \vec{\upsilon}' = \vec{\upsilon} \\ x' = (x - L_x) \ \in \ [0, L_x) \ \text{for} \ L_x \le x < 2L_x \\ y' = y \\ z' = z \end{cases}$$

Similarly, for particles leaving the computational domain through the lower boundary $x = 0$:

$$\begin{cases} \vec{\upsilon}' = \vec{\upsilon} \\ x' = (x + L_x) \ \in \ [0, L_x) \ \text{for} \ -L_x \le x < 0 \\ y' = y \\ z' = z \end{cases}$$

The second important aspect of periodic boundary conditions is the force and potential energy of interaction of particles from the boundary areas: $0 \le x < r_{cr}$ and $(L_x - r_{cr}) \le x < L_x$, where r_{cr} is the cutoff radius for the potential (it is assumed that one can neglect the forces at the distances $r > r_{cr}$).

Interaction of the particle i, which coordinate x_i is within the range of $(L_x - r_{cr}) \le x_i < L_x$, with the particles beyond the computational domain $L_x \le x'_j < (L_x + r_{cr})$, is modelled using the particles $0 \le x_j < r_{cr}$ from the computational domain with radius-vectors being corrected during calculating the force $\vec{F}_{ij} = \vec{F}_{(\ldots \vec{r}'_j \ldots)}(\vec{r}_i)$ in the following way:

$$\vec{r}'_j = \vec{r}_j + \vec{e}_x L_x \ ,$$

where $\vec{e}_x$ is the axis X unit vector.

Obviously, all of the above applies equally to the periodic boundary conditions along the coordinate axes Y and Z.

Computational algorithm. As the object of the study we chose a dielectric film with the thickness of Z = 32 nm along the primary axis and with total size of the computational domain of 268 nm along that axis. The particles of the vapor phase were removed from the computation upon reaching the boundaries (permeable reflectionless boundaries). The size of the computational domain was 8x8 nm along the axes X, Y, with periodic boundary conditions. The total initial number of particles was 96 000. The mass of the particles corresponded to the one of silicon. The computations were performed for Si (diamond lattice with the lattice constant of 5.43A) with periodic boundary conditions (3D problem). The

integration timestep was set to 2 fs.

The computational algorithm was based on the finite-difference Verlet scheme [34]. During modeling we used different statistical ensembles: the microcanonical ensemble (NVE), where the number of particles N, the volume V and the total energy E are constant, the canonical ensemble (NVT), where only the kinetic energy of the molecules (temperature) is fixed instead of the total energy, and isothermal-isobaric ensemble (NPT), which provides a constant pressure. The velocity (for NVT) and pressure (for NPT) adjustment was carried out by means of a thermostat and Berendsen barostat.

A more detailed description of the mathematical statement of the problem and its numerical realization can be found in [35],[36].

4 MODELING RESULTS, DISCUSSION

We used the following approaches to determine the parameters of the critical point.

a) Method of the meniscus [9].

This method allows determining in a clear way the range of temperatures and densities, where the critical point is located for each of the considered interaction potentials. The method is based on the direct observation of the liquid and vapor in the two phase system in the numerical experiment.

The computational domain is partially filled with the model liquid at the temperature knowingly below the critical point. In a series of experiments, the initial temperature was set to 4000K. The initial mass of liquid m_{liq} was set low enough so that the average density calculated as the relation of this mass to the total volume of the computational domain m_{liq}/V was certainly below the critical density. Next, the system is brought to a steady state, in which a dynamic equilibrium is set between the liquid and the saturated vapor when the flow of particles emitted from the fluid is equal to the flow of particles returning from the vapor to the liquid. This is the state when the values of the pressure as well as the values of the density of liquid and saturated vapor are measured in the system.

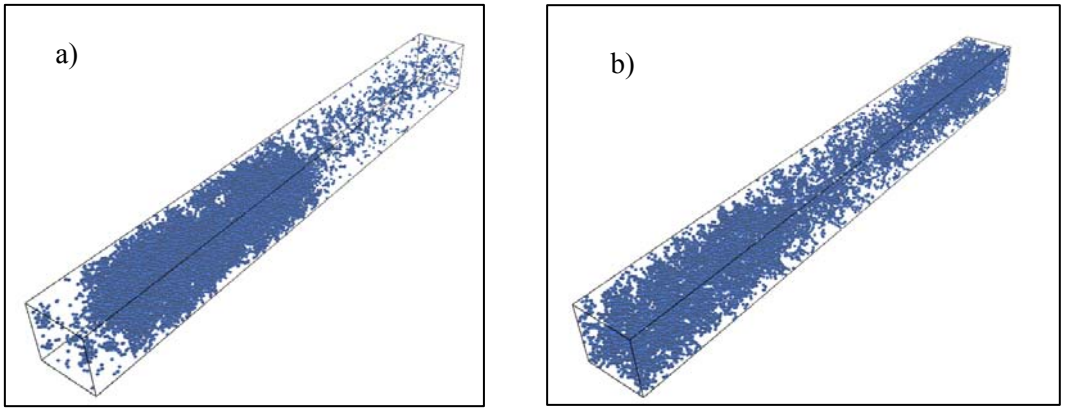

Fig.1. Steady states in the computational domain at 7000 K (a) and 8000 K (b) for the potential T-C.

This experiment and measurements are repeated at every step at the higher temperature

value. At some temperature value of T_0, the density becomes uniform across the whole computational domain. Fig. 1 shows an example of two steady states for the non-uniform (a) and uniform (b) distributions of density across the volume at the temperatures of 7000 K и 8000 K correspondingly. Since the initial mass of liquid was such that the average density was certainly below critical one, then $T_0 < T_{cr}$ as well, i.e. at such temperature the liquid will vaporize completely.

Then the initial mass of liquid (at constant size of the computational domain) is increased and a series of experiments with different temperatures is repeated again. The temperature T_0 is determined again, i.e. when the density becomes uniform across the volume of the computational domain for the new initial mass of liquid m_{liq}. The dependence $T_0(m_{liq})$ is non-monotonous and has a maximum equal to the critical temperature T_{cr} exactly when $m_{liq}/V = \rho_{cr}$. To clarify the position of this peak, we further use the method of Cailletet-Mathias [7]. Thus, the critical parameters are in the region of the transition from a state in which one can clearly distinguish the boundary between liquid and vapor (lower limit) to a state where the entire system is uniformly occupied with vapor (upper limit).

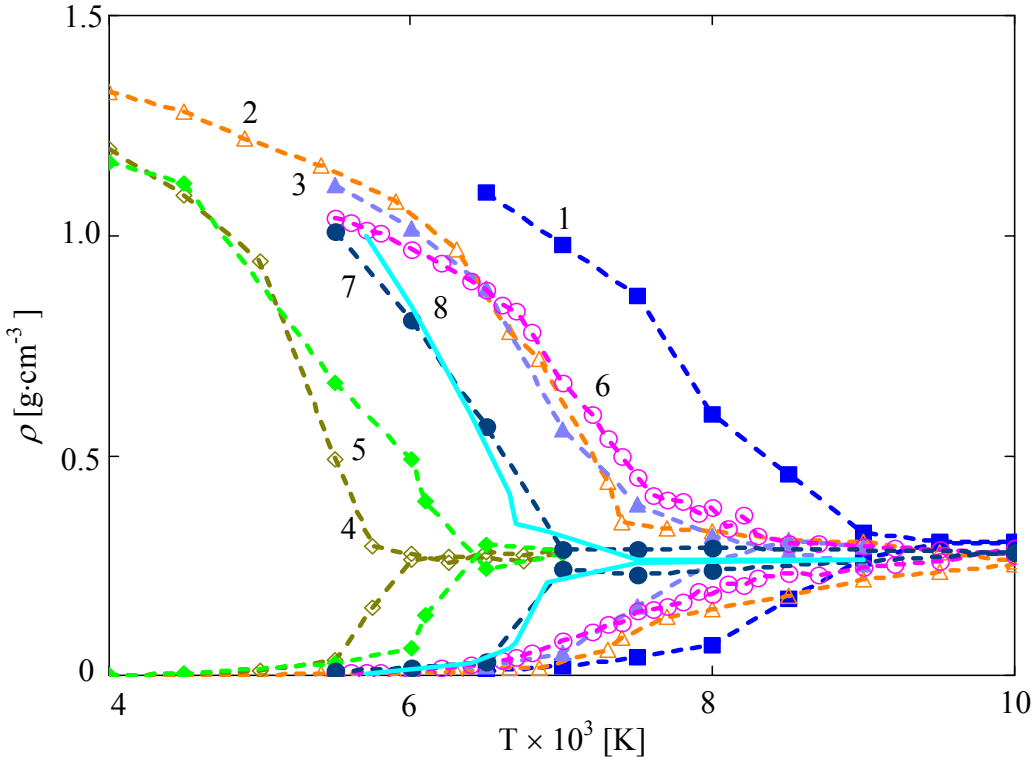

1 – SW; 2 – T-C; 3 – T-D; 4 – EA-1; 5 – EA-2; 6 – EDIP; 7 – KIHS; 8 – MIX.

Fig.2. Temperature dependence of the saturated vapor (below) and liquid (above) for different potentials.

b) Method of Cailletet and Mathias [7].

According to this method, the average density of the liquid and gaseous phases lie on a straight line, called the rectilinear diameter. The point of intersection of the rectilinear diameter with the density curve determines the critical value of the density and temperature.

Fig. 2 shows the temperature dependence of the densities of the liquid and vapor, resulting from a series of experiments described above, which are used to clarify the critical parameters using this method.

Thus, we used here the definition of the critical temperature as the temperature, at which the pressure and density of the vapor have a maximum, while the density of the liquid being in a dynamic equilibrium with the vapor is minimized.

c) Temperature dependence of the saturated vapor [7].

One can determine the critical pressure (at the known critical temperature) analyzing the temperature dependence of the pressure of the saturated vapor. The obtained temperature dependencies of the saturated vapor pressure are shown in Fig. 3. When passing through the critical point, there is a change of behavior: the strongly non-ideal saturated vapor described by an exponential function in the subcritical region is transformed into an ideal one with the linear dependence in the supercritical region.

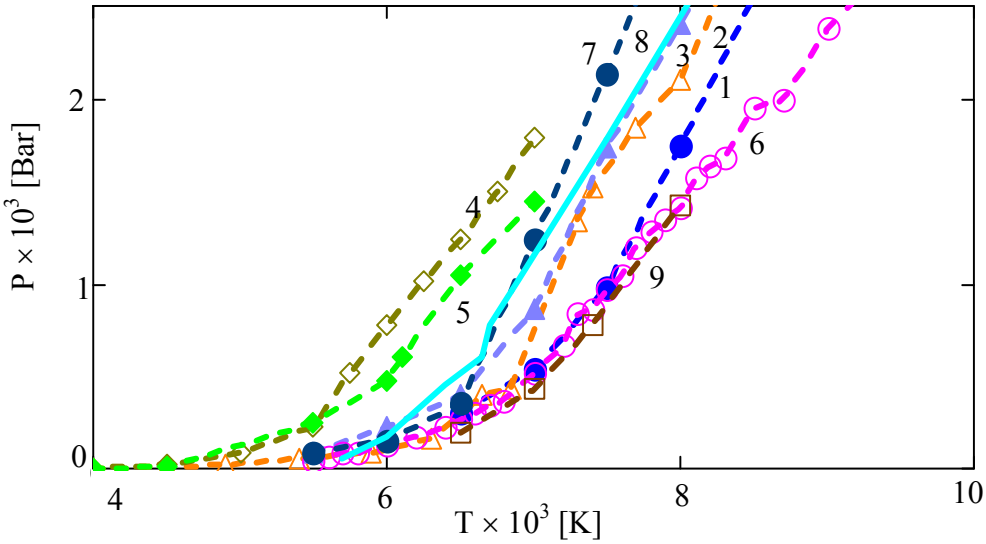

1 – SW; 2 – T-C; 3 – T-D; 4 – EA-1; 5 – EA-2; 6 – EDIP; 7 – KIHS; 8 – MIX; 9 – SWM.

Fig. 3. Temperature dependencies of the saturated vapor pressure for different potentials

d) Temperature dependence of the heat of vaporization [33].

Since in the critical point the dividing line between the properties of the gaseous and liquid phases disappears, the heat of vaporization, which is determined by the difference of the enthalpies of the liquid and gaseous phases, vanishes. In a series of computational experiments similar to those described above, the temperature dependencies of the enthalpy of the liquid phase and the vapor were measured. Next, we calculated the difference between them at the same temperatures and obtained a family of curves for different interaction potentials (Fig. 4). The point where the heat of vaporization vanishes was assumed as the critical temperature for each of the potentials used.

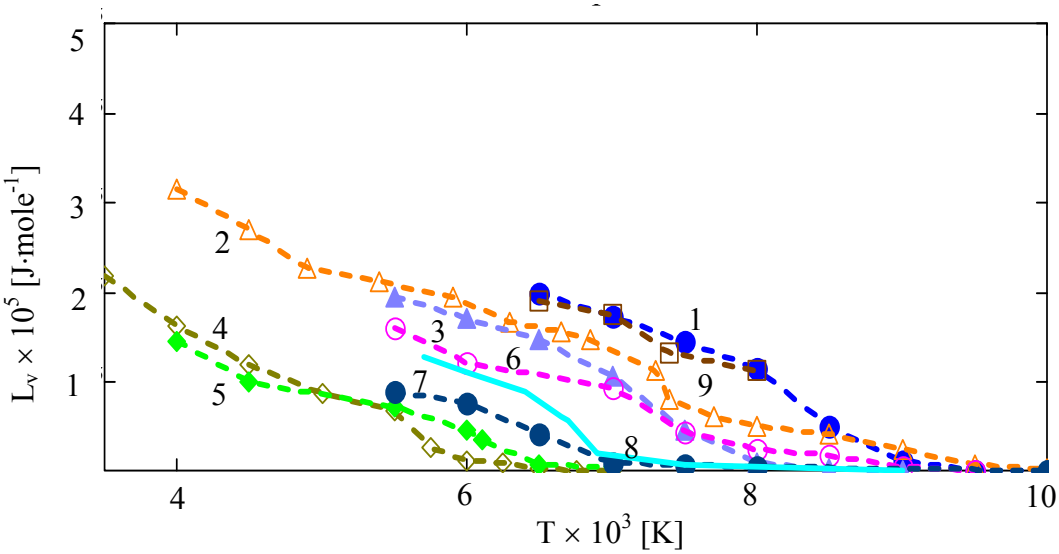

1 – SW; 2 – T-C; 3 – T-D; 4 – EA-1; 5 – EA-2; 6 – EDIP; 7 – KIHS; 8 – MIX; 9 – SWM.

Fig.4. Temperature dependence of evaporation heat

e) Temperature dependence of the average cluster size.

In the subcritical region, the density and pressure of saturated vapor increase with increasing temperature. In the near-critical region, atomic vapor particles begin to unite into clusters, which reach their maximum size just at the critical point. As the temperature increases further, the density no longer grows. In this case, the clusters begin to break up into smaller ones due to the increase of the kinetic energy of random motion. That is, the average size of the cluster must have a singularity at the critical point. This fact is used in this method to determine the critical temperature.

Mean number of atomic particles forming a cluster can be estimated using the formula

$$\langle N \rangle = \frac{n(T) k_B T}{P_{sat}(T)},$$

where $P_{sat}(T)$ is the saturated vapor pressure at the temperature T, $n(T)$ is the concentration of atomic particles in the saturated vapor.

The temperature dependence of $\langle N \rangle$ temperature has a typical bend at the critical point (Fig.5).

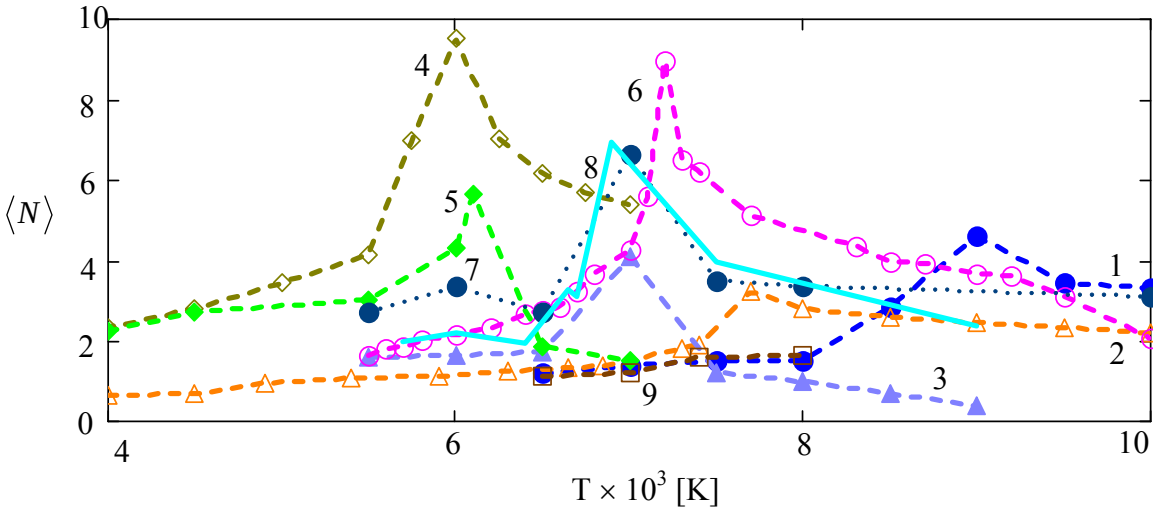

1 – SW; 2 – T-C; 3 – T-D; 4 – EA-1; 5 – EA-2; 6 – EDIP; 7 – KIHS; 8 – MIX; 9 – SWM.

Fig.5. Temperature dependence of the average cluster size

f) Method of isotherms (criteria of Van der Waals) [7,9].

It is known from the theory of van der Waals that in the critical point, the first and second derivatives of the pressure with regard to volume (density) vanish. For a set of fixed values of temperature (in the range of sub- and super-critical values), the dependencies (isotherms) of pressure vs. density for each of the potentials are plotted. To do this, a cubic computational domain with periodic boundary conditions in all three axes is completely filled with liquid at a fixed temperature. The system is brought to a steady state and then the pressure is measured. Further, the size of the computational domain without changing the number of particles and keeping the temperature constant is increased in the same three directions. Again, the system relaxes to a steady state and the pressure is measured.

Since the isotherms corresponding to a temperature below the critical one have a deflection and a clear minimum, one can select the isotherm, in which the deflection and minimum are absent (tangent to the graph is zero) - and it will be the closest to the critical isotherm. For example, for the potential of Erhart-Albe2 at T=5500 K, the isotherm has a clear deflection (Fig. 6). For the isotherm T=6250 K, it is almost imperceptible.

Received critical parameters of silicon (Fig. 1-6) are summarized in Table 1. Estimates of the parameters of the critical point [37, 38] used in the industry as well as the results of a simulation performed by the authors [39,40] Monte Carlo for a potential Stillenzhera - Weber placed there as well.

Critical temperature determined from the dependence (Fig. 1-6). The procedure for calculating the average cluster size was the most accurate. The critical pressure is determined from the temperature dependence of the saturated vapor, Fig. 3. Cailletet - Mathias method for determining the values of the critical density was used.

If the basis is recommended estimations [37, 38], the potentials of the EA-1, EA-2, KIHS and MIX show closest values of the critical parameters. Potentials WS and Tersoff show the largest deviation from the recommended estimations [37, 38].

At the same time the critical parameters for the potential Stillinger-Weber is in good agreement with the results for the SW obtained in the calculation [39, 40], which indicates that the decisive role of the interaction potential, rather than the method that was used.

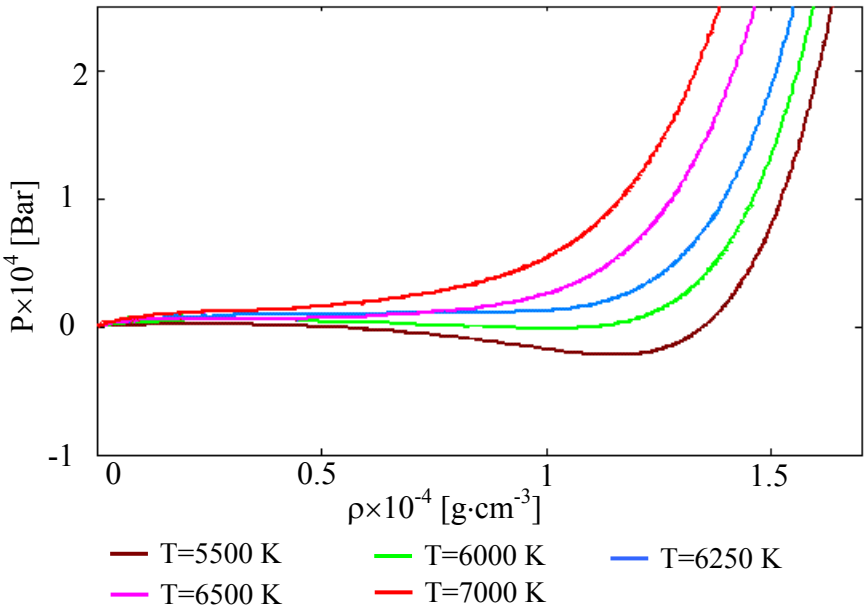

Fig.6. Method of isotherms to determine the critical temperature (potential of EA-2).

	Critical temperature, K	Critical density, g/cm^3	Critical pressure, bar
SW [20]	8550 ± 250	0.27 ± 0.06	2200 ± 400
T-C [23]	7750 ± 250	0.24 ± 0.04	1900 ± 100
EDIP [29]	7500 ± 250	0.31 ± 0.08	1000 ± 100
T-D [24]	7250 ± 250	0.23 ± 0.07	1300 ± 300
SWM [21]	7700 ± 250	0.25 ± 0.06	1200 ± 200
KIHS [27]	6850 ± 250	0.24 ± 0.06	800 ± 300
MIX [31]	6650 ± 250	0.22 ± 0.07	650 ± 100
EA-1 [26]	5750 ± 250	0.19 ± 0.05	500 ± 100
EA-2 [25]	6250 ± 250	0.24 ± 0.04	800 ± 100
Estimations [37, 38]	5160	0.1207	530
Calculations (SW) [39]	7500 ± 500	0.75 ± 0.1	-
Calculations (SW) [40]	7925 ± 250	0.76 ± 0.5	1850 ± 400

Table. 1. Critical parameters of silicon for different interaction potentials.

5 CONCLUSIONS

According to carried out computational experiments and analysis of the dependencies were determined critical values: pressure p_{cr}, density ρ_{cr} and temperature T_{cr} of the silicon to 9 interaction potentials. Statement of computational experiments carried out for 6 physical methods: meniscus [9], Cailletet - Mathias [7], the van der Waals isotherms [7,9], the temperature dependence of the saturated vapor [7], the temperature dependence of the heat of vaporization [33] and the average cluster size (method proposed by the authors).

Comparison of the simulation results (Table 1) with critical parameters used in practical applications [37,38] showed that the best agreement observed for potentials EA-1, EA-2, MIX and KIHS.

Comparison of the obtained critical parameters for the potential Stillinger -Weber [20] with results of calculations based on Monte-Karlo methods [39,40] for the same potential showed good agreement of results with each other, but with a large scatter of data [37,38]. Performed analysis allows us to recommend for modeling high-temperature processes ($T_m < T \le T_{cr}$) in silicon exactly potentials EA-1, EA-2, MIX and KIHS, in contrast to low-temperature processes ($T \le T_m$) where according to [31] classical potential Stillinger -Weber [20] and potentials KIHS, EA-2 and MIX have the advantage.

This work was supported by RFBR projects №13-07-00597, №15-07-05025.

REFERENCES

[1] Shang-Keng Ma, *Modern Theory of Critical Phenomena,* Benjamin, New York, (1976). Perseus, (2000).

[2] H. E. Stanley, *Introduction to Phase Transitions and Critical Phenomena,* Oxford University Press, Oxford and New York, (1971).

[3] Zel'dovich Ya B and Raizer Yu P, *Physics of Shock Waves and High-Temperature Hydrodynamic Phenomena*, New York: Academic, (1966).

[4] *Shock waves and extreme states of matter*, Under. Ed. V.E.Fortova, L.V.Altshulera et al., Moscow, Nauka, (2000).

[5] Soboleva E.B., "On the influence of the equation of state for simulation of convective flow and heat transfer in the near-critical fluids", *Teplofizika vysokikh temperature*, **38**, 6, 928 - 934, (2000).

[6] Povarnitsyn M.E, Itina T. E, Levashov P. R., Khishchenko K. V., "Simulation of ultrashort double-pulse laser ablation", *Applied Surface Science*, **257,** 5168–5171, (2011).

[7] V.A. Kirililin, V.V. Sychev, A.E. Sheindlin, *Technical thermodynamics*, M.: Izdatel`stvo MEI, (2008).

[8] Skripov V.P., *Metastable liquid,* M., Nauka, (1972).

[9] Leibfrid G., *Microscopic theory of mechanical and thermal properties of crystals*, M.: Fizmatgiz, (1963).

[10] Shambhu N. Sharma, Hiren G. Patel, *The Fokker-Planck equation. Stochastic Control*, Edited by Chris Myers, ISBN 978-953-307-121-3, Publisher Sciyo, Published in print edition August, InTech, (2010).

[11] Fortov V.E., Dremin A.N., Leont`ev A.A., "Estimation of the parameters of the critical point", *Teplofizika vysokikh temperature*, **13**, 5, 1072-1079, (1975).

[12] V.E.Fortov, I.V.Lomonosov, "Ia.B. Zeldovich and problems of equations of state of matter under extreme conditions", *UFN*, **184**, 3, 231 – 245, (2014).

[13] Morel V, Bultel A, Cheron B G., "The Critical Temperature of Aluminum", *Int. J. Thermophys*, **30**, 1853-1863, (2009).

[14] Porneala C, Willis D.A., "Time-resolved dynamics of nanosecond laser-induced phase explosion", *J. Phys. D: Appl. Phys*, **42**, 155503 (1-8) (2009).

[15] C.Wu, L.V. Zhigilei, "Microscopic mechanisms of laser spallation and ablation of metal targets from large-scale molecular dynamics simulations", *Appl. Phys. A*, **114**, 11-32, (2014).

[16] Lu Q., Mao S.S., Mao X., Russo R. E., "Delayed phase explosion during high-power nanosecond laser ablation of silicon", *Applied Physics Letters*, **80**, 17, 3072-3074, (2002).

[17] D. Autrique, G. Clair, D. L'Hermite, V. Alexiades, A. Bogaerts, B. Rethfeld, "The role of mass removal mechanisms in the onset of ns-laser induced plasma formation", *J.Appl. Phys.*, **114**, 023301 (1-10), (2013).

[18] Perez D, Lewis L.J., "Molecular-dynamics study of ablation of solids under femtosecond laser pulses", *Phys. Rev. B*, **67**, 184102 (1 –15), (2003).

[19] Cheng J., Liu C., Shang S., Liu D., Perrie W., Dearden G., Watkins K., "A review of ultrafast laser materials micromachining", *Optics & Laser Technology*, **46,** 88–102, (2013).

[20] H. Stillinger and T. A. Weber, "Computer simulation of local order in condensed phases of silicon", *Phys. Rev. B*, **31**, 5262-5271 (1985).

[21] L. Pizzagalli, J. Godet, J. Guenole, S. Brochard, E. Holmstrom, K. Nordlung, T. Albaret, "A new parameterization of the Stillinger-Weber potential for an improved description of defects and plasticity of silicon", *J. Phys, Condens. Matter* **25**, 055801, (2013).

[22] J. Tersoff, "New empirical model for the structural properties of silicon", *Phys. Rev. Lett.* **56**, 632-635 (1986).

[23] J. Tersoff, "New empirical approach for the structure and energy of covalent systems", *Phys. Rev. B*, **37**, 6991-7000, (1988).

[24] J. Tersoff, "Modeling solid-state chemistry: Interatomic potentials for multicomponent systems", *Phys. Rev. B,* **39**, 5566-5568, (1989).

[25] P. Erhart and K. Albe, "The role of thermostats in modeling vapor phase condensation of silicon nanoparticles", *Appl. Surf. Sci*., **226**, 12-18, (2004).

[26] P. Erhart and K. Albe, "Analytical potential for atomistic simulations of silicon, carbon, and silicon carbide", *Phys. Rev. B,* **71**, 035-211 (2005).

[27] T. Kumagai, S. Izumi, S. Hara, and S. Sakai, "Development of bond-order potentials that can reproduce the elastic constants and melting point of silicon for classical molecular dynamics simulation", *Comp. Mater. Sci*. **39**, 457, (2007).

[28] M. Z. Bazant, E. Kaxiras, "Modeling of covalent bonding in solids by inversion of cohesive energy curves", *Phys. Rev. Lett.* **77**, 4370 (1996).

[29] M. Z. Bazant, E. Kaxiras, J. F. Justo, "Environment-dependent interatomic potential for bulk silicon", *Phys. Rev. B*, **56**, 8542, (1997).

[30] J. F. Justo, M. Z. Bazant, E. Kaxiras, V. V. Bulatov, and S. Yip, "Interatomic potential for silicon defects and disordered phases", *Phys. Rev. B*, **58**, 2539 (1998).

[31] Mazhukin V. I., Shapranov A. V., Rudenko A. V., "Comparative analysis of potentials of interatomic interaction for crystalline silicon", *Mathematica Montisnigri*, **30**, 56-75, (2014).

[32] Kireev V.A. Short, *Course of Physical Chemistry*, M., (1970).

[33] J. O. Hirschfelder, Chf. Curtiss, R. B. Bird, *Molecular theory of gases and liquids*, Wiley, New York, (1954).

[34] Verlet L., "Computer "Experiments" on Classical Fluids. I. Thermodynamically Properties of Lennard-Jones Molecules." *Phys. Rev*., **159**, 98-103, (1967).

[35] Mazhukin V.I., Shapranov A.V., Samokhin A.A., Mazhukin A.V. Koroleva O.N., "Visualization and analysis of the results of molecular-dynamic modeling of intensive evaporation of liquid in the near-critical region", *Scientific Visualization,* **6**, 4, 72-95, (2014).

[36] Mazhukin V.I., Shapranov A.V., Samokhin A.A., Ivochkin A.Yu., "Mathematical modeling of non-equilibrium phase transition in rapidly heated thin liquid film", *Mathematica Montisnigri*, **27**, 65 - 90, (2013).

[37] *Innovative Engineering with Advanced Material Science*, SiFusion Polysilicon Furnaceware Technology, http://sifusion.ferrotec.com/products/sifusion/science/physical/.

[38] *Physical Properties and Critical Constants of Silicon*, Boston Electronics Corporation, http://www.boselec.com/products/matsiphy.html.

[39] N. Honda, Y. Nagasaka, "Vapour-liquid equilibrium of Silicon by Gibbs Ensemble Simulation", *Int. J. Thermophys*, **20**, 837 - 846, (1999).

[40] D. V. Makhov, Laurent J. Lewis, "Isotherms for the liquid-gas phase transition in silicon from NPT Monte Carlo simulations", *Phys. Rev. B*, **67**, 153202, (2003).

Received February, 10 2014

MATHEMATICA MONTISNIGRI
Vol XXXI (2014)

MODELING OF THE LASER METAL NANOPARTICLES FRAGMENTATION

I.N. ZAVESTOVSKAYA[1,2], A.P. KANAVIN[1,2]

[1]P.N. Lebedev Physical Institute, RAS, Moscow, 119991, Russia

[2]National Research Nuclear University "MEPhI",
Moscow, 115409, Russia

Abstract. The paper considers a physical model of metal nanoparticles fragmentation in liquids under the action of femtosecond laser pulses at the example of gold particles in water. The model is based on the electrolization of metal nanoparticles heated by a laser pulse, and their division under the development of instability of a charged drop of liquid metal. The process of hot electrons emission from the surface of a nanoparticle and further solvation in liquid has been studied. The critical fragmentation parameter, namely a particle charge, has been defined.

1 INTRODUCTION

Laser nanostructuring of materials is important in many scientific, technological and medical applications [1-4]. Of special interest are the metal nanoparticles, in particular the gold ones. Their unique optical properties stimulate the research of possible applications in optics, photonics, and biomedicine [5-15]. All the methods of producing nanoparticles may be conventionally divided into two groups: *wet chemistry* i.e., the chemistry using liquid components [16,17] and *dry processes* i.e., the processes with the use of plasma discharge or those that make use of the synthesis of the needed product in flame, as well as the material evaporation under the action of a laser pulse.

Laser ablation has manifested itself as one of most effective physical methods of nanofabrication [18-25]. However, the laser methods form rather large-sized nanoparticles with a wide size spectrum. In this connection, in order to reduce the size of nanoparticles their colloids are additionally treated by ultrashort laser pulses [25-28]. The mechanism of laser nanoparticles fragmentation in liquids has not been much studied and there is no consensus on this problem. They name the following possible mechanisms: the hydrodynamic instability of the melted metal drop arising due to its interaction with the liquid vapor [25]; the evaporation of gold atoms under heating the nanoparticles by laser radiation [26]; the Coulomb explosion [27,28].

A physical model of gold nanoparticles fragmentation in water under the action of femtosecond laser pulses is presented in this paper. When the colloids of relatively large gold nanoparticles (several tens of *nm*) are irradiated by femtosecond laser pulses, one can observe their fragmentation into smaller nanoparticles (up to several nm). In the process the particle is heated up to the melting temperature and turns into a drop of liquid. The heating is accompanied by thermionic emission from the drop surface. The emitted electrons take away the negative charge, and the drop of melted metal turns to be positively charged. Thus the model of fragmentation is based on the electrolization of metal nanoparticles heated by a laser

2010 Mathematics Subject Classification: 82D80, 81T80, 37N20.
Key words and Phrases: Nanoparticle fragmentation, femtosecond laser pulses, solvation, particle charge.

pulse, and their division under the development of instability of a charged drop of liquid metal. As a mechanism of electrolization we have considered the emission of hot electrons from the surface of a nanoparticle with further salvation in liquid. The problem of gold particles heating at femtosecond laser pulse absorption has been solved. Time dependence of electron thermionic emission current from the particle surface has been found. The particle fragmentation parameter has been defined. The estimates are given of nanoparticle charge gained under the action of the laser pulse in water.

2 EXPERIMENTAL RESULTS

Laser ablation is an effective method of nanofabrication. The method presents an ablation of a solid target by strong laser radiation, and this leads to the ejection of the target components, and formation of nanoclusters and nanostructures. Generally, the size and structure of nanoobjects produced with the help of laser ablation are influenced by the following factors:

- The laser radiation characteristics: intensity, pulse duration, and the wavelength.
- Target material properties: absorption at different wavelengths, the melting, vaporization and crystallization temperatures.
- The environment properties: vacuum, gas, liquid.

When laser radiation is focused onto the solid target surface there takes place the absorption of the laser energy, which results in thermal and nonthermal heating of the target material, melting and ablation of the material in the form of atoms and nanoclusters.

At the same values of laser intensity the mass of particles produced by ablation depends on the amount of energy absorbed from the laser pulse. Micro- and nanosecond pulses contain more energy as compared to pico- and femtosecond ones, and this makes the ablation with longer pulses more effective to produce a greater mass of particles. However, one should note that ultrashort pulse ablation leads to the ejection of particles of higher energy due to high intensity of the laser pulse.

Target laser ablation may be accompanied by hot plasma formation. If the plasma is produced near the target, it may decrease the efficiency of energy transfer to the target surface, as well as give rise to secondary ablation of the material due to the target heating or cavitation phenomena (in liquid media). These effects are well illustrated in [21], in which the authors studied the dependence of the size of nanoparticles produced in water on the position of the focal plane of the lens focusing the laser radiation relative to the target surface. The produced nanoparticles may be devided into two groups: narrow-dispersed (particle average size, 10-20 *nm*) nanoparticles and wide-dispersed ones (particle average size, 60-70 *nm*). The authors attribute the origin of the first group to the ablation due to the laser interaction with target material, and the second group is a result of interaction with the produced plasma. It was found that the produced plasma intensity correlates with the amount of ablated material, as well as the average size of nanoparticles related to the wide-dispersed group. The authors assume that plasma heating of the target or mechanical target destruction due to the collapse of plasma-induced cavitation bubble are possible mechanisms of secondary ablation connected with plasma.

If the target is ablated in vacuum or gas medium, the nanoclusters may be transported to a substrate located at some distance from the target and form a nanostructured film. Ablation in

liquids (e.g., water solutions) leads to the ejection of nanoparticles into the environment and to the formation of colloidal solutions.

Ablation in liquids makes it possible to obtain pure nanomaterials, which are free of surface contamination typical of chemical methods. Nanoparticles obtained in a pure well-controlled medium are especially important for the application *in vivo* biodetection and visualization. Ablation in liquids has a number of specific features, namely:

- The presence of an optical breakdown in a dense medium, which absorbs a significant part of laser energy (typical time up to 50 μm); an effective transfer of energy from the laser plasma to the ambient liquid and formation of a cavitation bubble that is growing up to 150-250 μs and then collapsing yielding a large amount of mechanical energy;
- Absorption of an incident laser radiation by produced suspended nanoparticles. May cause various effects: secondary ablation of the material [29], fragmentation of colloidal particles [30], formation of complex chemical structures [31].
- The presence of self-focusing phenomenon and generation of a continuum for ultrashort pulses. In particular, the filamentation may take place when ultrashort laser pulses pass through the optical medium, and appears as a result of a balance between the laser pulse self-focusing and de-focusing effect of the plasma produced under high laser intensity in self-focusing area [32].

Laser ablation in liquids is an effective method to produce nanoparticles in the form of colloidal solutions. One should note that at ablation in water or other solutions under the absence of chemically active components the produced nanoparticles are of rather large size. This is associated with the coagulation and aggregation of atoms subjected to ablation. Nanosecond laser pulses, for example, give the particles of 10-300 *nm* in size and 50-300 *nm* dispersion [33].

Ultrashort laser pulse ablation offers better chances to control the size and dispersion of nanoparticles. A possibility to control effectively the nanoparticle size by changing the the laser flux density (F) has been shown in [23]. The size of nanoparticles varied from 4 to 120 *nm* when F changed from 60 up to 1000 J/cm^2. Two populations of nanoparticles have been produced in the experiments. The first one was produced under low density of the laser flux and included the particles of small size and narrow dispersion. At average F values both populations were observed. At high F the particles had large average size and wide dispersion. The mentioned populations are similar to those produced in the experiments on changing the position of the focal surface of a focusing lens discussed above. So, one can conclude that different mechanisms are responsible for the occurrence of each of the populations: the ablation due to the incident radiation and ablation due the effects caused by plasma formation.

To control the size of produced nanoparticles the water solutions of surface-active agents are used frequently, for example, sodium dodecyl sulfate, which cover the nanoparticles just after the ablation and prevent further agglomeration [34]. A drawback of the method lies in the fact that the nanoparticles covered by surface-active agents have no free chemical bonds, and the area of its further application is limited.

Paper [14] presents the results from the experiments on the ablation of gold in water solutions containing neutral α-cyclodextrins, β-cyclodextrins, or γ- cyclodextrins. A Ti/sapphire laser was used in the experiments (pulse duration, 110 *fs*; wavelength, 800 *nm*;

pulse maximum energy, 1 *mJ*). A sharp decrease in the size of nanoparticles was observed in comparison with the experiments in water. The nanoparticles produced at ablation in the solution of β-cyclodextrins (10 *mMole*) had the average size 2.1-2.3 *nm*, the dispersion did not exceed 1 nm. The solution was of saturated red color. The produced colloids turned to be very stable.

To make smaller the nanoparticles produced by ablation in a liquid medium the colloids are additionally treated by ultrashort laser pulses. In [27] the 11±5 *nm* nanoparticles were produced by laser ablation of a gold plate in a sodium dodecyl sulfate solution. Then, using a sprayer, the colloid 80 μm droplets were produced and subjected to structural changes with the help of single nanosecond laser pulses (wavelength, 532 *nm*; pulse duration, 10 *ns*; pulse energy, 30 *mJ*). The experiment resulted in obtaining the nanoparticles of 3.7 *nm* average size. The authors assume that, as a result of laser energy absorption, nanoparticles are heated up to the temperature of metal melting, and then are ionized due to thermal emission. The electrons emitted from the particles' surface are temporarily solvated in water. As a result, a multiply charged gold nanoparticle becomes unstable and fragmented owing to the Coulomb explosion. A similar scenario of fragmentation is considered in [28]. At the first stage the 8±5 *nm* nanoparticles were produced by ablation of a gold plate in sodium dodecyl sulfate solution. Then, the nanoparticles were subjected to laser radiation (the wavelength, 355 *nm*; pulse duration, 10 *ns*; pulse energy, 50 *mJ*; pulse repetition rate, 10 *Hz*). The nanoparticles reduced in size to 1.5 *nm*.

In [15], as a result of gold shells ablation in pure deionized water the produced gold nanoparticles had an average size of 55 *nm* and 34 *nm* dispersion. At the second stage, the obtained colloids were subjected to laser irradiation with the following characteristics: (pulse duration, 140 *fs*; wavelength, 800 *nm*; pulse energy, 500 *mJ*; pulse repetition rate, 1 *kHz*). After 30 minutes of irradiation of the colloid, the average size of nanoparticles reduced to 11±5 *nm*. Figures 1 and 2 illustrate size distribution of nanoparticles before and after irradiation.

Under further treatment (up to two hours) the nanoparticle average size increased gradually, and finally stabilized at 20-30 *nm*. The obtained colloids demonstrated excellent stability – up to several months. The authors consider the nanoparticle fragmentation to be a consequence of Coulomb explosion. Originally the size of nanoparticles reduces sharply due to the absorption of the incident 800 *nm* laser radiation. Further decrease is caused by absorption of energy from the white continuum, which occurs due to nonlinear optical interaction between the incident radiation and medium.

An absence of nanoparticles of intermediate size even at a very short time of irradiation speaks in favor of a concept of Coulomb explosion. The presence of such particles is typical for nanoparticle size reduction due to thermal evaporation of matter.

In [26] the colloids of gold 5-50 *nm* nanoparticles were obtained by the method of chemical reduction. Later, a laser with the wavelength of 532 nm, pulse duration 7 ns and flux density 210 mJ/cm^2 was used in the experiments on nanoparticle size reduction. The time of laser irradiation was 10 minutes. As a result, the nanoparticles having the size of 20 to 50 *nm* disappeared, and the number of nanoparticles of the size up to 10 nm sharply increased. TEM pictures of nanoparticles before and after laser irradiation are shown in Fig. 3.

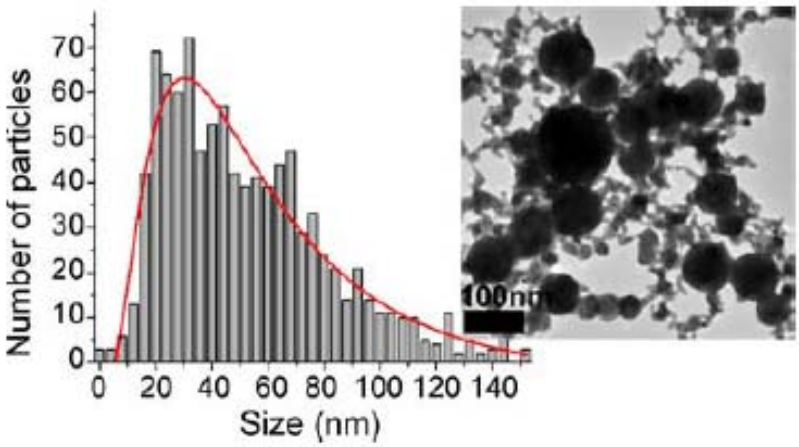

Fig. 1. TEM picture of Au nanoparticles produced by target ablation in water. Size distribution of nanoparticles.

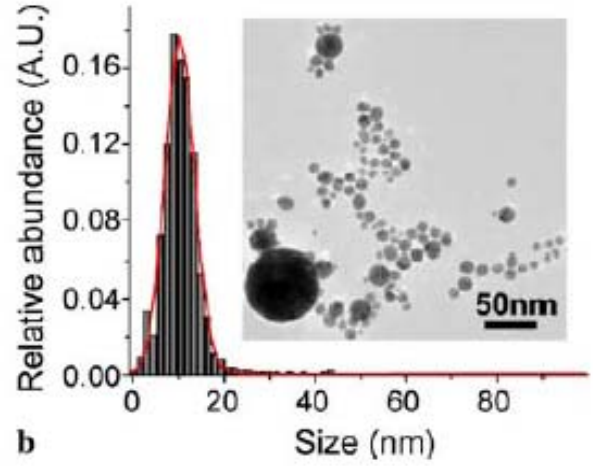

Fig. 2. TEM picture of Au nanoparticles after 30 minutes of irradiation by femtosecond laser pulses. Size distribution of nanoparticles.

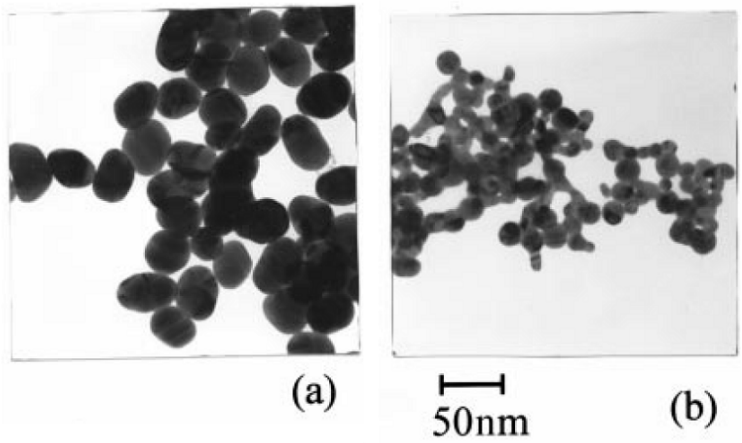

Fig. 3 TEM picture of Au nanoparticles before (a) and after (b) 10 minutes of laser irradiation; the laser flux density 210 mJ/cm^{-2}

The influence of laser irradiation time and laser flux density on nanoparticle size distribution was also studied in the paper. At a fixed laser flux density of 140 mJ/cm^2 , the maximum size of nanoparticles after 5 minutes of irradiation was 22 *nm*. Further irradiation did not change this value, and this shows that nanoparticle maximum size value may be considered as a certain threshold value. When laser flux density increased from 30 up to 500 mJ/cm^2 , there was observed a decrease in nanoparticle maximum size. The authors suggested as a mechanism of nanoparticle size reduction the evaporation of Au atoms under nanoparticle heating by laser radiation up to the temperature exceeding the gold melting temperature.

A possibility to reduce the nanoparticle size by means of laser treatment has been demonstrated for silver as well [35]. The colloids of silver 40-60 *nm* nanoparticles were obtained by the method of chemical reduction of $AgNO_3$ in water with an addition of sodium citrate at a temperature close to the boiling temperature. Then, the produced nanoparticles were subjected to laser radiation: pulse duration, 18 *ps*; wavelength, 355 and 532 *nm*; pulse energy, 2-3 *mJ*. As a result, 5-10 *nm* nanoparticles were produced. It was established that the choice of laser wavelength affects the selectivity of cluster fragmentation. For example, when the wavelength was changed for 532 *nm*, there was observed the fragmentation of large nanoparticles only, or irregular-shaped nanoparticles. The authors stated that there takes place an electron photoemission as a result of laser action on silver nanoparticles. The nanoparticles become charged and disintegrate into the smaller ones.

3 THEORETICAL MODELING

The papers are available which consider various aspects of laser interaction with metal nanoparticles. Paper [36] is devoted to numerical simulation of the interaction between short laser pulses and gold nanoparticles in water. The authors made use of a hydrodynamic model, which describes, with the help of Navier-Stokes equations, the heat and mass transfer in the system, and includes the equations of state (EOS) for water, two-temperature description of electron-phonon equilibrium in a metal nanoparticle, as well as the description of thermoelastic response of the particle matter. The modeling was made for moderate laser fluxes ($F < 100$ J/m^2), when the temperature is lower or slightly higher than the critical temperature in water; nanoparticle radius lies within the limits 25-200 *nm*; pulse duration is 0.1-1 *ps*. It was found that irradiation of nanoparticles by femtosecond laser pulses results in a propagation of a compression wave in the direction from the particle, and the width of the wave depends on the viscosity and heat conductivity of the ambient liquid. For 50 *nm* nanoparticles irradiated by 200 *fs* laser pulses and $F = 60$ J/m^2, the vapor formation on the surface of the particle starts at $t \approx 23$ ps, and the vapor layer is produced up to the time $t \approx 84$ *ps*. It was established that a total amount of evaporated matter remains relatively small, and the effect ofvapor formation on the temperature profilesis insignificant. The water temperature near the nanoparticle surface reaches the boiling temperature at flux density of 18 J/cm^2, and the critical temperature at 72 J/cm^2. At higher fluxes there is observed a continuous transition from liquid to the vapor without vapor-liquid common existence near the surface of a nanoparticle.

Paper [37] presents a kinetic theory of laser-metal nanoparticle interaction in a matrix of a wide-band dielectric (SiO_2). The formalism is based on Boltzmann equation for the electrons of an open system adapted to the description of nanoparticle electron losses owing to

thermionic emission and photoelectric effect. The simulations of energy transfer and re-distribution are presented, as well as those of electron emission within the framework of the study into the destruction processes resulting from laser-gold nanoparticle interaction in a SiO_2 matrix. The calculations were made for 1.3 *nm* and 2.6 *nm* nanoparticles in SiO_2 matrix irradiated by 351 nm laser pulses with pulse duration 0.5 ns and 50 *ps*, and flux density 0.3 *J/cm2* and 0.15 *J/cm2*, respectively. It was shown that under such regimes a considerable number of electrons can be ejected from the nanoparticles due to thermionic emission. In both cases the electron effective temperature in nanoinclusions reached saturation at > 1*eV* (5000-6000*K*), and the grating temperature was relatively low (620*K* and 390*K*, respectively) due to energy transfer to the aambient glass and the emission of high-energy electrons.

Paper [38] presents a model which allows one to determine the dynamics of electron and ion temperature in a gold nanoparticle dipped into dielectric of a finite volume under the action of subpicosecond laser pulses. The model is based on a two-temperature model destined for the calculation of nanoparticle temperature and ballistic-diffusion approximation (BDA) for the estimation of heat transfer from the particle and its propagation in a dielectric environment. The model was applied to gold 10 *nm* nanoparticles in Al_2O_3 shell, and the shell thickness varied from 0.54 to 54 *nm*. The laser pulse duration constituted 110 *fs*. Time dependences of electron and grating temperature were found with the help of Fourier law and BDA for 5.4 *nm* thick shell.

We consider such scenario of gold nanoparticles fragmentation in water under the action of femtosecond laser pulses. When the colloids of relatively large gold nanoparticles (several tens of *nm*) are irradiated by femtosecond laser pulses, one can observe their fragmentation into smaller nanoparticles (up to several *nm*). In the process the particle is heated up to the melting temperature and turns into a drop of liquid. The heating is accompanied by thermionic emission from the drop surface. The emitted electrons take away the negative charge, and the drop of melted metal turns to be positively charged. Thus the model of fragmentation is based on the electrolization of metal nanoparticles heated by a laser pulse, and their division under the development of instability of a charged drop of liquid metal. As a mechanism of electrolization we have considered the emission of hot electrons from the surface of a nanoparticle with further salvation in liquid. The problem of gold particles heating at femtosecond laser pulse absorption has been solved. Time dependence of electron thermionic emission current from the particle surface has been found. The particle fragmentation parameter has been defined. The estimates are given of nanoparticle charge gained under the action of the laser pulse in water.

To develop a physical model and optimize the regimes of laser irradiation for producing nanoparticles one needs to solve the following problems:

- The problem of nanoparticle heating under the action of laser radiation;
- Find the current of electron thermionic emission from the surface of a nanoparticle;
- Calculate the fragmentation parameter for gold nanoparticles;
- Evaluate the charge gained by the nanoparticle as a result of thermionic emission and electron salvation

4 THE PROBLEM OF NANOPARTICLE HEATING

A two-temperature model [3] has been used to solve the problem of metal nanoparticles heating by femtosecond laser pulses:

$$\begin{cases} C_e \dfrac{\partial T_e}{\partial t} - div(\lambda \cdot grad T_e) = \dfrac{P}{V} - g(T_e - T_{ph}) \\ C_{ph} \dfrac{\partial T_{ph}}{\partial t} = g(T_e - T_{ph}) \end{cases} \quad (1)$$

T_e , is the electron subsystem temperature; T_{ph} , the phonon subsystem temperature; C_e, C_{ph} , the electron and phonon heat capacity; *g*, the factor of electron-phonon coupling, which describes the rate of energy exchange between the electrons and the lattice; λ, the coefficient of heat conductivity; *P,* the laser radiation power absorbed by a nanoparticles; V , the nanoparticles volume.

Each of the equations represents the energy conservation law. The equation for the electrons illustrates the change in their temperature due to the heat transfer to the phonons, and laser radiation and laser radiation absorption. The phonons' temperature changes only due to the heat exchange with electron, since the phonons do not absorb the laser radiation.

One can use an approximation of homogeneously heated nanoparticle for the nanoparticles with the radii smaller than the distance covered by the heat from the incident radiation during the pulse action. The distance covered by the heat during the pulse is:

$$l = 2\sqrt{\chi_e \tau}\ ,\ \chi_e = \frac{\upsilon_F^2}{3\nu_e}$$

where τ is the pulse duration; χ_e the temperature conductivity of the metal electron subsyste; υ_F , the Fermi velocity; ν_e, the frequency of electron collisions. For the metals the electron collision frequency consists of the electron-phonon and electron-electron collisions. The grating temperature При температурах решетки T_{ph} being higher than Debye temperature Θ_D (for Au $\Theta_D = 170K$), the frequency of electron-phonon collisions is proportional to T_{ph} . When the electron thermal energy $k_B T_e$ is snaller than Fermi energy ε_F , the frequency of electron-electron collisions ν_{e-e} depends quadratically on the electron temperature. Bearing this in mind, let us neglect the contribution of electron-phonon collisions and consider $\nu_e \approx \nu_{e-e}$. At $\nu_{e-e} = 0.93 \cdot 10^{14}\, s^{-1}$, $\upsilon_F = 1.4 \cdot 10^8\, cm/s$, we get $\chi_e = 70\, cm/s$. At 100 *fs* pulse duration we get $l = 52$ nm. So, for the particles having the radii smaller than 52 nm, one can neglect the thermal fluxes directed from the areas with higher temperatures to the areas with lower temperatures. Finally we have the following system of equations:

$$\begin{cases} C_e \dfrac{\partial T_e}{\partial t} = -g(T_e - T_{ph}) + \dfrac{P}{V} \\ C_{ph} \dfrac{\partial T_{ph}}{\partial t} = g(T_e - T_{ph}) \end{cases} \quad (2)$$

The initial conditions:

$$\begin{cases} T_e(0) = T_{in} \\ T_{ph}(0) = T_{in} \end{cases}$$

Here T_{in} is the temperature of the environmental area considered to be equal to 300K.

If the electron subsystem temperature is much lower than Fermi temperature (for Au T_F = 63 900), only the electrons near Fermi surface are charged, and the electron heat capacityis presented in the form of linear temperature dependence:

$$C_e\left(T_e\right) = C_e^{'} \cdot T_e \tag{3}$$

where $C_e' = \pi^2 k_B^2 n_e / 2\varepsilon_F$ and n_e is the concentrationof free electrons; k_B, the Boltzman constant; ε_F, the Fermi energy.

Theoretical and experimental research shows that the Au d zone, located close to Fermi level, has a very complex structure. The electrons of U d zone introduce significant correction into the number of thermally excited electrons, and, hence, influence the electron heat conductivity [39]. The use of linear approximation for temperature dependence of electron heat conductivity may lead to an essential overestimation of electron subsystem temperature in a state of partial thermodynamic equilibrium with the phonon subsystem. Such equilibrium is usually realized under the action of femtosecond laser pulses onto the metals.

Thermally excited electrons of *d* zone also make contribution into the interaction between the electron and phonon susbsystems. That is why the temperature dependence of *g* was taken into account in the solution of the thermal problem. Figure 4 illustrates the temperature dependence of *g* factor.

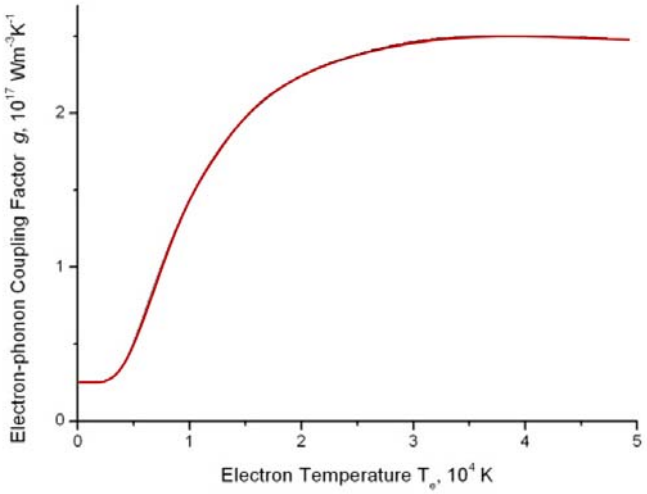

Fig.4. Dependence of electron-phonon coupling factor on the electron subsystem temperature.

Define the dependence of electron maximum temperature on the laser pulse energy density using a linear dependence between the electron heat conductivity and temperature. At the stage of heating by the laser pulse (100 *fs*) one can neglect the term responsible for the energy exchange between the electrons and phonons in the first equation of system (2). We get:

$$V \cdot C_e \cdot \frac{\partial T_e}{\partial t} = P = \sigma_{abs} \cdot q\,, \tag{4}$$

where V is the nanoparticle volume; P , the absorbed laser radiation; σ_{abs}, the absorption crosssection considered to be equal to a geometrical crosssection πa^2; and a, the nanoparticle radius; q, the laser flux. After time integration of equation (4) to the pulse duration we get the ratiobetween the electron maximum temperature $T_e^{(0)}$ on the laser pulse energy density F:

$$T_e^{(0)} = \sqrt{\frac{3}{2}\frac{F}{a \cdot C_e'}} \tag{5}$$

The obtained dependences between the maximum electron temperature $T_e^{(0)}$ and laser pulse energy density are given in Fig. 5. As seen from the figure, the maximum electron temperature calculated with the use of linear approximation for electron heat capacity is twice as much as the one obtained with account for d-electron contribution to heat conductivity.

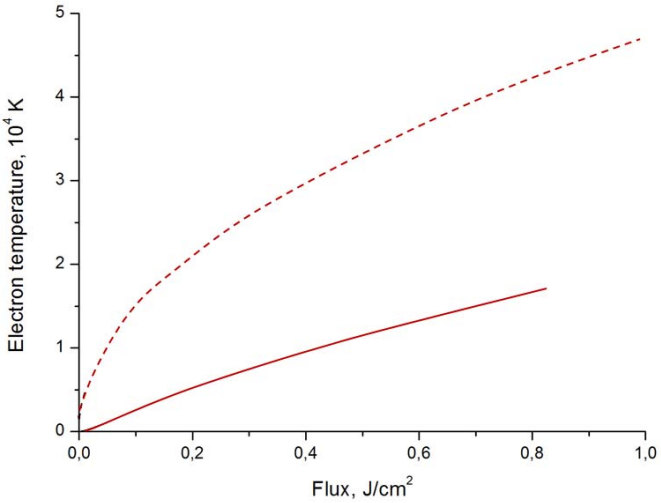

Fig. 5 Electron subsystem temperature vs flux density. Solid line: d-electron contribution taken into account; dashed line: linear approximation with no account for d-electron contribution.

At the initial stages of heating the electron subsystem temperature is much higher than the temperature of phonon subsystem ($T_e >> T_{ph}$), and, so, we may neglect the grating temperature in the system (2):

$$\begin{cases} C_e' \cdot T_e \dfrac{\partial T_e}{\partial t} = -g \cdot T_e \\ C_{ph} \dfrac{\partial T_{ph}}{\partial t} = g \cdot T_e \end{cases} \tag{6}$$

The solution of the system (6) has the following form:

$$\begin{cases} T_e(t) = T_e^{(0)}\left(1 - \dfrac{g \cdot t}{C_e' \cdot T_e^{(0)}}\right) = T_e^{(0)}\left(1 - \dfrac{t}{\tau_c}\right) \\ T_{ph}(t) = \dfrac{g \cdot T_e^{(0)}}{C_{ph}}\left(t - \dfrac{t^2}{2\tau_c}\right) \end{cases} \quad (7)$$

τ_c, the typical time of electron subsystem cooling. For Au we have $g = 2.5\times10^{10}$ W/cm^3K, $C_e'=6.27\times10^{-5}$ J/cm^3K^2. From the first equation of the system (7) we may estimate the typical time of electron subsystem cooling: if $T_e^{(0)} \approx 10^4\,K$, then $\tau_c \approx 25nc$.

Figure 6 illustrates the results from solution of systems (2) and (6) for the laser pulse energy density 100 mJ/cm^2.

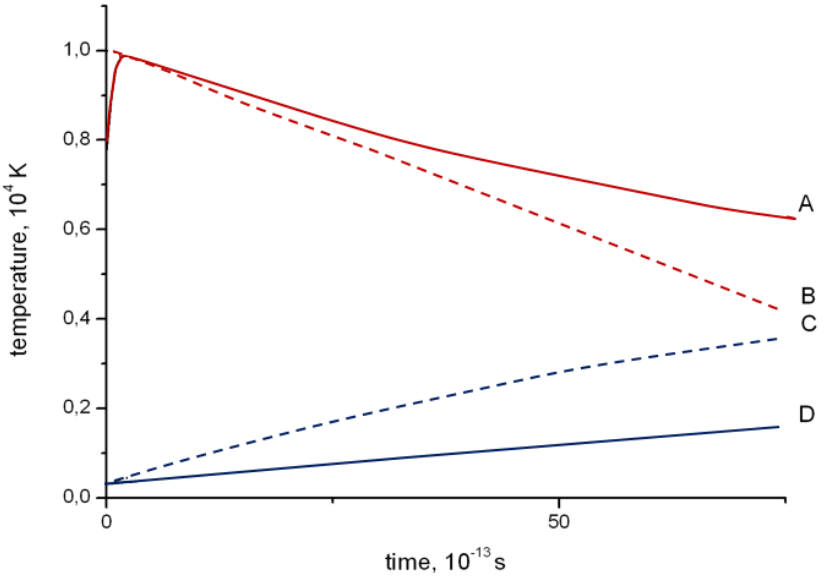

Fig.6 Time temperatures profile of the electron (A,B) and phonon (C,D) subsystems. Solid lines – numerical solution; dashed lines – analytical solution.

In the calculations the absorption cross-section was assumed to be equal to the geometrical cross-section πa^2, where a = 100 nm is the particle radius. As seen from Fig.1, after the end of the laser pulse the electron temperature reaches about ten thousands degrees, and then drops linearly during the time of tens of picoseconds. The final temperature of the nanoparticles lattice exceeds the melting temperature of gold (T=1337 K), i.e. the nanoparticles is transformed into a liquid state.

5 DEPENDENCE ON THE SIZE OF NANOPARTICLES

The absorption crosssection σ_{abs} for the nanoparticles depends on their size. The efficiency of laser radiation absorption Q_{abs} is defined as follows: $Q_{abs} = \dfrac{\sigma_{abs}}{\pi a^2}$. The

dependence of the efficiency of laser radiation (800 *nm*) absorption by gold nanoparticles in water is shown in Fig. 7.

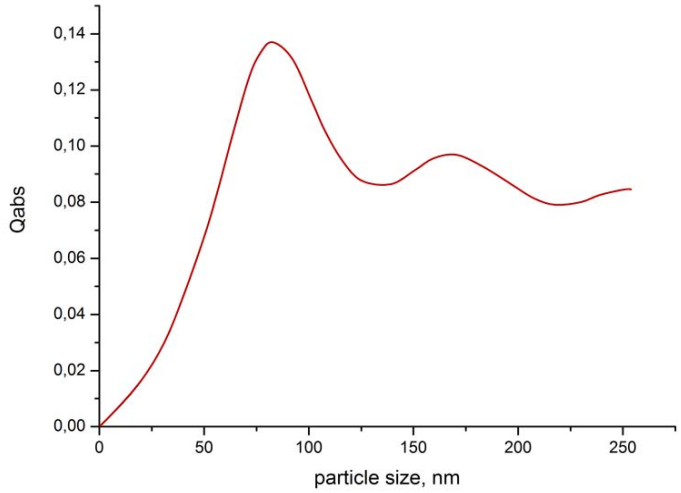

Fig.7. The dependence of absorption efficiency for for the incident laser radiation with λ=800 nm.

For the calculations we have used the program package MatLab [40], based on the Mie scattering theory of a plane electromagnetic wave on a homogeneous sphere of random size. As seen from the figure 7, the absorption crosssection increases with an increase in the nanoparticle size, and reaches its maximum for the nanoparticles with the radius of about 75 nm.

The incident laser energy is absorbed by the metal electron subsystem and leads to its heating. This means that that the change in the absorption crosssection under the change of nanoparticle size results in the change of electron temperature. Figure 8 presents the dependence of electrom maximum temperarture on the size of nanoparticles for different densities of the the incident laser flux obtained by equation (4). Maximum temperature of the heated electron subsystem corresponds to the absorption maximum efficiency, and falls at 75 nm nanoparticles.

The electron subsystem transfers the energy to the grating, and this leads to the temperature growth. Let us estimate estimate the amount of heat *H*, which is necessary for the gold nanoparticle to be melted under the action of a laser pulse. $H = C_{Au} \cdot (T_{пл} - T_0) + \Delta H_{пл}$, here $C_{Au} = 25.4\ J/mole \cdot K$ is the gold heat capacity; $T_{пл}$, the melting temperature of Au; $T_0 = 300K$, the initial temperature; $\Delta H_{пл} = 12.6 \cdot 10^3\ J/mole$, the melting molar heat. Then $H = 3.8kJ/mole \cdot K = 3{,}7kJ/cm^3$.

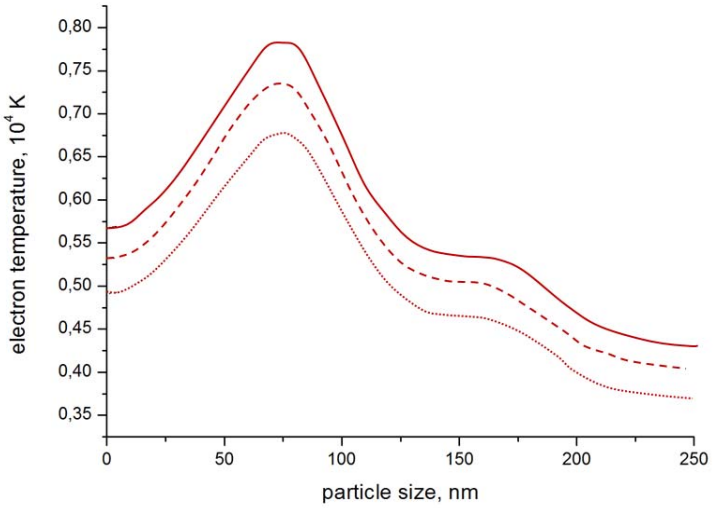

Fig. 8. Maximum electron temperature vs nanoparticle size for the laser flux density of 200 mJ/cm^2 (dotted line), 250 mJ/cm^2 (dashed line), 300 mJ/cm^2 (solid line).

If one knows the H value, the, by using formula (4) it is possible to find the dependence between the threshold flux density of the laser flux F_{th} and the nanoparticle size. Under the threshold density of the laser flux we mean here its minimal value needed to transfer to the particle the amount of heat sufficient to melt it.

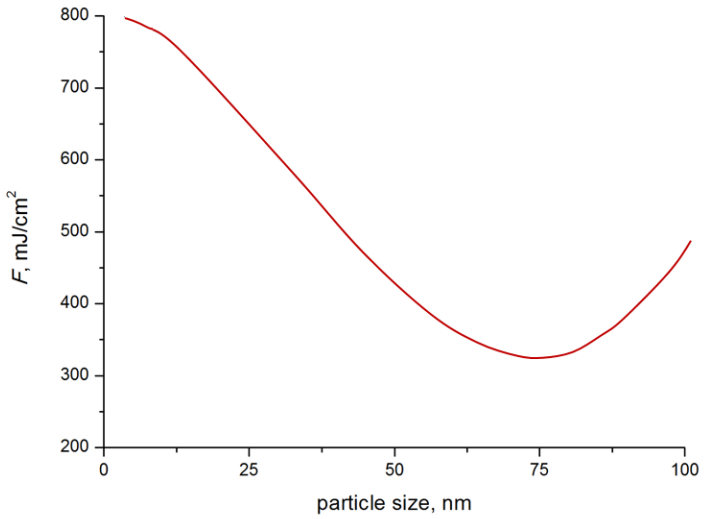

Fig. 9. Laser flux threshold density vs nanoparticle size.

One can see from Fig. 9 that the F_{th} value lies within the limits of 300 to 800 mJ/cm^2 for 100 *nm* nanoparticles. The smaller is the absorption efficiency the more energy should be given to the nanoparticle in order to reach the metal melting temperature. This is well seen from a comparison of Fig.8 and Fig. 9: the growth of absorption efficiency corresponds to the decrease in laser flux density.

6 THERMIONIC EMISSION

A thermionic emission from the surface of heated gold nanoparticles is observed. The value of electron thermionic emission current is defined by the temperature of the metal electron subsystem:

$$j = A \cdot T_e^2 \cdot \exp(-\frac{W}{kT_e}) \tag{8}$$

Here A, is the Richardson constant; $A \approx 120 \ \frac{A}{cm^2 \cdot K^2}$, W=5,1 eV, the work of the gold yield; T_e, the electron temperature.

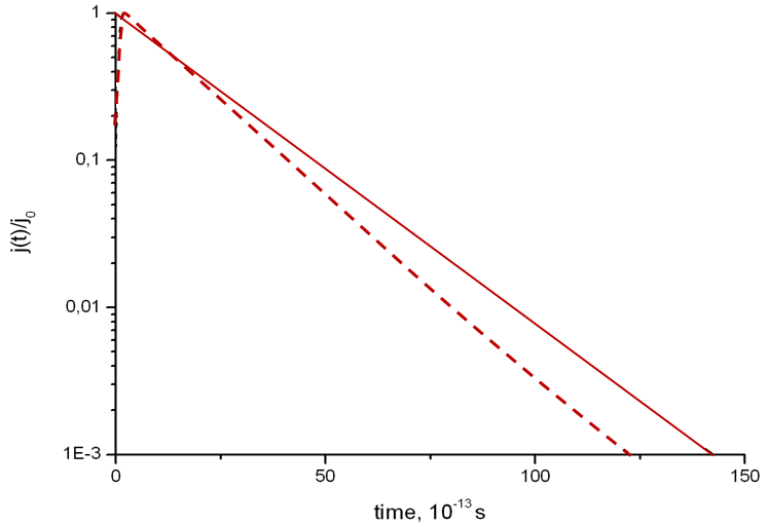

Fig. 10. Time profile of thermionic emission current. Solid line –analytical solution, dashed line – numerical solution.

Fig. 10 illustrates time dependence of thermionic emission current for laser fluence $F = 100\ mJ/cm^2$. Maximal density of thermionic current is ~ $10^6\ A/cm^2$. One can see from the Fig. 10 that, in accordance with the numerical and analytical solutions, the current drops exponentially after the end of the laser pulse during a typical time of several picoseconds.

7 SALVATION OF ELECTRONS IN WATER

The electrons emitted from the surface of a nanoparticle are rapidly thermolized.

The interaction electrostatic forces occurr berween the water dipoles and electrons emitted from the nanoparticle surface due to thermionic emission. Water molecules are polarized by electron and captured, i.e. the electrons are solvated in water.

Typical time of salvation is about 250 fs [3]. The mobility of electrons sharply drops here. As a result, an electric double layer of a space charge is formed near the nanoparticle surface.

Pure deionized water presents an amorphous dielectric with the forbidden zone E_g=6.5±0.5 eV [3]. Hence, the motion of emitted electrons in water can be considered as electron motion in a semiconductor in the space charge self-field.

This field grows with the growth of the number of emitted electrons, and it becomes more and more difficult for the new electrons to leave the nanoparticle surface. As a result, the emission current decreases, and, hence, the field becomed weaker. When the field decreases, it is easier for the electrons to leave the nanoparticle surface, and the emission current grows. Such electric field is called a self-consistent field.

Water molecules are heavier than electrons, and, so, the capture of electrons by water molecules in salvation prevents the electron motion by the electric field. Consequently, the molility and the depending (by Einstein relation) diffusion coefficient of slvated electrons sharply drop down to ~ 10^{-4} cm^2/s [3].

In this case salvation is similar to electron capture on a capture center. The above considerations allow one to use the elements of the solid body theory to describe the electron motion in water. Namely, the equations of electron motion in a dielectric medium with account for the space self-charge have the form [41]:

$$\begin{cases} \dfrac{\partial n_e}{\partial t} = D_e \Delta n_e - \mu_e \cdot div\left(n_e \cdot \vec{E}\right) - \dfrac{n_e}{\tau_s} \\ \dfrac{\partial n_s}{\partial t} = D_s \Delta n_s - \mu_s \cdot div\left(n_s \cdot \vec{E}\right) + \dfrac{n_e}{\tau_s} \\ -\varepsilon_0 \Delta\varphi = 4\pi e\left(n_e + n_s\right) \\ \vec{E} = -grad\varphi \end{cases} \tag{9}$$

e is the electron charge; n, the concentration of electrons; D, the electron diffusion coefficient in water; μ, the electron mobility in water; E, the electron spatial self-consistent field; ε_0, the dielectric constant of water; φ, the electric potential of the self-field of electrons, the indices e and s refer to the emitted and solvated electrons, respectively.

The first two equations in (9) describe the motion of the emitted and solvated electrons due to the diffusion and drift in a self-consistent electric field and the solvation in water, respectively. The third equation of the system is derived from the Maxwell equation for the rotor of the magnetic field vector provided that our problem is a spherically symmetric one (assume the nanoparticle to be sphere-shaped).

The boundary conditions are as follows:

$$\begin{cases} n_e\big|_{r=a} = \dfrac{j_T}{\langle \upsilon_T \rangle \cdot e} \\ \left(D_s \dfrac{\partial n_s}{\partial r} - \mu_s n_s \vec{E} \right)\Bigg|_{r=a} = 0 \end{cases} \tag{10}$$

Here j_T is the emission current and $\langle \upsilon_T \rangle$, the average velocity of the emitted electrons.

The first equation of system (10) shows that the concentration of electrons emitted at nanoparticle boundary is defined by the emission current only; the second one shows that the current at the boundary of a nanoparticle equals zero.

Since the mobility and diffusion coefficient of solvated electrons are small, we neglect the terms corresponding to the diffusion and drift of solvated electrons. Finally, instead of system (9) we get the following system of equations:

$$\begin{cases} \dfrac{\partial n_e}{\partial t} = D_e \Delta n_e - \mu_e \cdot div\left(n_e \cdot \vec{E}\right) - \dfrac{n_e}{\tau_s} \\ \dfrac{\partial n_s}{\partial t} = \dfrac{n_e}{\tau_s} \\ -\varepsilon_0 \Delta\varphi = 4\pi e\left(n_e + n_s\right) \end{cases} \tag{11}$$

Systems (10) and (11) determine the electric field *E(r,t)* and *n(r,t)*, at the given parameters j_T and $\langle \upsilon_T \rangle$, and the parameters ε_0, μ and *T*. For further solution of the system it is convenient to introduce dimensionless functions and variables. In a dimensionless form in a spherical system of coordinates we have the system of equations where all the values are dimensionless:

$$\begin{cases} \dfrac{\partial n_e}{\partial t} = \dfrac{1}{r^2}\dfrac{\partial}{\partial r}\left(r^2 \dfrac{\partial n_e}{\partial r}\right) - \dfrac{1}{r^2}\dfrac{\partial}{\partial r} r^2\left(n_e E_r\right) - \dfrac{n_e}{\tau_s} \\ \dfrac{\partial n_s}{\partial t} = \dfrac{n_e}{\tau_s} \\ \dfrac{1}{r^2}\dfrac{\partial}{\partial r}\left(r^2 E_r\right) = n_e + n_s \end{cases} \tag{12}$$

Numerical solution of (12) resulted in obtaining time dependence of a space charge self-consistent field value. It is well known that the field value and the value of the generating charge are related as follows: $E = \dfrac{Ze}{a^2}$, *E* is the electric field; *Ze* , the charge, *a* , the size of a nanoparticle.

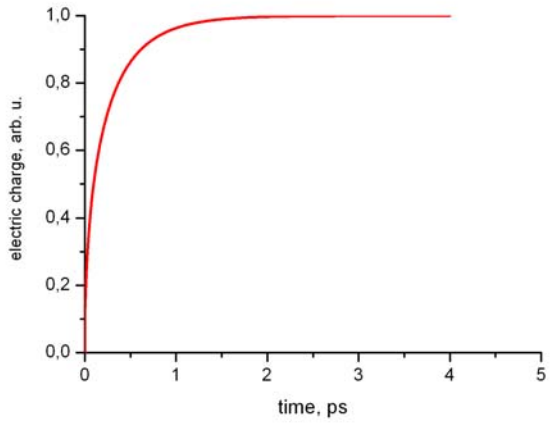

Fig.10. Electric charge (in relative units) vs time.

Figure 10 illustrates the time of a space charge. The obtained time dependence of the space charge indicates that a sharp growth of the electric field is observed for the times of ~1 *ps*, i.e., the times corresponding to a sharp growth of the thermionic emission current (see Fig. 10).

After this one can observe an exponential drop of the thermionic emission current, and the electric charge reaches the saturation. The estimated electric charge gained by a nanoparticles as a result of electron emission from its surface $Z_0 \approx 10^6$.

8 FRAGMENTATION PARAMETER

It has been shown that under irradiation of colloids of relatively large gold nanoparticles (several tens of ns) by femtosecond laser pulses one observes the fragmentation of these nanoparticles into smaller nanoparticles (up to several ns). The nanoparticle is heated to up to the metal boiling temperature and turns into a drop of liquid. The heating is accompanied by electron thermionic emission from the surface of a drop. The emitted electrons take away the negative charge, and the drop of melted metal becomes positively charged.

The problem of charged spherical drop stability depending on the ratio between the surface and Coulomb energy was solved by Rayleigh in 1882 [42]. The fission parameter X is defined as follows:

$$X = \frac{E_c}{2E_s}$$

where E_c, is the Coulomb repulsion force, E_s, the surface tension force.

It's well known that the fragmentation is observed at $X \geq 1$; at $0.3 < X < 1$ one can observe both the fragmentation and evaporation of single atoms from the the nanoparticle surface; at $X < 0.3$ only the evaporation of single atoms is observed [43].

The fission parameter for the metal (gold) nanoparticles is defined as $X = A\frac{q^2}{n}$, q, the particle charge; n, the number of atoms in the nanoparticle; $A = \frac{e^2\rho}{6 \cdot \sigma \cdot M_a} \approx 2$; e, the electron charge; $\rho = 19.3 g/cm^3$, the gold density; $\sigma = 1.125 \cdot 10^3 erg/cm^2$, the surface tension coefficient of melted gold; $M_a = 196.97 g/mole$, the gold molar mass.

The drop is stable in the face of extreme deformations – splitting into two identical parts at $Q_{cr}^2 = 0{,}36 \times 16\pi a^3 \sigma$, where a - particle size, $Q=Ze$, σ, surface tension coefficient of the liquid.

One can estimate the minimal number of electrons, q_{min}, which should leave the drop surface to make it unstable and fragmented.

Figure 12 presents the dependence of q_{min} on the size of nanoparticle. Mimimum number of electrons needed for fragmentation grows as function $a^{2/3}$, where a is the nanoparticle radius.

The typical values of q_{min} for the nanoparticles at a diameter $a=100nm$ should be an order $Z_{cr}=10^4$. Comparing the typical values with the charge estimates obtained from numerical solution of (9), one can obtain that

$$Z_0 / Z_{cr} >> 1$$

The charge gained by the nanoparticle from the electron thermionic emission is sufficient to make the particle unstable and fragmented.

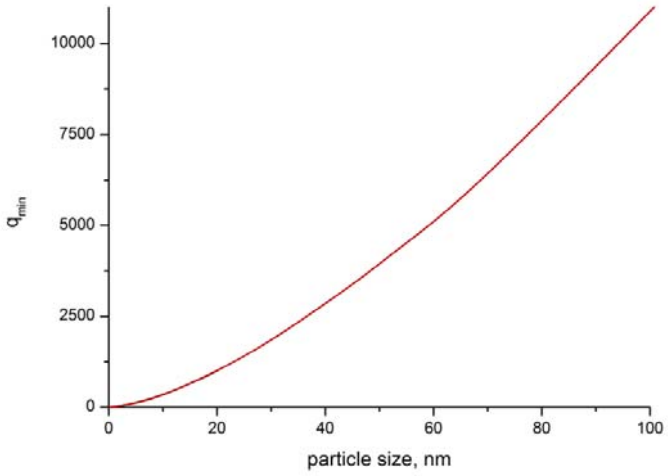

Fig. 12. Minimum number of electrons needed for fragmentation vs nanoparticle size. .

9 CONCLUSION

Theoretical modeling of metal nanoparticles fragmentation in water under the action of femtosecond laser pulses is discussed. The problem of heating a gold nanoparticle by laser pulses of femtosecond duration has been solved. The value and typical time of the drop of thermionic emission current from the nanoparticle surface due to the heating of the particle by the laser radiation field has been found. On the basis of the Rayleigh drop model the criterion of nanoparticle fragmentation has been found. The estimates of the charge gained by the nanoparticle due to the electron thermionic emission and their further solvation have been obtained. It was shown that the charge exceeds the threshold value given by the Rayleigh criterion. It is possible to conclude that as a result of the influence of laser radiation the particle becomes unstable and the nanoparticles fragmentation takes place.

The results of theoretical modeling may be used to optimize the laser operation regime destined to produce the nanoparticles of the given size.

Acknowledgments. This work was supported by the Russian Academy of Sciences (grants 21P and 7OF) and Russian Foundation for Basic Research (grant 02-12-00761)

REFERENCES

[1] I.N. Zavestovskaya, "Laser-assisted metal surface micro- and nanostructurization", *Laser and Particle Beams,* **28**, 437 (2010).

[2] I.N. Zavestovskaya, "Laser Nanostructurization of metal surfaces", *Quantum Electronics*, **40**, 942 (2010).

[3] I.N. Zavestovskaya, A.P. Kanavin, S.D. Makhlysheva "Theoretical modeling of laser fragmentation of nanoparticles in liquid media. *Bulletin of the Lebedev Physics Institute,* **40**, 335 (2013)
[4] I.N. Zavestovskaya, "Laser nanocrystallization of Metals", in *Fundamentals of Laser-Assisted Micro- and Nanotechnologies*, Ed. By V.P. Veiko and V.I. Konov, Springer, p. 51-75 (2014).
[5] P.N. Prasad, *Introduction to Biophotonics*, Wiley-Interscience, Boston, (2003).
[6] A.V. Kabashin, Ph. Delaporte, A. Pereira, D. Grojo, R. Torres, Th. Sarnet, M. Sentis, "Nanofabrication with Pulsed Lasers", *Nanoscale Res. Lett.,* **5**, 454 (2010).
[7] Y. Vorobyev, C. Guo, "Enhanced absorptance of gold following multipulse femtosecond laser ablation", *Phys. Rev. B,* **72**, 195422(1-5) (2005).
[8] J. B. Pendry, "Playing Tricks with Light", *Science*, **285**, 1687 (1999).
[9] G.A. Shafeev, "Laser-based formation of Nanoparticles" in *Laser in Chemistry*, **2,** Ed. By M. Lackner, Wiley VCH Verlag, Wienheim, p.713, (2008)
[10] E.V. Barmina, E. Stratakis, K. Fotakis, U.A. Shafeev, "Generation of nanostructurs under laser metal ablation: New results", *Quantum Electronics*, **40**, 1012 (2010).
[11] R.R. Letfullin, C. Joenathan, T.F. George, V.P. Zharov, "Laser-induced explosion of gold nanoparticles potential role for nanophotothermolysis of cancer", *Nanomedicine*, 1, 4, 473 (2006)
[12] T. Wang, X. Hu, S. Dong, "The Fragmentation of Gold Nanoparticles Induced by Small Biomolecules", *The Royal Scociety of Chemistry C,* (2008)
[13] S. Eustis, G. Krylova, A.Eremenko, N. Smirnova, A.W. Schill, M. El-Sayed, "Growth and fragmantation of silver nanoparticles in their synthesis with a fs laser and CW light photo-sensitization with benzophenone", *Photochem. Photobiol,* **4**, 154 (2005).
[14] A.V. Kabashin, M. Meunier, C. Kingston, J.H.T. Luong, "Fabrication and Characterization of Gold Nanoparticles by Femtosecond Laser Ablation in Aqueous Solution of Cyclodextrins", *J. Phys. Chem. B*, **107**, 4527 (2003)
[15] S. Besner, A.V. Kabashin, M. Meunier, "Two-step femtosecond laser ablation-based method for the synthesis of stable and ultra-pure gold nanoparticles in water", *Appl.Phys. A* (2007), DOI:10.1007/s00339-007-4001-1.
[16] L.I. Boguslavskiy, "Metody polucheniya nanochastits I ih razmerno-chuvstvitelnyye parametry" *Vestnik MITHT*, **5**, 3 (2010) (in Russia).
[17] S. Bhattacharya, A. Srivastava, "Sinthesis of gold nanoparticles stabilized by metal-chelator and the controlled formation of close-packed aggregates by them", *Proc. Indian Acad. Sci., Chem. Sci.,* **115**, 613 (2003)
[18] Yu.V. Afanasiev, V.A. Isakov, I.N. Zavestovskaya, B.N. Chichkov, F. Von Alvensleben, H. Welling, "Hydrogynamic regimes of UV laser ablation of polymers", *Appl. Phys. A* **64**, 561 (1997);
[19] I.N. Zavestovskaya, P.G. Eliseev, O.N. Krokhin, N. A. Men'kova, "Analysis of the nonlinear absorption mechanisms in ablation of transparent materials by high-intensity and ultrashort laser pulses", *Appl. Phys. A* **92**, 903 (2008).
[20] E.V. Zavedeev, A.V. Petrovskaya, A.V. Simakin, G.A. Shafeev, "Nanostructures production under Laser silver ablation in liquid", *Quant. El.* **36**, 978 (2006).
[21] J.–P.Sylvestre, A.V. Kabashin, E. Sacher, M. Munier, "Femtosecond laser ablation of gold in water: influence of the laser-produced plasma on the nanoparticle size distribution", *Appl. Phys. A* **80**, 753 (2005)
[22] S. Barcikowski, A. Hahn, A.V. Kabashin, B.N. Chichkov, "Properties of nanoparticles generated during femtosecond laser machining in air and water", *Appl.Phys. A* **87**, 47 (2007)
[23] A.V. Kabashin, M. Meunier, "LASER Ablation-Based Synthesis nanomaterials" in *Recent advances in laser processing of materials*, Elsever, Amsterdam, 1, (2006).
[24] E. Giorgetti, A. Giusti, F. Giammanco, P. Marselli, "Production and

Photofragmentation of Au Nanoparticles by 355 nm Picosecond radiation", *Optics and Spectrosc*., **107**, 474 (2009)

[25] F. Boson-Verdyura, R. Brayner, V.V. Voronov, "Nanoparticles production under laser metal ablation in liquid", *Quant. El*., **33**, 8, 714 (2003)

[26] Takami, H. Kurita, and S. Koda, "Laser-induced Size reduction of Noble metal Particles", *J. Phys. Chem. B,* 103, 1226 (1999)

[27] H. Muto, K. Miyajima, F. Mafune, "Mechanism of Laser-Induced Size Reduction of Gold Nanoparticles as Studied by Single and Double Laser pulse Exitation", *J. Phys. Chem. C,* **112**, 5810 (2008)

[28] K. Yamada, Y. Tokumoto, T. Nagata, F. Mafune, "Mechanism of Laser-Induced Size-rechection of Gold nanoparticles as Studied by nanosecond transient absorption Spectroscopy", *J. Phys. Chem. B,* **110**, 11751 (2006)

[29] T. Tsuji, Y. Tsuboi, N. Kitamura, "Microsecond-resolved imaging of laser ablation at solid–liquid interface: investigation of formation process of nano-size metal colloids", *Appl. Surf. Sci*., **229**, 365 (2004)

[30] F. Mafuné, J.-Y. Kohno, Y. Takeda, "Full Physical Preparation of Size-Selected Gold Nanoparticles in Solution: Laser Ablation and Laser-Induced Size Control", *J. Phys. Chem. B*, **106**, 7575 (2002)

[31] F. Mafuné, F., J. –Y. Kohno,Y. Takeda. "Formation of Gold Nanonetworks and Small Gold Nanoparticles by Irradiation of Intense Pulsed Laser onto Gold Nanoparticles" *J. Phys. Chem. B*, **107**, 1258 (2003)

[32] G. Daminelli, J. Krüger, W. Kautek, "Femtosecond laser interaction with silicon under water confinement" *Thin Solid Films*, **467**, 334 (2004)

[33] S.I. Dolgaev, A.V. Simakin, V.V. Voronov at al., "Nanoparticles produced by laser ablation of solids in liquid environment", *Appl. Surf. Sci*., **186**, 546 (2002)

[34] F. Mafune, J.-Y. Kohno, Y. Takeda, "Dissociation and Aggregation of Gold Nanoparticles under Laser Irradiation", *J. Phys. Chem*., **105**, 9050 (2001)

[35] P. V. Kamat, M. Flumiani, G. V. Hartland. "Picosecond dynamics of Silver nanoparticles. Photoejection of Electrons and fragmentation", *J. Phys. Chem. B*, **102**, 3123 (1998)

[36] A.N. Volkov, C. Sevilla, L.V. Zhigilei. "Numerical modeling of short pulse laser interaction with Au nanoparticles surrounded by water", *Appl.Surface Sci.*, **253**, 6394 (2007)

[37] P. Grua, J. P. Morreeuw, H. Bercegol, "Electron kinetics and emission for metal nanoparticles exposed to intense laser pulses", *Phys. Rev. B*, **68**, 035424 (2003).

[38] M. Rashidi-Huyeh, S. Volz and B. Palpant, "Non-Furier heat yransport in metal-dielectric core-shell nanopareticles under ultrashort laser pulse exitation", *Phys. Rev. B*, **78**, 125408 (2008)

[39] D.A. Thomas, Z. Lin, L.V. Zhigilei, E.G. Gurevich, S. Kittel, R. Hrgenroder "Atomic modeling of femtosecond laser-indused melting and atomoc mixing in Au film-Cu substrate system", *Appl. Surface Sci*. **255**, 9605 (2009).

[40] Christian Mätzler, *MATLAB Functions for Mie Scattering and Absorption*, *Version 2*, University of Bern, Bern, (2002).

[41] M. A. Lampert, P. Mark, *Current injection in solids* Ac. press, NY, (1970).

[42] L. D. Landau, E.M. Lifshits, *Theoretical Physics* v.8, Nauka, Moscow (1982) (in Russian).

[43] U. Na¨her, S. Bjørnholm, S. Frauendorf, F.Garsias, C.Guet, "Fission of metal clusters", *Phys. Rep.* **285**, 245 (1997).

Received March, 10 2014

The journal *Mathematica Montisnigri* publishes original scientific works from all fields of mathematics and mathemat ical modelling which comprise new and significant results with complete proofs, which are of interest for a larger mathematical community. It also contains expository articles. The journal does not publish works of polemical or methodological interest, as well as works that have been offered for publishing in other journals. The journal publishes papers in English, Russian, French and German. It is usually issued thrice a year.

Instructions to the authors:

Authors should submit the Manuscript electronically at the address:

zarkop@ac.me,
borkov@ac.me,
orgcom@LPpM3.ru.

The paper should be prepared in MS Word by the instructions, which can be found at the web page: **lppm3.ru/en/pub/manusc** .

The file has to be translated into Portable Document Format (PDF) before submission to the Editorial board of the journal.

The papers should have a precise and informative title. 2010 Mathematics Subject Classification and Key words and Phrases should be included at the bottom of first page of the paper.

Theorems, other statements and formulae must be clearly marked, separating the results of the authors from the already known results. The list of references has to be enclosed in alphabetical or chronological order at the end of the paper as well as the affiliation of the author.

Subscription for one volume is 40 USA dollars for institutions and 20 USA dollars for individuals.

For subscriptions and exchange please refer to the above address.

Computer processing of the press Olga Koroleva, Moscow, Russia.
Print: AP Print, Podgorica, Montenegro.

CIP – Каталогизација у публикацији
Централна народна библиотека, Цетиње, 51(05)

MATHEMATICA Montisnigri = Математика Црне Горе/ главни и одговорни уредник Жарко Павићевић. - Књ. 1 (1993) - Подгорица (Џорџа Вашингтона бб) : Друштво математичара и физичара Црне Горе: Природно – математички факултет Универзитета Црне Горе, 1993 – (Подгорица: АП Принт). - 30 cm

Три пута годишње. – Текст на руском и енг. језику.

ISSN 0345-2238 – Mathematica Montisnigri
COBISS.CG-ID 150244359

MATHEMATICA MONTISNIGRI
VOLUME XXXI-2014